NASA-CR-174765
19850018950

A CR-174765

Contract NAS3-23687

Component-Specific Modeling

Annual Status Report
1984

Prepared By:
R.L. McKnight, Principal Investigator

Approved By:
J.A. McKenzie, Program Manager
M.L. Roberts, Technical Manager

NATIONAL AERONAUTICS AND SPACE ADMINSTRATION
LEWIS RESEARCH CENTER
21000 BROOKPARK ROAD
CLEVELAND, OHIO 44135

GENERAL ⟨ge⟩ ELECTRIC

AIRCRAFT ENGINE BUSINESS GROUP
ADVANCED TECHNOLOGY PROGRAMS DEPARTMENT
CINCINNATI, OHIO 45212

ENTER:D 85N27261
       DISPLAY 85N27261/2
       85N27261*#   ISSUE 16   PAGE 2799   CATEGORY 39   RPT#: NASA-CR-174765 NAS
       1.26:174765 ASR-1   CNT#: NAS3-23687   84/00/00   115 PAGES   UNCLASSIFIED
DOCUMENT
UTTL: Component-specific modeling   TLSP: Annual Status Report
AUTH: A/MCKNIGHT, R. L.
CORP: General Electric Co., Cincinnati, Ohio.   CSS: (Aircraft Engine Business
       Group.)   AVAIL.NTIS
SAP: HC A06/MF A01
COI: UNITED STATES
MAJS: /*COMPONENT RELIABILITY/*COMPUTER PROGRAMS/*HEAT TRANSFER/*MISSION
       PLANNING/*STRESS ANALYSIS
MINS: / COMBUSTION CHAMBERS/ DEFORMATION/ PERFORMANCE PREDICTION/ STRESS-STRAIN
       RELATIONSHIPS/ TEMPERATURE/ TURBINE BLADES
ABA: Author
ABS: A series of interdisciplinary modeling and analysis techniques that were
       specialized to address three specific hot section components are
       presented. These techniques will incorporate data as well as theoretical
       methods from many diverse areas including cycle and performance analysis,
       heat transfer analysis, linear and nonlinear stress analysis, and mission
       analysis. Building on the proven techniques already available in these
       fields, the new methods developed will be integrated into computer codes
       to provide an accurate, efficient and unified approach to analyzing

MORE   ENTER:P
       DISPLAY 85N27261/2
combustor burner liners, hollow air-cooled turbine blades and air-cooled
turbine vanes. For these components, the methods developed will predict
temperature, deformation, stress and strain histories throughout a
complete flight mission.

1. Report No. CR-174765	2. Government Accession No.	3. Recipient's Catalog No.
4. Title and Subtitle Component-Specific Modeling		5. Report Date
		6. Performing Organization Code
7. Author(s) R.L. McKnight		8. Performing Organization Report No.
		10. Work Unit No.
9. Performing Organization Name and Address General Electric Company Aircraft Engine Business Group Advanced Technology Programs Dept. Cincinnati, OH 45215		11. Contract or Grant No. NAS3-23687
		13. Type of Report and Period Covered First Annual Status Report
12. Sponsoring Agency Name and Address National Aeronautics & Space Administration Washington, D.C. 20546		14. Sponsoring Agency Code RTOP 533-04-1A

15. Supplementary Notes

16. Abstract

The overall objective of this program is to develop and verify a series of interdisciplinary modeling and analysis techniques that have been specialized to address three specific hot section components. These techniques will incorporate data as well as theoretical methods from many diverse areas including cycle and performance analysis, heat transfer analysis, linear and nonlinear stress analysis, and mission analysis. Building on the proven techniques already available in these fields, the new methods developed through this contract will be integrated into computer codes to provide an accurate, efficient and unified approach to analyzing combustor burner liners, hollow air-cooled turbine blades and air-cooled turbine vanes. For these components, the methods developed will predict temperature, deformation, stress and strain histories throughout a complete flight mission.

17. Key Words (Suggested by Author(s)) Finite element analysis, structural analysis, mission modeling, nonlinear analysis	18. Distribution Statement Unclassified, Unlimited

19. Security Classif. (of this report) Unclassified	20. Security Classif. (of this page) Unclassified	21. No. of Pages 108	22. Price*

NASA-C-168 (Rev. 10-75)

N85-27261 #
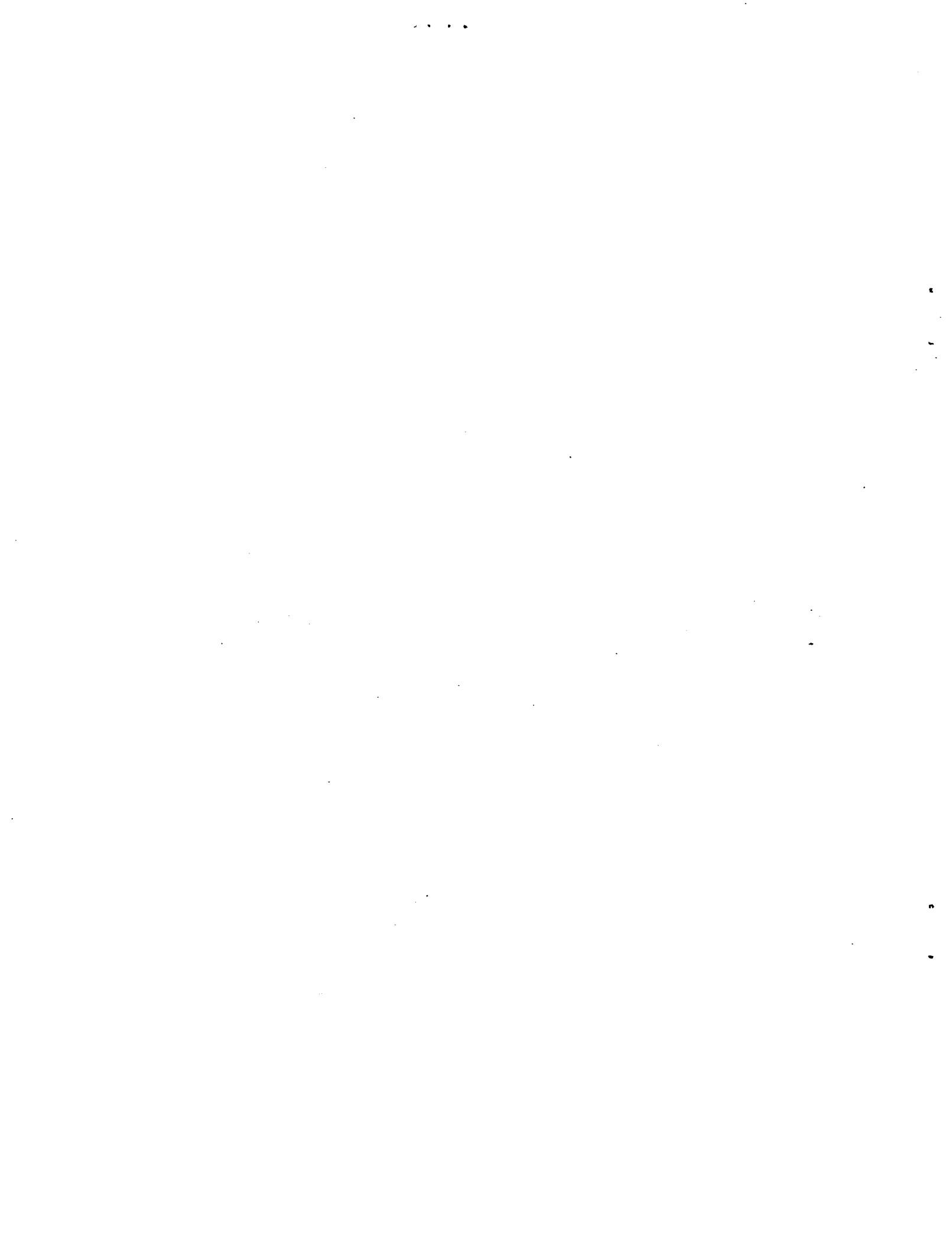
FOREWORD

This report has been prepared to expedite early domestic dissemination of the information generated under the contract. The data and conclusions must be considered preliminary and subject to change as further progress is made on this program. This is a progress report covering the work done during the second 12 months of the contract, and it is not a final report.

TABLE OF CONTENTS

LIST OF ILLUSTRATIONS

LIST OF TABLES

1.0 INTRODUCTION

Modern jet engine design imposes extremely high loadings and temperatures on hot section components. Fuel costs dictate that minimum weight components be used wherever possible. In order to satisfy these two criteria, designers are turning toward improved materials and innovative designs. Along with these approaches, they also must have more accurate, more economical, and more comprehensive analytical methods.

Numerous analytical methods are available that can, in principle, handle any problem that might arise. However, the time and expense required to produce acceptable solutions is often excessive. This program addresses this problem by setting out a plan to create specialized software packages which will provide the necessary answers in an efficient, user-oriented, stream-lined fashion. Separate component-specific models will be created for burner liners, turbine blades, and turbine vanes using fundamental data from many technical areas. The methods developed will be simple to execute, but they will not be simple in concept. The problem is extremely complex and only by a thorough understanding of the details can the important technical approaches be extracted. The packaging of these interdisciplinary approaches into a total system must conform to the modular requirements for useful computer programs.

The overall objective of this program is to develop and verify a series of interdisciplinary modeling and analysis techniques that have been specialized to address three specific hot section components. These techniques will incorporate data as well as theoretical methods from many diverse areas including cycle and performance analysis, heat transfer analysis, linear and nonlinear stress analysis, and mission analysis. Building on the proven techniques already available in these fields, the new methods developed through this contract will be integrated to provide an accurate, efficient, and unified approach to analyzing combustor burner liners, hollow air-cooled turbine blades, and air-cooled turbine vanes. For these components, the methods developed will predict temperature, deformation, stress, and strain histories throughout a complete flight mission.

This program, to a great extent, draws on prior experience. This base of experience is invaluable for understanding the highly complex intersctions among all the different technical disciplines as well as for estimating the importance of different engine parameters. In particular, there are four specific areas in which experience is especially beneficial.

First, with the recent increases in fuel costs, greater emphasis has been placed on more accurate solutions for stresses and strains in order to understand and improve the durability and life of hot section components; Conventional linear elastic analyses are no longer sufficient instead, they now provide the boundary values for more refined creep and plasticity calculations. These nonlinear analyses are now performed routinely as part of the design process at General Electric. This extensive experience with these plasticity and creep methods contributes directly to developing component specific models.

Second, advances in 3-D modeling capability are being achieved by the concepts developed under the NASA-supported ESMOSS program. ESMOSS concepts provide the basis to develop an efficient modeling system for geometric and discretized models of engine components.

Third, the NASA-funded Burner Liner Thermal/Structural Load Modeling Program contributes strong support to this program. The specific area addressed, transfer of data from a 3-D heat transfer analysis model to a 3-D stress analysis model, will provide the background and framework for the data interpolation required for all thermomechanical models in this contract.

Fourth, over the past 10 years General Electric has developed internally a family of computer programs: LASTS, OPSEV, and HOTSAM; These programs all have the common thread of using selected points from cycle data, heat transfer, and stress analyses and a decomposition/synthesis approach to produce accurate values of temperature, stress, and strain throughout a mission. These programs are totally consistent with the overall objectives of this program, and represent a proven technology base upon which the component specific models are being developed. Significant advances being made are the inclusion of nonlinear effects and the introduction of improved modeling and data transfer techniques.

The program is organized into nine tasks which can logically be separated into two broadly parallel activities (Figure 1). On the right of Figure 1 we have the Component Specific Thermomechanical Load Mission Modeling path. Along this path a Decomposition/Synthesis approach is being taken. In broad terms, methods are being developed to generate approximate numerical models for the engine cycle and the aerodynamic and heat transfer analyses needed to provide the input conditions for hot parts stress and life analysis.

The left path, Component Specific Structural Modeling provides the tools to develop and analyze finite element nonlinear stress analysis models of combustor liners and turbine blades and vanes. These two paths are shown in more detail in Figures 2 and 3.

Software Development, Task IV, consists of planning and writing the computer programs for both paths, with the necessary interconnections, using a structured, top down approach.

In the Thermomechanical Load Mission Modeling portion of the program (Figure 2), we are developing in Task III a Thermodynamic Engine Model which generates the engine internal flow variables for any point on the operating mission. The method for doing this is described below. Task V is developing techniques to decompose flight missions into characteristic mission segments. In Task VII a Thermomechanical Mission Model is being developed. This uses the flow variables from the Thermodynamic Model to determine metal temperature and pressure distributions for a representative combustor liner and turbine blade and vane.

Individual tasks for the Structural Modeling activity are shown in Figure 3. The requirements of Software Design, Task II, have been factored into Task VI, the evaluation of the structural analysis methods which were selected for evaluation in Task I. Task VIII provides the capability for structurally modeling current state-of-the-art combustor liners and hollow turbine blades and vanes, given the defining dimensional parameters. These parameters will be chosen to facilitate parametric studies.

The component specific models are being developed in two steps. In the first a geometric modell is defined. In the application of the Component

```
                    ┌─────────────────┐
                    │    Task I -     │
                    │     Survey      │
                    └─────────────────┘
                             │
        ┌────────────────────┼────────────────────┐
        ▼                    ▼                    ▼
┌───────────────┐  ┌─────────────────┐  ┌─────────────────────┐
│  Component-   │  │    Software     │  │    Component-       │
│   Specific    │  │   Development   │  │     Specific        │
│  Structural   │  │                 │  │  Thermomechanical   │
│   Modeling    │  │   ─────────     │  │   Load Mission      │
│               │  │                 │  │     Modeling        │
│   ─────────   │  │    Task IV      │  │                     │
│               │  └─────────────────┘  │   ─────────         │
│   Task II     │                       │                     │
│   Task VI     │                       │    Task III         │
│   Task VIII   │                       │    Task V           │
│               │                       │    Task VII         │
└───────────────┘                       └─────────────────────┘
        │                                          │
        └────────────────────┬─────────────────────┘
                             ▼
                    ┌─────────────────┐
                    │   Reporting     │
                    │    Task IX      │
                    └─────────────────┘
```
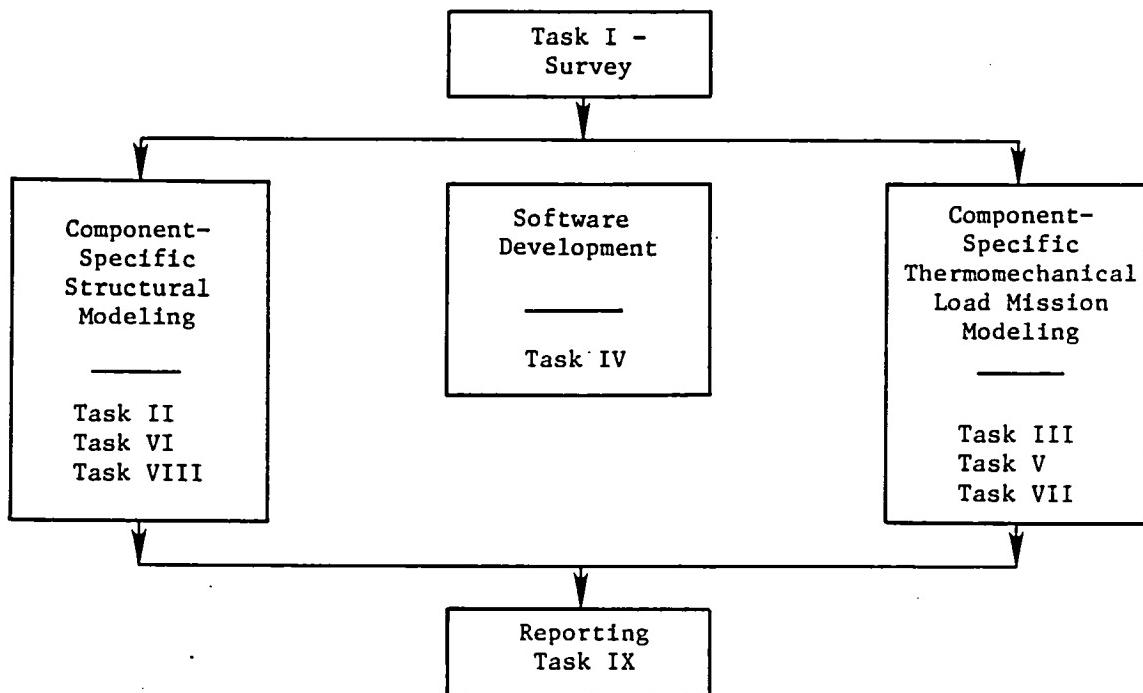
Figure 1.   Component Specific Modeling Base Program.

```
┌─────────────────┐                    ┌─────────────────┐
│    Task III      │                   │    Task V        │
│                 │                    │                 │
│  Thermodynamic  │                    │  Mission Model  │
│  Engine Model   │                    │  Decomposition  │
└─────────────────┘                    └─────────────────┘
        │                                      │
        │        ┌─────────────────────┐       │
        │        │     Task VII        │       │
        │        │                     │       │
        └───────▶│ Thermomechanical Load│      │
                 │   Mission Model      │      │
                 │   Development        │      │
                 │ ─ ─ ─ ─ ─ ─ ─ ─ ─ ─ │      │
                 │Decomposition/Synthesis│◀─────┘
                 │   Capability         │
                 │ ─ ─ ─ ─ ─ ─ ─ ─ ─ ─ │
                 │   Verification       │
                 └─────────────────────┘
```
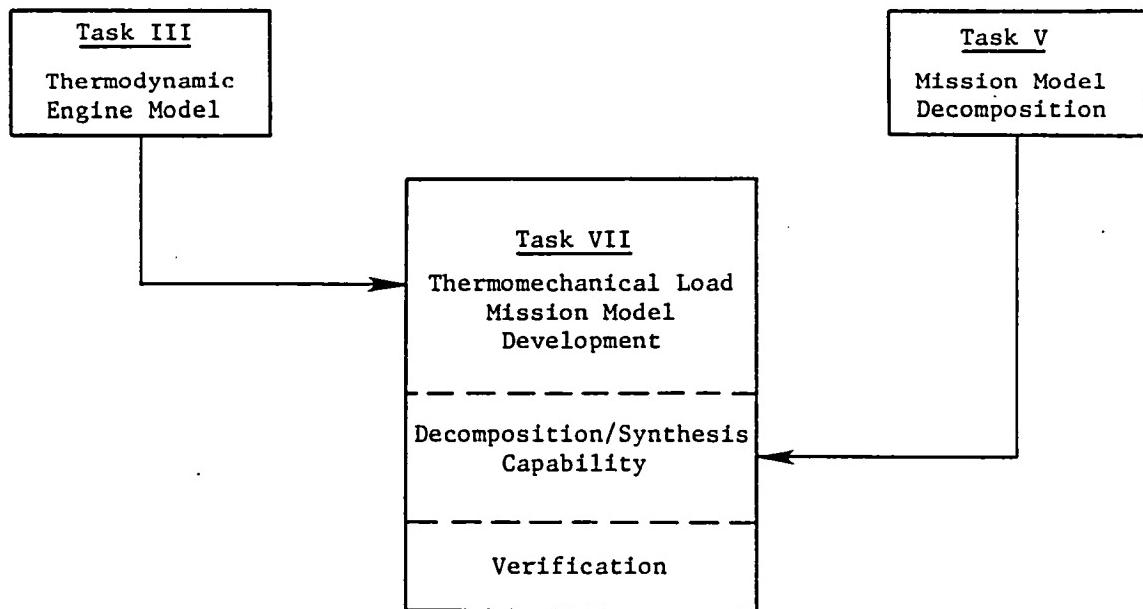
Figure 2.   Component Specific Thermomechanical Load
            Mission Modeling.

4
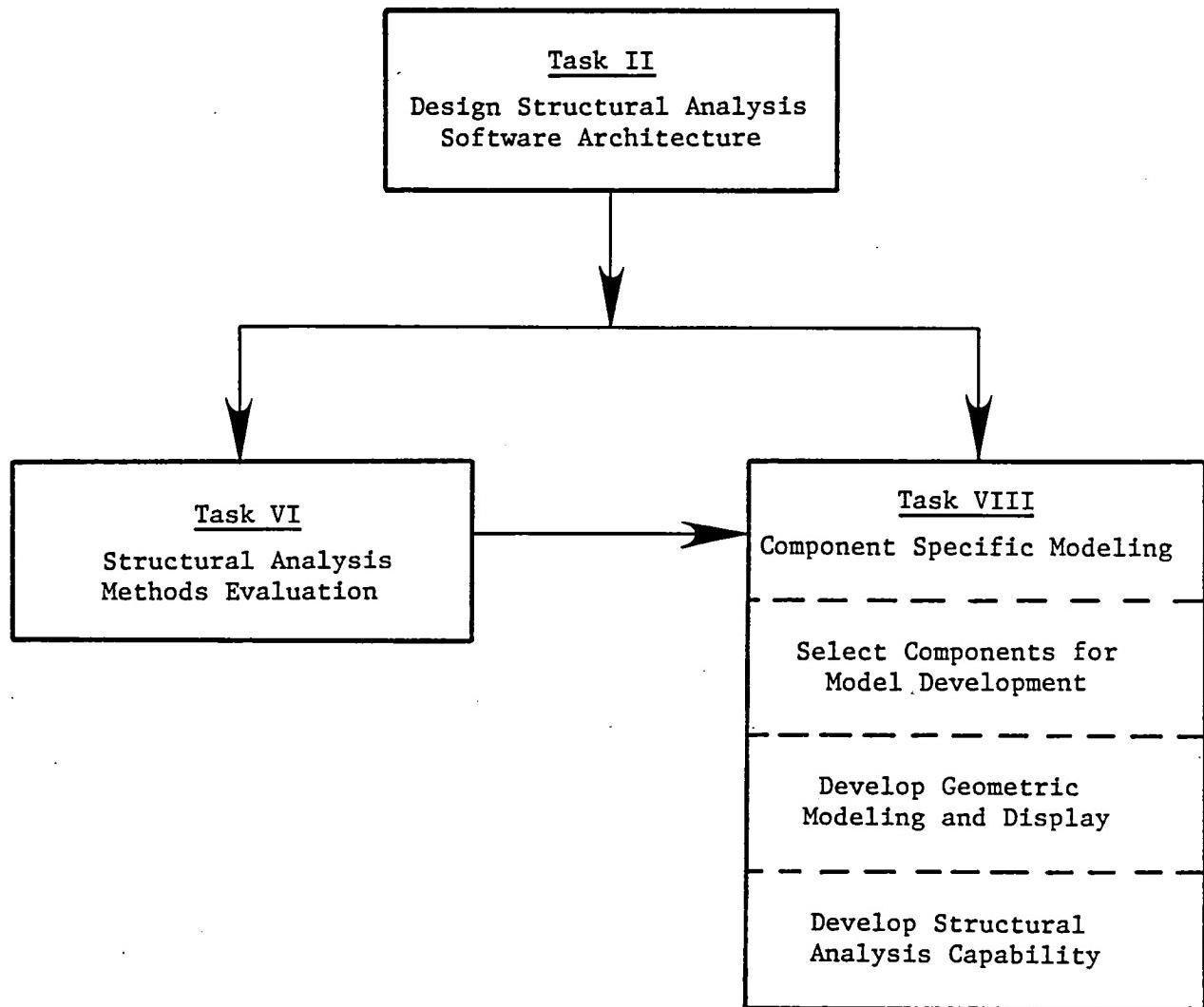
Figure 3.   Component Specific Structural Modeling.

Specific Modeling Program these data are then transferred to the Thermomechanical Load Mission Model to provide the geometry for determining component pressures and temperatures. Thus, a data transfer link is being developed to do this in Task IV, Software Development. The capability for generating from the geometric model a discretized, finite element model is also a part of Task VIII. At this point another link between the two paths is needed to transfer the component temperatures and pressures from the Thermomechanical Load Model to the finite element model, interpolating the data as needed to define nodal temperatures and pressures. This also is being completed in Task IV.

2.0 TECHNICAL PROGRESS

2.1 TASK I - LITERATURE SURVEY

The first task of this program was to perform a literature survey of available methods, techniques, and solution strategies that can be used to geometrically model, display, and structurally analyze burner liner, turbine blades and vanes. NTIS, NASA, DTIC, and internal General Electric Company documents were searched. As a result of this survey, 85 papers and 8 books and procedures were discovered with pertinent information. As a result of evaluating this information, recommendations were made on the technology to be incorporated into the base and advanced portions of this program to the NASA Program Manager. The NASA Program Manager approved the following program content:

GEOMETRIC SHAPE GEOMETRIES

Base Program

- ESMOSS - considered commercial and university codes

Advanced Program

- ESMOSS

LINEAR AND NONLINEAR FINITE ELEMENT METHODS

Base Program

- 8-, 16-, and 20-noded isoparametric elements - considered beams, plates, and shells

Advanced Program

- Supplements from 3D inelastic program
- Decomposition and synthesis methods

SPECIALTY ELEMENTS

Base Program

- None - considered slave, large FEM, hybrid, embedded hole

Advanced Program

- Supplements from 3D inelastic program
- Decomposition and synthesis methods

NON-FINITE ELEMENT METHODS

Base Program

- None - considered finite difference, boundary integral

Advanced Program

- Supplements from 3D inelastic program
- Decomposition and synthesis methods

STIFFNESS AND MASS MATRIX ASSEMBLY TECHNIQUES

Base Program

- Element level algorithm

Advanced Program

- Frontal solution methods
- Supplements from 3D inelastic program

MATERIAL BEHAVIOR CHARACTERISTICS

Base Program	Elastic	Inelastic
- Isotropic	X	X
- Orthotropic	X	
- Temperature-dependent	X	X
- Cyclic Plasticity		X
- Creep		X

Advanced Program	Elastic	Inelastic
● Viscoplasticity		X
● Anisotropic	X	X

SOLUTION TECHNIQUE

Base Program

- SESOL (sparse matrix solver, skyline storage scheme)

Advanced Program

- Vectorized COLSOL (active column solver, compacted storage)
- Frontal solution methods

LINEAR AND NONLINEAR SUBSTRUCTURES

Base Program

- Superelements
- Conventional finite element

Advanced Program

- Multilevel substructuring

SOLUTION STRATEGIES

Base Program

- Dynamic time incrementation
- Dynamic load incrementation
- Solution acceleration schemes - Aitkens extrapolation, Over-relaxation scheme

Advanced Program

- Supplements from 3D inelastic program
- Padovan's techniques

CENTRIFUGAL STIFFNESS MATRIX FORMULATION

Base Program

- Two-step method

Advanced Program

- Large deformation method (updated Lagrangian)

EIGENVALUE AND EIGENVECTOR EXTRACTION

Base Program

- Subspace iteration
- Master nodes

Advanced Program

- Lanczos method

AUTOMATIC DISCRETIZATION PROCEDURE

Base Program

- ESMOSS
- Master regions - considered commercial and university codes

Advanced Program

- ESMOSS

REMESHING AND GRID OPTIMIZATION

Base Program

- Progressive subdivision
- Constraint equations

Advanced Program

- Total realignment
- Element upgrade

DATA DISPLAY

Base Program

● ESMOSS

Advanced Program

● NASA in-house

PROVEN DATA SETS

Stress-Strain Decomposition and Synthesis Techniques

● Turbine blade nonlinear structural life analysis
● Multiaxial cyclic thermoplasticity analysis with Besseling's sub-volume method

Component Temperature and Pressure Synthesis Techniques

● CF6-50 rolled ring combustor
● CF6-80A high pressure sector test
● CF6-6 single shank turbine blade
● CF6-80 and 80A turbine vanes
● Thermodynamic engine model
● Thermomechanical loads model - build on in-house expertise: OPSEV, OPSEV-A, LASTS, HOTSAM

Survey of 3-D Heat Transfer Codes

● Used survey results from "burner liner thermal structural load modeling"
● Use internal THT-D program for development work
● Thermal loads transfer module uses MARC or SINDA available to NASA

2.2 TASK II - DESIGN OF STRUCTURAL ANALYSIS SOFTWARE ARCHITECTURE

The software architecture was designed using the methodology developed on the ESMOSS program. This development was carried out by a team whose members provided expertise in all of the pertinent areas. The architecture approved by the NASA Program Manager is contained in Appendix A. In addition to the program architecture, the preprocessor and postprocessor attributes are defined.

2.3 TASK III - THERMODYNAMIC ENGINE MODEL

The Thermodynamic Engine Model (TDE) was completed and approved by the NASA Program Manager in 1983[1].

2.4 TASK IV - SOFTWARE DEVELOPMENT

This task consists of planning and writing the computer codes for both paths of this program with the necessary interconnectors. As such, it is a continuous and ongoing effort with the substance being covered under the other task headings.

2.5 TASK V - MISSION MODEL DEVELOPMENT

2.5.1 Component Temperature and Pressure Decomposition and Synthesis

Based on our efforts in 1983 and the developments described below, a Component Temperature and Pressure Decomposition and Synthesis Plan was approved by the NASA Program Manager. This plan is outlined in Appendix B.

2.5.1.1 Combustor Liner Temperature and Pressure Decomposition and Synthesis

An expression for the temperature gradient through the material thickness can be derived from the cooling effectiveness, the compressor discharge temperature, and the combustor exit temperature. The temperature gradient through the material can be calculated from

---

[1] R.L. McKnight, "Component - Specific Modeling," Annual Status Report, NAS3-23687, 1983.

12

$$T_H - T_C = \frac{Q/A^t}{K} \qquad\qquad (1)$$

where

T_H = Hot side metal temperature, $^\circ$ F

T_C = Cold side metal temperature, $^\circ$ F

Q/A = Heat flux through material $\frac{Btu}{hr\text{-}ft^2}$

t = Material thickness, ft

K = Metal conductivity $\frac{Btu}{ft^2\text{-}hr\text{-}^\circ F}$

The heat flux can be calculated from

$$Q/A = (h_c + hr)(T_C - T_3) \qquad\qquad (2)$$

or it is proportional to $(T_{Liner} - T_3$

$$Q/A = (h_c + hr)(T_{Liner} - T_3) \qquad\qquad (3)$$

where

h_c = Convection heat transfer coefficient $Btu/hr\text{-}ft^2\text{-}^\circ$ F

hr = Equivalent heat transfer coefficient for radiation to casing $Btu/hr\text{-}ft^2\text{-}^\circ$ F

T_{Liner} = Bulk liner temperature, $^\circ$ F

Substituting the heat flux expression into the gradient equation (1) gives

$$\frac{T_H - T_C}{(T_{Liner} - T_3)} \ \alpha \ \frac{(h_c + hr)t}{k} \qquad\qquad (4)$$

using the equation for cooling effectiveness,

$$y_c = \frac{T_4 - T_{Liner}}{T_4 - T_3} \qquad\qquad (5)$$

An equation for $(T_{Liner} - T_3)$ can be written as follows:

$$(T_{Liner} - T_3) = (1 - y_c) T_y + (y_c - 1) T_3 \qquad (6)$$

Substituting Equation 6 into the expression (4) gives

$$\frac{T_H - T_3}{(1 - y_c) T_4 + (y_c - 1) T_3} \; \alpha \; \frac{(h_c + hr)t}{k} \qquad (7)$$

The convection term, h_c, varies with pressure and thus the gradient through the material thickness should be correlated with pressure.

A THTD analysis was done at several pressure conditions and the calculated temperature gradients were plotted vs P3 for several axial locations and the results are shown in Figure 4. The locations and coordinates are shown in Figure 5. As shown in the figure, the gradient data are correlated with pressure. The constants m and b in the equation

$$\frac{T_H - T_C}{T_{Liner} - T_3} = \frac{T_H - T_C}{(1 - y_c) T_y + (h_c - 1) T_3} = mP_3 + b \qquad (8)$$

are tabulated in Table I.

Table I. Linear Fit Constants for Equation (8).

Location	X, inches	m	b
1	0.094	12.3×10^{-5}	0.100
2	0.438	14.1×10^{-5}	0.061
3	0.654	9.0×10^{-5}	0.061
4	0.854	10.7×10^{-5}	0.092
5	1.114	28.1×10^{-5}	0.168
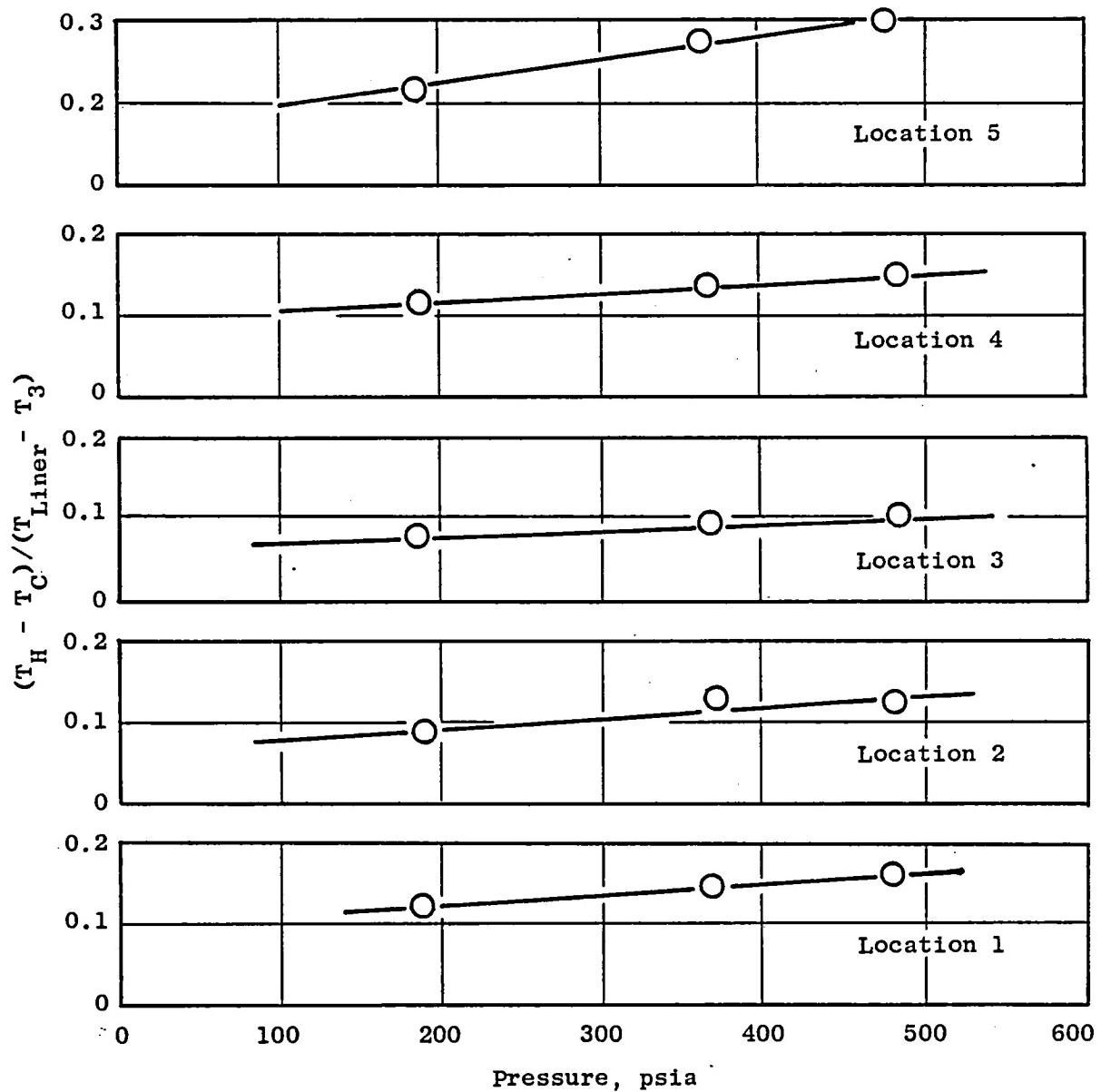
Figure 4. Material Thickness Temperature Gradient.
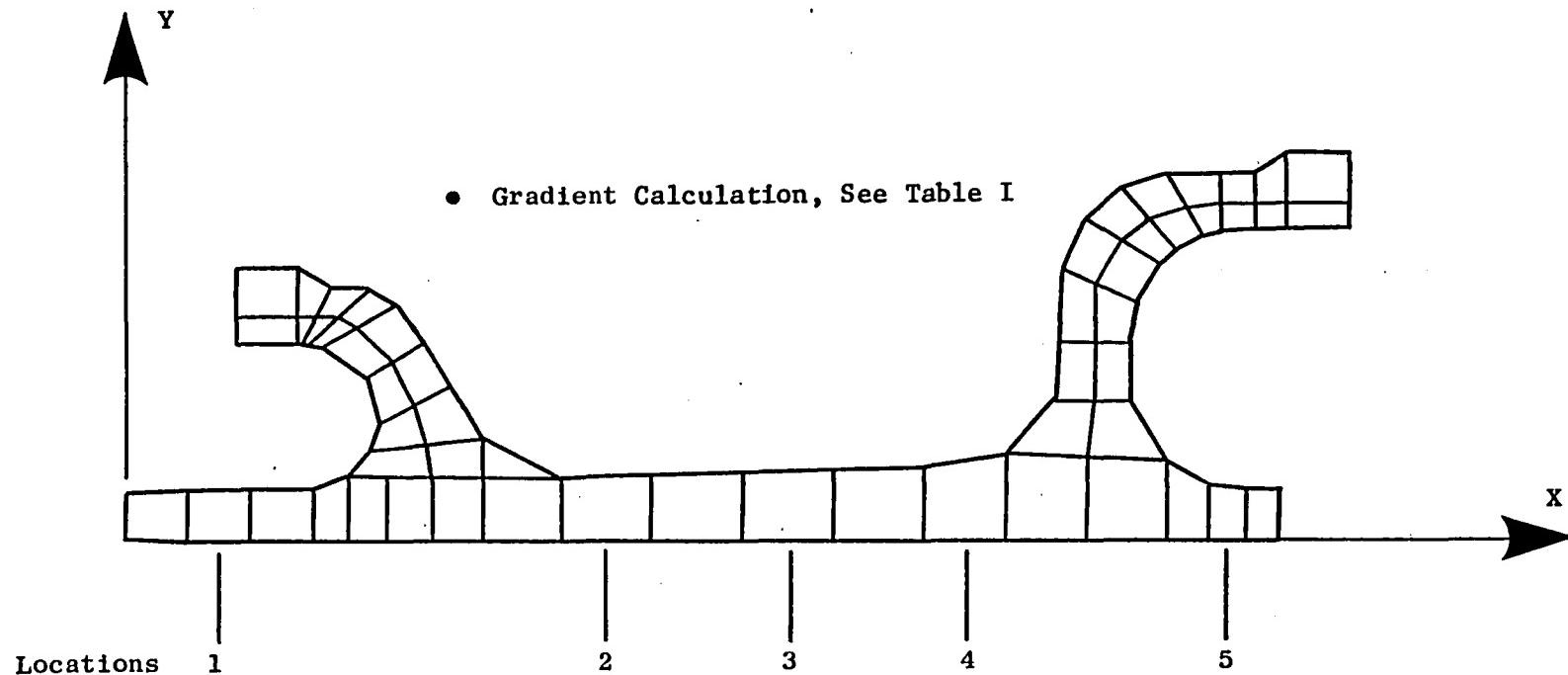
Figure 5. Coordinate System for Cooling Effectiveness.

Given the combustor exit temperature, T_y, the compressor discharge pressure, P_3, and the compressor discharge temperature, T_3, the temperature gradient through material thickness can be calculated from Equation 8 using the cooling effectiveness and the constants from Table I.

2.5.1.2 Turbine Blade and Vane Temperature and Pressure Decomposition and Synthesis

The spanwise distribution of overall local cooling effectiveness has been completed for the CF6-50 and B-1B NESIP (similar to CFM56-2) Stage 1 HP turbine blades; The results are compared in the attached Figure 6 which is based on THTD runs for 15, 50, and 77 % of blade span. The ratio of $\eta_{c,local}/\eta_{c,50\%}$ is unity by definition at the 50% span location. At the other two spans, the η_c ratio is identified for each of the sixteen points around the airfoil. The curves have been terminated at the locus or the average η_c ratio for each span.

For the CF6-50 blade, this procedure defined a single curve for the pressure and suction surfaces. However, the B-1B blade is better represented by a two-branch curve at the 77% span (Figure 7). We have reviewed the two blade designs for possible explanations of this characteristic. There is no obvious single cause. It is undoubtedly the combined result of configuration, coolant circuitry, the application of film cooling and variations in gas-side heat-transfer coefficients.

It appears best to allow for incorporating separate curves for the pressure and suction surfaces, with freedom to input these curves for different blade designs. This is probably the thing to do for the B-1B blade, defining a separate curve for the pressure surface between Points 2 and 6. Points 7 and 8 appear to be represented quite well by the curve for the suction surface. Using the suction surface curve for Points 2 through 6 could overpredict the temperatures by about 135° F at the 77% span.

2.5.2 Stress-Strain Decomposition and Synthesis

The decomposition and synthesis of stresses, strains, and deformations is technically the most challenging portion of this program. It requires

HPT Stage 1 Blade

$Wc = 2.95\% \ W25$

$$\eta = \frac{T_{41} - T_M}{T_{41} - T_3}$$

$T_{41} = 2618°\ F$ } at Takeoff
$T_3 = 1095°\ F$ }

$\dfrac{\eta}{\eta_{50\%}}$
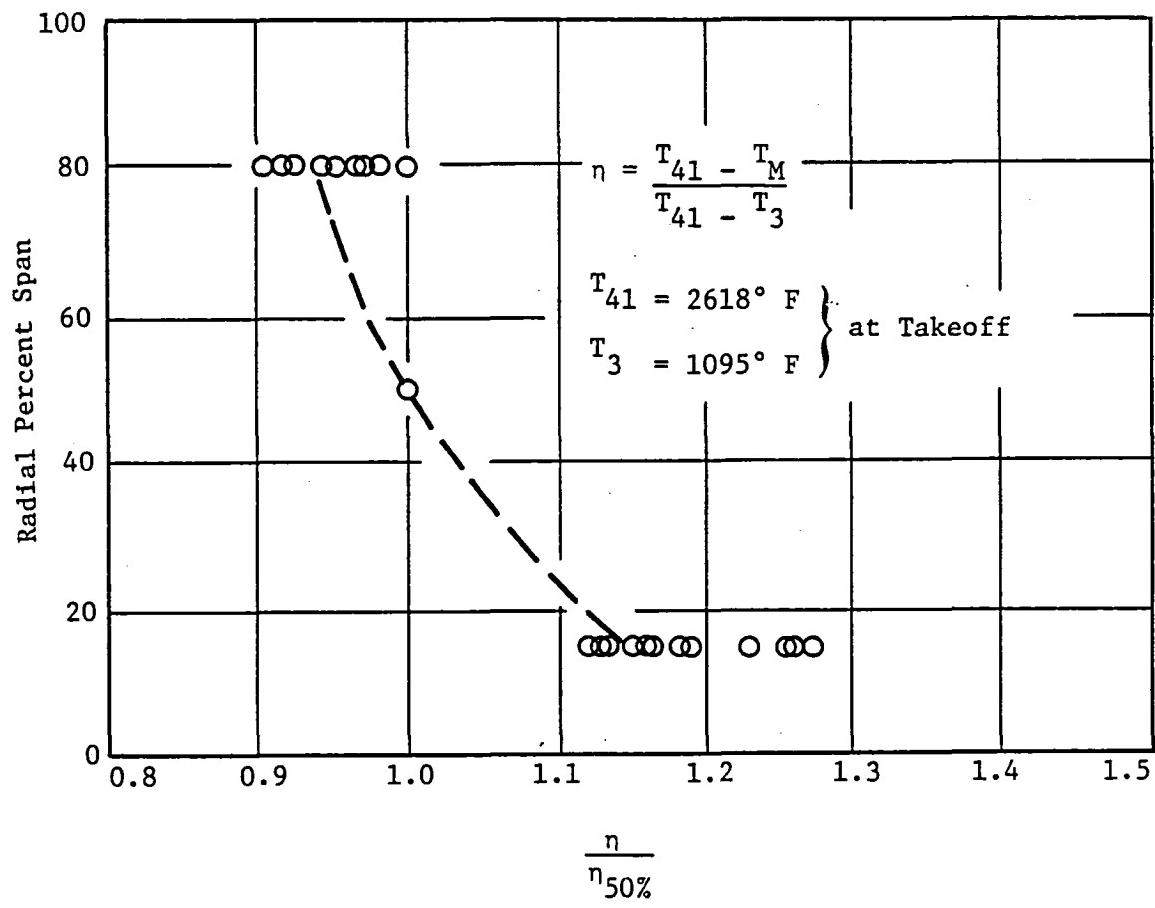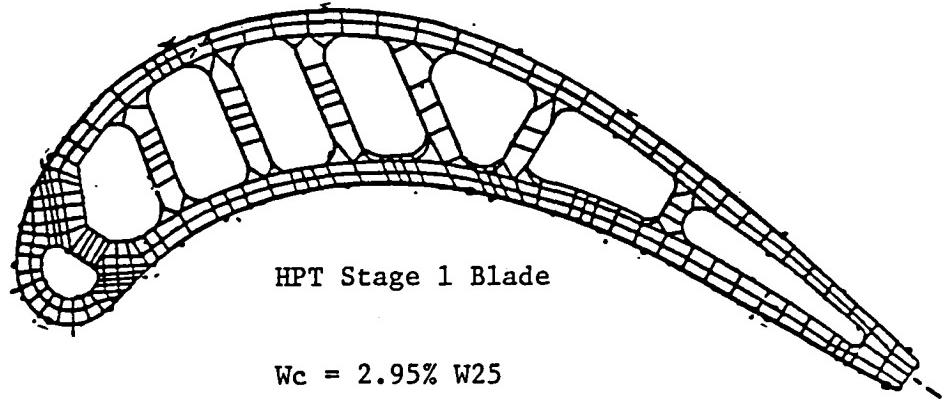
Figure 6.   HPT Stage 1 Blade Cooling Effectiveness.
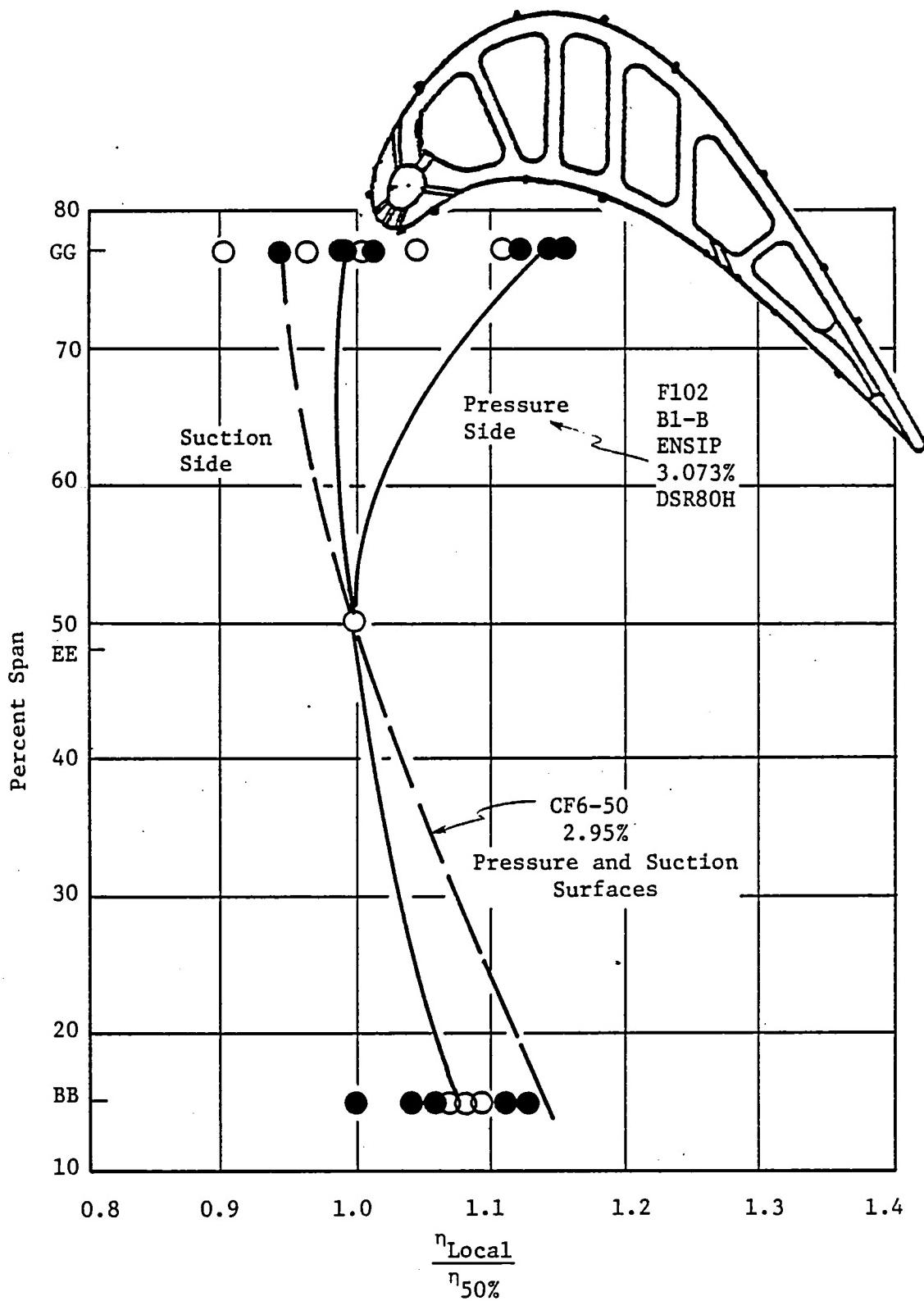
Figure 7. F102 B1-B HPT Blade Cooling Effectiveness.

innovative methods to produce usable results for burner liners, turbine blades, and vanes. Thus, our goal under this task has been to compile a library of possible decomposition and synthesis techniques and to assess their validity. Among the techniques being considered are the following:

- Assume that the structure remains totally elastic at all stress levels and do the decomposition and synthesis based on an elastic "pseudostress."

- Assume that the structure is deformation-controlled (strain range invariance). The first level of decomposition and synthesis would be based on deformations (total strains). A second level of synthesis could then introduce the effects of plasticity and creep by using the material response characteristics to partition the total strain into elastic, plastic, and creep components.

- Assume that the structure is load-controlled (stress invariance). Decomposition and a first level of synthesis would be based on load terms reflecting the centrifugal loadings and the temperature and pressure distributions. A second level of synthesis could then introduce the effects of plasticity and creep by using the material response characteristics to determine the elastic, plastic, and creep strains that would be caused by the total load.

- Use simplified nonlinear finite element modeling to decompose and synthesize the stresses, strains, and deformations in terms of the set of analyzed mission components. These simplified models could be either one 2D or 3D element or a nonlinear substructure. These models could use boundary conditons from the detailed analysis or they could be run as an intimate part of the detailed analysis.

- Apply the method of superposition for the decomposition and sysnthesis of stresses, strains, and deformations. This method would be investigated based on the following hierarchy of calculated parameters:
  - deformations
  - strains
  - stresses

  We will determine to what degree these parameters can be decomposed and synthesized by superposing the results from the individual loading functions (temperature, pressure, rpm).

- Use linear and nonlinear interpolation of the results of a detailed analysis for decomposing and synthesizing stresses, strains, and deformations. The interpolating parameters would be second-level predicted temperatures, pressures, and rpm's.

- Form look-up tables of deformations, stresses, and strains as functions of temperatures, pressures, and rpm's. These tables would then be used to decompose and synthesize the mission cycles.

- Finally, generate from test data an empirical model relating stresses, strains, and deformations to temperatures, pressures, and rpm's. With this model, mission cycles could be decomposed and new ones synthesized.

We have developed the following general methodology:

A. Know the component in question.

B. Know the thermomechanical load cycle.

C. Know the total response of the generic component through a detailed finite element analysis.

    1. The detailed analysis will encompass total thermomechanical loading conditions.

    2. From the detailed analysis:

        a. Can locate and categorize the critical location(s) in a specific component

- User defined
- Automated procedure

        b. Categorize the stress/strain response at the critical location

- Uniaxial
- Biaxial
- Triaxial

        c. Identify the generic mode of load application

- Tension
- Compression
- Thermal
- Pressure
- RPM (Inertia)
- Strain (Displacement) Control
- Load Control

      - Consider the effect of load split and the super-position of loads

        d. Material Behavior

- Elastic
- Elastic/Plastic
- Elastic/Creep
- Elastic/Plastic/Creep
- Flow Rule and Yield Criteria Used
- Creep Formulation Used

      - Rank and/or prioritize the ability to synthesize desired material response

Decomposition Techniques:

A. Assess the methodology used to-date in our attempt to decompose the thermomechanical response history of baseline models.

B. Serving as baseline data sets are two models previously validated under other NASA programs.

1. "Turbine Blade Tip Model" NASA CR-165268

    ● Uniaxial strain cycling conditions

    ● Simulation of complex strain/temperature cycling conditions

2. "Inelastic Shingled Combustor Hot Spot" NASA CR-2278

    ● Biaxial strain cycling conditions
    ● Simulation of a very complex thermal cycle

C. Have used CYANIDE, our in-house nonlinear finite element code to analyze such models under select conditions

1. Have economically and efficiently created a preliminary data base.

2. Have resorted to use of the code because we have little or no relevant experimental data having direct application to our specific needs.

3. Have yet to determine if the content of the data base encompasses all the information we may require in the synthesis of stress, strains and deformations.

D. Are presently evaluating the concept of degenerating thermomechanical response into component parts.

1. For our situation, is the superposition of thermomechanical response a valid technique and does it suit our needs?

    ● Can the total response be characterized as a sum, a function of the sum, or some function of the individual response?

    ● To date we have concerned ourselves only with elemental results – strains in particular. Can the concept be extended to include displacements and/or stresses?

Synthesis Techniques:

A. For each specific component, construct an algorithm to compute fixed point mission-time profiles of "local" stresses, strains, and displacements. Essential to this effort is the assumption that we need only synthesize the response on the local level.

22

B. Will base the synthesis techniques on a defined set mission-segment component-station characteristics.

  • This may include the TML matrix and the characterization procedure noted in general methodology.

C. Once the response at the critical location has been characterized, the synthesis of local response can proceed along assorted paths.

  • Generate empirical relations between loads and deformation states.

  • Generate closed form solutions.

  • Perform a parallel path solution utilizing another analysis code.

D. Assemble the parameters defining local response and make them available to the user.

This year's effort in the stress/strain decomposition and synthesis techniques has focused on the development of methods to predict structural behavior in response to a defined set of loads. These methods are based on the premise that the structural response to an arbitrary set of loads can be accurately predicted, provided that the current loads are perceived as being small pertubations of the loads used in a previous analysis. We are examining the use of linear and nonlinear interpolation routines to use the information obtained from a prior analysis to synthesize current nonlinear strain response.

To circumvent the complex behavior exhibited in a two or three-dimensional analysis, it was decided to first limit ourselves to simple uniaxial conditions. For our work we would examine a uniaxial specimen under the following conditions:

1. No time-dependent material behavior

  • Total strain can be separated into elastic and plastic components

2. Consider only small inelastic and plastic components

  • Range from 0.4% to 0.6%

3. Consider a limited temperature range

  • Range from 600° F to 1200° F

4. Will examine only simple load cycles

Our in-house nonlinear finite element code was used to analyze a uniaxial model under various loading conditions; The results from the analyses that constitute our data base are tabulated and presented in Table II. Equations that express the plastic strain as a function of load and temperature were defined and are presented in Table III. These equations and linear interpolation were used to predict plastic strain response for various load cycles.

Table II. Data Base.

T/P	600	700	800	900	1000	1100	1200
Total Strains							
110	4381	4480	4580	4683	4787	4892	5000
120	4995	5101	5207	5312	5417	5521	5625
130	5630	5735	5839	5943	6057	6187	6320
140	6314	6442	6572	6705	6840	6979	7158
Plastic Strains							
110	430	468	505	542	579	615	650
120	685	724	761	795	827	855	880
130	961	993	1023	1049	1084	1132	1180
140	1296	1336	1385	1435	1485	1534	1622

Having the data base in place and the relationship for plastic strain defined, assorted load cycles could be defined to test the quality (accuracy) of the strain prediction techniques. Four load cycles are presented in Figure 8. Table IV illustrates the results obtained when the plastic strains are defined as being a function of stress. In Table V, predicted strains are those determined via our synthesis techniques and the computed strains are those strains obtained directly from our finite element code. Table VI illustrates the results obtained for cycle No. 4 when four separate methods of strain prediction are compared.

In our investigation of stress-strain decomposition and synthesis techniques we continued to use the combustor liner shingle segment model presented in Footnote 1. Noting that the thermal stress-strain response of the model is biaxial, our efforts are directed toward examining the nonlinear stress-strain behavior (or the history) of a defined critical location.

24

Table III. Plastic Strain as a Function of Temperature and Pressure.

Plastic Strain = f (Temperature)

$$\varepsilon_p = AT^B$$

Pressure (ksi)	A	B
110	9.33347E-6	0.5977902
120	6.66123E-5	0.3643609
130	1.515E-4	0.2868058
140	1.633E-4	0.3208346

Plastic Strain = (Pressure)

$$\varepsilon_p = AP^B$$

Temperature (° F)	A	B
600	2.59397E13	4.522953
700	7.35291E-13	4.317914
800	1.18710E-12	4.140312
900	4.07319E-12	3.982063
1000	7.94597E-12	3.85249
1100	1.29902E-11	3.772658
1200	1.27499E-11	3.772658

Plastic Strain = f (Temperature & Pressure)

$$\varepsilon_p = A + BT + CP$$

where,   A = 03.1091E-3

B = 3.96503E-7

C = 2.96807E-3
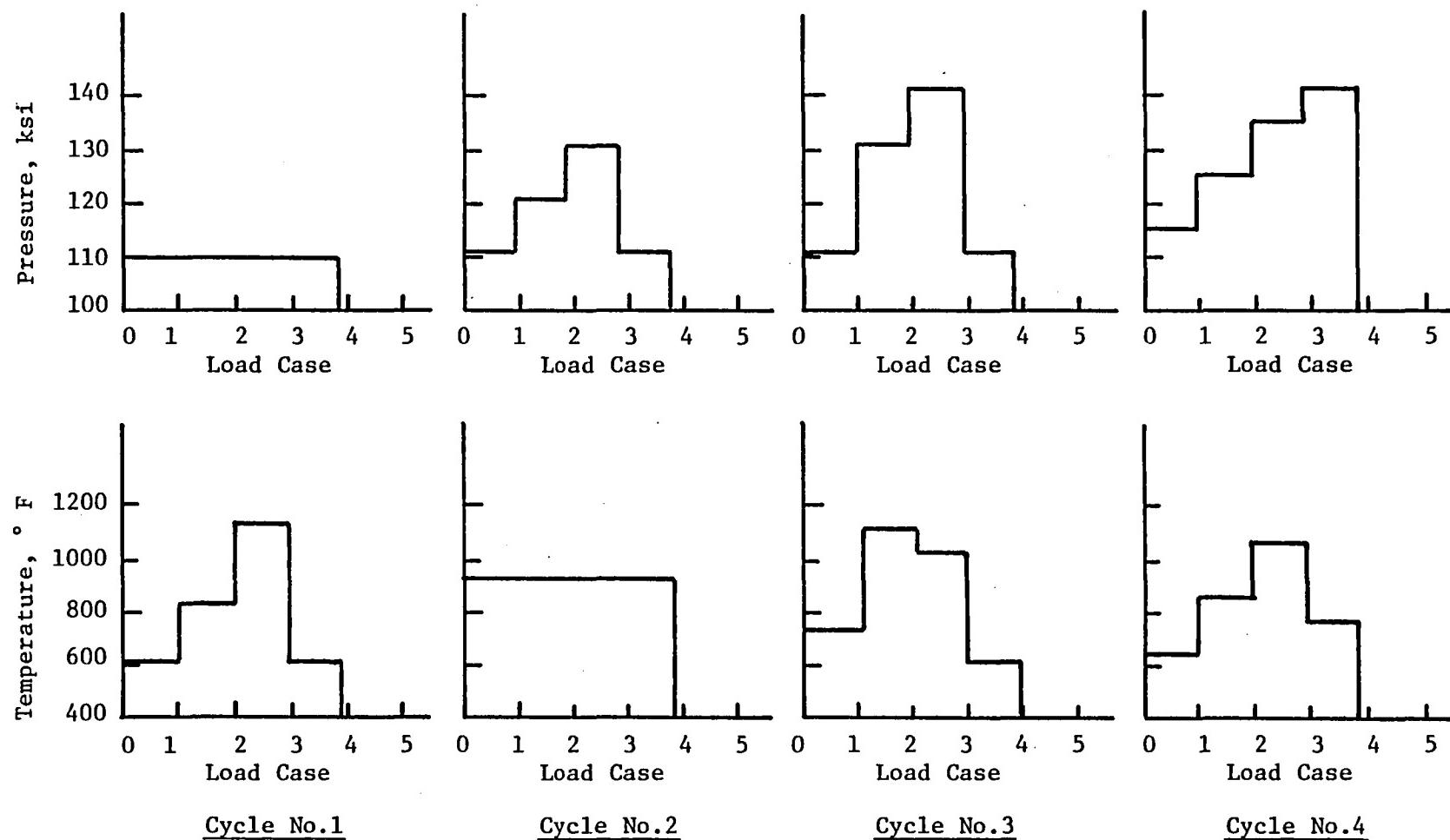
Figure 8. Load Cycles 1, 2, 3, and 4.

Table IV. Details for the Four Load Cycles.

Load Cases	Pressure, ksi	Temperature, ° F
Cycle 1		
1	110	600
1	110	800
3	110	1100
4	110	600
Cycle 2		
1	110	900
2	120	900
3	130	900
4	110	900
Cycle 3		
1	110	700
2	130	1100
3	140	1000
4	110	600
Cycle 4		
1	115	650
2	125	850
3	135	1150
4	140	750

Table V. Predicted Plastic Strain Response for the Fan Load Cycles.

Load Case	Synthesized	Computed	Percent Error
Cycle 1			
1	427	430	-0.7
2	507	505	+0.4
3	614	615	-0.2
4	614	615	-0.2
Cycle 2			
1	548	542	+1.1
2	775	795	-2.5
3	1066	1049	+1.6
4	1066	1049	+1.6
Cycle 3			
1	480	468	+2.6
2	1150	1132	+1.6
3	1472	1485	-0.9
4	1472	1485	-0.9
Cycle 4			
1	561	576	-2.6
2	892	908	-2.8
3	1356	1358	-0.1
4	1377	1360	+1.2

Table VI. Comparison of the Plastic Strain Prediction Methods.

Load Cases	Synthesized	Computed	Percent Error
• Example A - Nonlinear Response Computed as a Function of Stress			
1	561	576	-2.6
2	892	908	-1.8
3	1356	1358	-0.1
4	1377	1360	+1.2
• Example B - Nonlinear Response Computed as a Function of Temperature			
1	576	576	0
2	914	908	+0.6
3	1354	1358	-0.3
4	1366	1360	+0.4
• Example C - Nonlinear Response Computed Directly From Data Base Using Straight Linear Interpolation			
1	576	576	0
2	907	908	-0.1
3	1367	1358	+0.7
4	1366	1360	0
• Example C - Nonlinear Response Computed as a Function of Temperature/ Pressure			
1	562	576	-2.4
2	938	908	+3.3
3	1354	1358	-0.3
4	1343	1360	-1.2

The shingle combustor segment model was generated having a thermal dis-
continuity, and this hot spot is our critical location. In our current work,
we have chosen to impose elastic constraints on the region of local inelas-
ticity. The inelastic region is surrounded on all sides by purely elastic
material, and it is our intention to examine overall structural and material
behavior as the size of this critical location is altered.

In our analysis, incremental cyclic plasticiity is performed using the
Besseling subvolume method and employing the Von Mises yield criteria and the
Prandtle Ruess flow rule. A strain-hardening creep law equation of the
following form is used to describe the creep response of the material.

$$\varepsilon_c = k\sigma^n t^m + q\sigma^r t$$

where the constants m, n, k, q and r are material and temperature dependent
creep coefficients.

It is our desire to determine if the size of the nonlinear region has
significant effect on our stress-strain decomposition and synthesis tech-
niques. Reduction in the number of nonlinear elements in the model can pro-
duce significant savings in computational costs associated with a nonlinear
analysis. For such an investigation the combustor shingle model was run for
two separate analysis conditions. One being that the inelastic region is
defined by eight elements and the other being that the inelastic region is
defined by a single element. These two test conditions were each run three
separate times to separate the effects of creep and plasticity.

The shingle segment is shown in Figure 9 and modeled as illustrated in
Figure 10. The thermal condition of the combustor shingle at peak temperature
is shown in Figure 11(a) and the thermal cycle at the center of the hot spot
is presented in Figure 11(b). The hot spot encompasses 12 elements with 1
element (No. 99) exhibiting the maximum nonlinear material behavior (or total
strain response).

The baseline condition for the current model was contained in NASA
CP-2271. The baseline case represents the condition when all elements in the
model are capable of nonlinear material behavior. Noting that we treated the
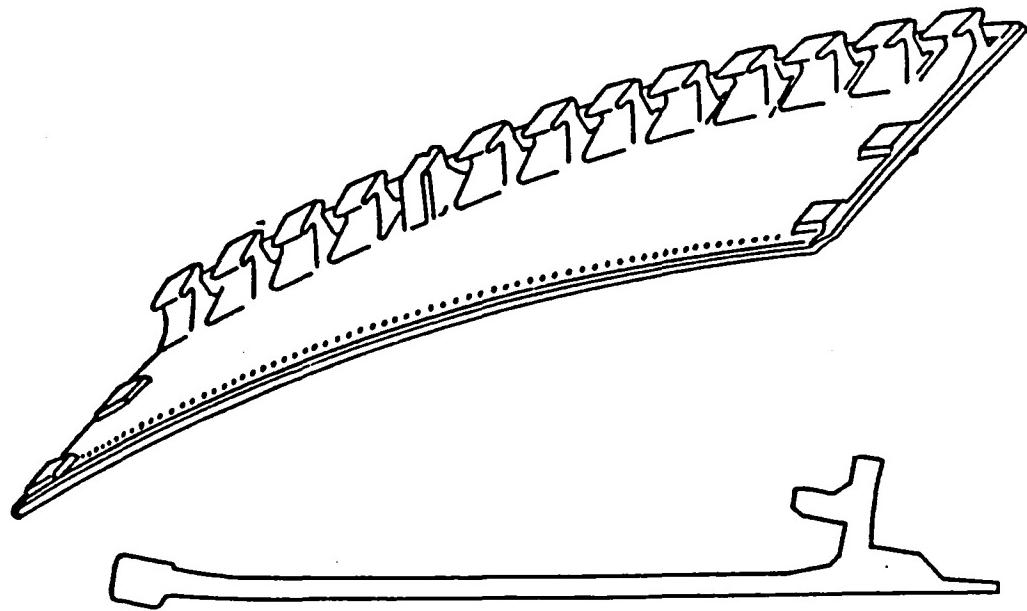
Figure 9. Shingle Segment.

Figure 10. CYANIDE Model.

Solid Line – Distribution Through Center
of Hot Spot
Dashed Line – Normal Distribution

(a)

SHINGLE HOT SPOT R80 (HSR80)
LOAD CASE   5
TEMPERATURE   START   1000.000 INCR   50.000
CYANIDE ANALYSIS

(b)
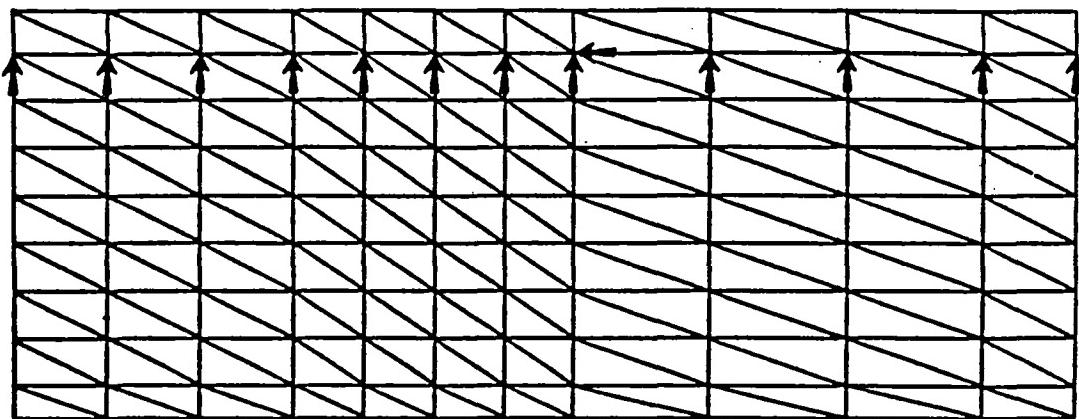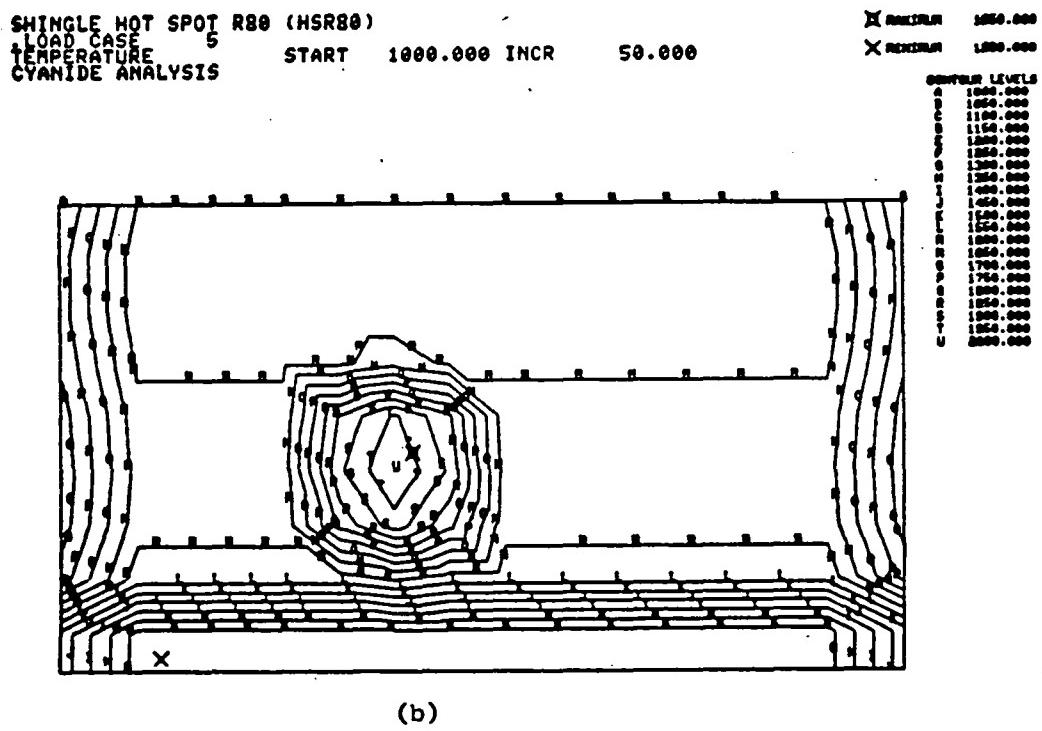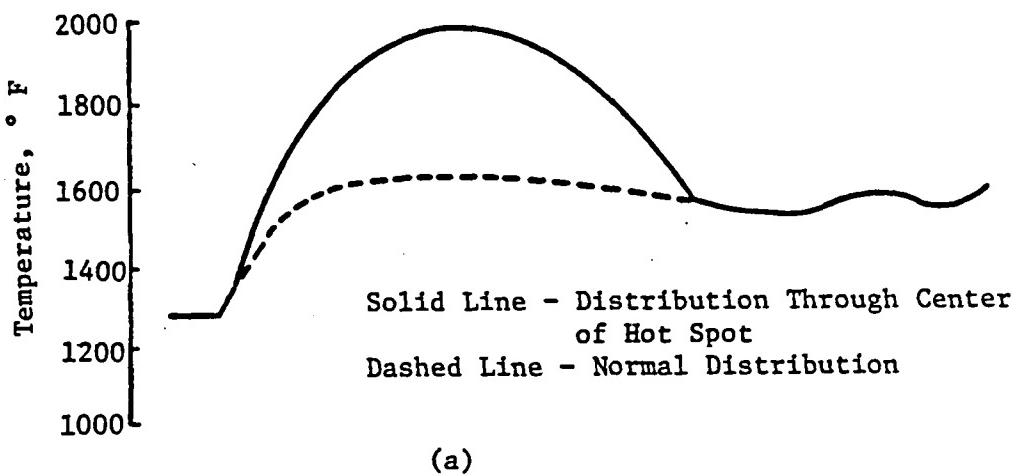
Figure 11.   Temperature Distribution on Shingle at Peak Condition.

inelastic region as being one of eight elements in size and that the defined critical element denotes behavior of the model, we can observe the effects of material nonlinearity. Tables VII through XII give the results at the critical element for the associated test conditions.

Case 1: Baseline - All elements may be inelastic.

Case 2: Inelastic region is eight elements in size: Elements 75-78, 97-100 (See Figure 12).

Case 3: Inelastic region is one element in size: Element 99 (See Figure 12).

It can be observed that when compared to the baseline case, original model behavior is best approximated when the inelastic region is eight elements in size.

In support of the functional decomposition techniques, we investigated the influence of mechanical loads on our baseline models. The baseline models are those presented in NASA CR-165268 and NASA CP-2271. Tables XIII and XIV give pertinent data pertaining to the superposition of the mechanical loads. Simple pressure loads were sued for such purposes.

In reference to Table XIII, the turbine blade tip model:

D = Original model with imposed displacement boundary conditions.

P = Original model with simple pressure load (8000 psi).

DP = Original model with imposed displacement boundary conditions and simple pressure load.

In reference to Table XIV, the shingle combustor model:

E = Elastic only

ED = Elastic/Plastic

EPC = Elastic/Plastic/Creep

EPCP = Elastic/plastic/Creep With 1500 psi Pressure Load

In support of the functional decomposition and synthesis techniques, we have investigated the influence of creep time on our baseline models. Six cases were examined and are presented here. The model used was the shingle combustor model and creep times were increased from 0.05 hour to 1.0 hour.

Table VII.   Case 1 Results – R Components of Strain.

R-Total Strain

	1	2	3	4	5	6	7	8	9	10	11	12	13	14	15	16
EC	-122	-780	-978	-1184	-1963	-1113	-460	-975	-656	-633	-380	-809	-558	-544	-321	-314
EP	-123	-835	-1092	-1420	-2601	-1888	-1003	-1474	-1155	-1131	-879	-1318	-1070	-1056	-833	-826
EPC	-123	-835	-1092	-1420	-2736	-2037	-1126	-1582	-1262	-1239	-986	-1420	-1171	-1157	-934	-926

R-Plastic Strain

	1	2	3	4	5	6	7	8	9	10	11	12	13	14	15	16
EC	0	0	0	0	0	0	0	0	0	0	0	0	0	0	0	0
EP	0	-113	-208	-448	-1516	-1635	-1053	-1129	-1129	-1129	-1129	-1170	-1170	-1170	-1170	-1170
EPC	0	-113	-208	-448	-1516	-1650	-1099	-1118	-1118	-1118	-1118	-1136	-1136	-1136	-1136	-1136

R-Creep Strain

	1	2	3	4	5	6	7	8	9	10	11	12	13	14	15	16
EC	0	0	0	0	-736	-736	-736	-736	-736	-736	-736	-736	-736	-736	-736	-736
EP	0	0	0	0	0	0	0	0	0	0	0	0	0	0	0	0
EPC	0	0	0	0	-301	-301	-301	-301	-301	-301	-301	-301	-301	-301	-301	-301

Table VIII. Case 3 Results - R Components of Strain.

R-Total Strain

	1	2	3	4	5	6	7	8	9	10	11	12	13	14	15	16
EC	-122	-780	-978	-1184	-1996	-1122	-463	-982	-663	-640	-388	-819	-568	-554	-331	-327
EP	-122	-841	-1081	-1375	-2152	-1325	-469	-990	-672	-649	-396	-834	-583	-569	-346	-342
EPC	-122	-841	-1081	-1375	-2272	-1326	-551	-1069	-750	-727	-475	-906	-656	-642	-418	-414

R-Plastic Strain

	1	2	3	4	5	6	7	8	9	10	11	12	13	14	15	16
EC	0	0	0	0	0	0	0	0	0	0	0	0	0	0	0	0
EP	0	-120	-209	-402	-1107	-1190	-695	-708	-708	-708	-708	-739	-739	-739	-739	-739
EPC	0	-120	-209	-402	-1107	-879	-618	-618	-618	-618	-618	-625	-625	-625	-625	-625

R-Creep Strain

	1	2	3	4	5	6	7	8	9	10	11	12	13	14	15	16
EC	0	0	0	0	-759	-759	-759	-759	-759	-759	-759	-759	-759	-759	-759	-759
EP	0	0	0	0	0	0	0	0	0	0	0	0	0	0	0	0
EPC	0	0	0	0	-278	-278	-278	-278	-278	-278	-278	-278	-278	-278	-278	-278

Table IX. Case 2 Results - R Components of Strain.

R-Total Strain

	1	2	3	4	5	6	7	8	9	10	11	12	13	14	15	16
EC	-122	-780	-978	-1184	-2231	-1369	-712	-1227	-908	-885	-633	-1061	-811	-797	-574	-567
EP	-122	-866	-1143	-1517	-2825	-2121	-1177	-1727	-1408	-1385	-1133	-1578	-1327	-1313	-1090	-1083
EPC	-122	-866	-1143	-1517	-3088	-2492	-1473	-1997	-1680	-1657	-1405	-1841	-1591	-1597	-1354	-1346

R-Plastic Strain

	1	2	3	4	5	6	7	8	9	10	11	12	13	14	15	16
EC	0	0	0	0	0	0	0	0	0	0	0	0	0	0	0	0
EP	-	-128	-234	-480	-1702	-1849	-1268	-1352	-1352	-1346	-1352	-1402	-1402	-1402	-1402	-1402
EPC	0	-128	-234	-480	-1702	-1984	-1399	-1432	-1432	-1432	-1432	-1454	-1454	-1454	-1454	-1454

R-Creep Strain

	1	2	3	4	5	6	7	8	9	10	11	12	13	14	15	16
EC	0	0	0	0	-852	-852	-852	-852	-852	-852	-852	-852	-852	-852	-852	-852
EP	0	0	0	0	0	0	0	0	0	0	0	0	0	0	0	0
EPC	0	0	0	0	-349	-349	-349	-349	-349	-349	-349	-349	-349	-349	-349	-349

Table X. Case 1 Results – Z Components of Strain.

Z –Total Strain

	1	2	3	4	5	6	7	8	9	10	11	12	13	14	15	16
EC	-835	-1643	-1885	-2144	-3301	-2260	-1465	176	-373	-459	-938	268	410	-224	-618	-613
EP	-834	-1753	-2115	-2565	-4084	-3171	-2341	-551	-1100	-1187	-1667	-402	-810	-877	-1272	-1267
EPC	-834	-1753	-2115	-2565	-4389	-3507	-2527	-824	-1373	-1460	-1940	-683	-1092	-1159	-1554	-1548

Z–Plastic Strain

	1	2	3	4	5	6	7	8	9	10	11	12	13	14	15	16
EC	0	0	0	0	0	0	0	0	0	0	0	0	0	0	0	0
EP	0	-325	-549	-1027	-2635	-2825	-2366	-2197	-2197	-2197	-2197	-2062	-2062	-2062	-2062	-2062
EPC	0	-325	-549	-1027	-2635	-2783	-2176	-2072	-2072	-2072	-2072	-1960	-1960	-1960	-1960	-1960

Z–Creep Strain

	1	2	3	4	5	6	7	8	9	10	11	12	13	14	15	16
EC	0	0	0	0	-1420	-1420	-1420	-1420	-1420	-1420	-1420	-1420	-1420	-1420	-1420	-1420
EP	0	0	0	0	0	0	0	0	0	0	0	0	0	0	0	0
EPC	0	0	0	0	-472	-472	-427	-472	-472	-472	-472	-472	-472	-472	-472	-472

Table XI. Case 2 Results - Z Components of Strain.

Z-Total Strain

	1	2	3	4	5	6	7	8	9	10	11	12	13	14	15	16
EC	-835	-1643	-1885	-2144	-3556	-2506	-1706	-66	-615	-701	-1181	25	-400	-467	-862	-857
EP	-835	-1817	-2191	-2652	-4170	-3249	-2365	-553	-1101	-1188	-1667	-374	-799	-865	-1260	-1255
EPC	-835	-1817	-2191	-2652	-4493	-3566	-2532	-819	-1359	-1445	1925	-642	-1067	-1133	-1528	-1522

Z-Plastic Strain

	1	2	3	4	5	6	7	8	9	10	11	12	13	14	15	16
EC	0	0	0	0	0	0	0	0	0	0	0	0	0	0	0	0
EP	0	-357	-601	-1059	-2753	-2935	-2446	-2239	-2239	-2239	-2239	-2081	-2081	-2081	-2081	-2081
EPC	0	-357	-601	-1059	-2753	-2823	-2219	-2082	-2082	-2082	-2082	-1947	-1947	-1947	-1947	-1947

Z-Creep Strain

	1	2	3	4	5	6	7	8	9	10	11	12	13	14	15	16
EC	0	0	0	0	-1562	-1562	-1562	-1562	-1562	-1562	-1562	-1562	-1562	-1562	-1562	-1562
EP	0	0	0	0	0	0	0	0	0	0	0	0	0	0	0	0
EPC	0	0	0	0	-472	-472	-472	-472	-472	-472	-472	-472	-472	-472	-472	-472

Table XII. Case 3 Results - Z Components of Strain.

Z-Total Strain

	1	2	3	4	5	6	7	8	9	10	11	12	13	14	15	16
EC	-835	-1643	-1885	-2144	-3210	-2147	-1343	296	-253	-339	-819	386	-39	-106	-501	-498
EP	-835	-1763	-2076	-2467	-3423	-2446	-1456	194	-353	-440	-920	320	-103	-170	-565	-563
EPC	-835	-1763	-2076	-2467	-3570	-2431	-1503	137	-412	-499	-979	239	-184	-251	-645	-643

Z-Plastic Strain

	1	2	3	4	5	6	7	8	9	10	11	12	13	14	15	16
EC	0	0	0	0	0	0	0	0	0	0	0	0	0	0	0	0
EP	0	-337	-542	-921	-2005	-2204	-1688	-1649	-1649	-1649	-1649	-1535	-1535	-1535	-1535	-1535
EPC	0	-337	-542	-921	-2005	-1696	-1371	-1371	-1371	-1371	-1371	-1327	-1327	-1327	-1327	-1327

Z-Creep Strain

	1	2	3	4	5	6	7	8	9	10	11	12	13	14	15	16
EC	0	0	0	0	-1403	-1403	-1403	-1403	-1403	-1403	-1403	-1403	-1403	-1403	-1403	-1403
EP	0	0	0	0	0	0	0	0	0	0	0	0	0	0	0	0
EPC	0	0	0	0	-413	-413	-413	-413	-413	-413	-413	-413	-413	-413	-413	-413

Figure 12.   Nonlinear Patch in Elastic Matrix.

Table XIII. Turbine Blade Tip Model.

Temperature, ° F								
	1	2	3	4	5	6	7	8
● R-Total Strain								
D	0	-2850	-2550	-2925	-2800	250	-600	0
P	0	0	0	0	0	0	0	0
DP	0	-2850	-2550	-2925	-2800	250	-600	0
● R-Plastic Strain								
D	0	-1222	-1222	-1262	-1262	-1129	-1129	-1129
P	0	-47	-47	-59	-59	-59	-59	-59
DP	0	-1551	-1551	-1734	-1734	-1298	-1298	-1223
● R-Creep Strain								
D	0	-51	-52	-265	-611	-611	-611	-611
P	0	-2	-2	-16	-50	-50	-50	-50
DP	0	-57	-57	-258	-617	-617	-617	-617
● Z-Total Strain								
D	0	1201	1085	1279	1279	226	483	306
P	0	1460	1368	1842	2156	1755	1846	980
DP	0	3370	3164	3932	4332	2071	3218	2147
● Z-Plastic Strain								
D	0	611	611	631	631	555	555	555
P	0	365	365	480	480	480	480	480
DP	0	1765	1765	2007	2007	1802	1802	1750
● Z-Creep Strain								
D	0	26	26	132	305	305	305	305
P	0	17	17	153	535	535	535	535
DP	0	65	66	342	985	985	985	985

Table XIV. Case 1 Results – Z Components of Strain.

Z-Total Strain

	1	2	3	4	5	6	7	8	9	10	11	12	13	14	15	16
EC	-835	-1643	-1885	-2144	-3301	-2260	-1465	176	-373	-459	-938	268	410	-224	-618	-613
EP	-834	-1753	-2115	-2565	-4084	-3171	-2341	-551	-1100	-1187	-1667	-402	-810	-877	-1272	-1267
EPC	-834	-1753	-2115	-2565	-4389	-3507	-2527	-824	-1373	-1460	-1940	-683	-1092	-1159	-1554	-1548
EPCP	-866	-1787	-2150	-2603	-4370	-3512	-2543	-813	-1391	-1478	-1958	-700	-1110	-1177	-1571	-1563

Z-Plastic Strain

	1	2	3	4	5	6	7	8	9	10	11	12	13	14	15	16
EC	0	0	0	0	0	0	0	0	0	0	0	0	0	0	0	0
EP	0	-325	-549	-1027	-2635	-2825	-2366	-2197	-2197	-2197	-2197	-2062	-2062	-2062	-2062	-2062
EPC	0	-325	-549	-1027	-2635	-2783	-2176	-2072	-2072	-2072	-2072	-1960	-1960	-1960	-1960	-1960
EPCP	0	-328	-557	-1017	-2584	-2806	-2190	-2091	-2091	-2091	-2091	-1980	-1980	-1980	-1980	-1980

Z-Creep Strain

	1	2	3	4	5	6	7	8	9	10	11	12	13	14	15	16
EC	0	0	0	0	-1420	-1420	-1420	-1420	-1420	-1420	-1420	-1420	-1420	-1420	-1420	-1420
EP	0	0	0	0	0	0	0	0	0	0	0	0	0	0	0	0
EPC	0	0	0	0	-472	-472	-472	-472	-472	-472	-472	-472	-472	-472	-472	-472
EPCP	0	0	0	0	-482	-482	-482	-482	-482	-482	-482	-482	-482	-482	-482	-482

Table XIV. Case 1 Results - R Components of Strain (Concluded).

R-Total Strain

	1	2	3	4	5	6	7	8	9	10	11	12	13	14	15	16
EC	-122	-780	-978	-1184	-1963	-1113	-460	-975	-656	-633	-380	-809	-558	-544	-321	-314
EP	-123	-835	-1092	-1420	-2601	-1888	-1003	-1474	-1155	-1131	-879	-1318	-1070	-1056	-833	-826
EPC	-123	-835	-1092	-1420	-2736	-2037	-1126	-1582	-1262	-1239	-986	-1420	-1171	-1157	-934	-926
EPCP	12	-680	-921	-1220	-2377	-1612	-697	-1289	-851	-828	-576	-1019	-769	-756	-533	-533

R-Plastic Strain

	1	2	3	4	5	6	7	8	9	10	11	12	13	14	15	16
EC	0	0	0	0	0	0	0	0	0	0	0	0	0	0	0	0
EP	0	-113	-208	-448	-1516	-1635	-1053	-1129	-1129	-1129	-1129	-1170	-1170	-1170	-1170	-1170
EPC	0	-113	-208	-448	-1516	-1650	-1099	-1118	-1118	-1118	-1118	-1136	-1136	-1136	-1136	-1136
EPCP	0	-79	-154	-342	-1254	-1229	-721	-750	-750	-750	-750	-769	-769	-769	-769	-769

R-Creep Strain

	1	2	3	4	5	6	7	8	9	10	11	12	13	14	15	16
EC	0	0	0	0	-736	-736	-736	-736	-736	-736	-736	-736	-736	-736	-736	-736
EP	0	0	0	0	0	0	0	0	0	0	0	0	0	0	0	0
EPC	0	0	0	0	-301	-301	-301	-301	-301	-301	-301	-301	-301	-301	-301	-301
EPCP	0	0	0	0	-269	-269	-269	-269	-269	-269	-269	-269	-269	-269	-269	-269

1. All elements in the model are capable of nonlinear material behavior.

2. An isolated patch of elements is capable of nonlinear material behavior.

3. A single element is capable of nonlinear material behavior.

Shown in Tables XV and XVI are the results of the study.

Case 1 - Elastic/Plastic/Creep Behavior

Case 2 - Elastic/Creep Behavior Only

We also examined the following two conditions:

1. All elements in the model are capable of nonlinear material behavior.

2. An isolated patch of eight elements are capable of nonlinear material behavior. The nonlinear region is surrounded by purely elastic material.

For the above conditions the analysis was performed using creep times of 0.05, 0.1, 0.5, and 1.0 hours. The results are summarized in Tables XVII through XX.

The following outline summarizes our thoughts on the direction of the decompositon and sysnthesis methods.

II. DECOMPOSITION TECHNIQUES

    A. Component Identification

    1. Will concern only the following components:

- Combustor Liner
- Turbine Blade
- Turbine Vane

    2. No mesh generation or mesh refinement will be permitted once decomposition procedures have begun.

    B. Thermomechanical Loads

    1. Operating Conditions are identified by temperatures, pressures, and rotational speed.

Table XV. Case 1 Results.

R-Total Strain															
1	**2**	**3**	**4**	**5**	**6**	**7**	**8**	**9**	**10**	**11**	**12**	**13**	**14**	**15**	**16**
(a) -123	-835	-1092	-1420	-3636	-2654	-1941	-2402	-2082	-2059	-1807	-2227	-1974	-1960	-1738	-1725
(b) -122	-866	-1143	-1517	-4430	-3244	-2489	-2970	-2649	-2626	-2374	-2783	-2532	-2518	-2296	-2881
(c) -122	-780	-978	-1183	-2657	-1789	-1127	-1637	-1318	-1295	-1043	-1469	-1218	-1204	-981	-971

R-Creep Strain															
(a) 0	0	0	0	-1683	-1683	-1683	-1683	-1683	-1683	-1683	-1683	-1683	-1683	-1683	-1683
(b) 0	0	0	0	-2204	-2204	-2204	-2204	-2204	-2204	-2204	-2204	-2204	-2204	-2204	-2204
(c) 0	0	0	0	-2286	-2286	-2286	-2286	-2286	-2286	-2286	-2286	-2286	-2286	-2286	-2286

Z-Total Strain															
(a) -834	-1753	-2115	-2565	-5886	-4527	-3608	-1951	-2500	-2587	-3066	-1817	-2232	-2299	-2693	-2681
(b) -835	-1817	-2191	-2652	-5857	-4476	-3572	-1877	-2423	-2509	-2988	-1724	-2149	-2215	-2610	-2598
(c) -835	-1642	-1885	-2144	-3993	-2958	-2158	-510	-1059	-1146	-1625	-416	-841	-968	-1303	-1297

Z-Creep Strain															
(a) 0	0	0	0	-2666	-2666	-2666	-2666	-2666	-2666	-2666	-2666	-2666	-2666	-2666	-2666
(b) 0	0	0	0	-2591	-2591	-2591	-2591	-2591	-2591	-2591	-2591	-2591	-2591	-2591	-2591
(c) 0	0	0	0	-3578	-3578	-3578	-3578	-3578	-3578	-3578	-3578	-3578	-3578	-3578	-3578

Table XVI. Case 2 Results.

R-Total Strain

	1	2	3	4	5	6	7	8	9	10	11	12	13	14	15	16
(a)	-122	-780	-978	-1184	-3215	-2416	-1774	-2276	-1957	-1934	-1682	-2102	-1851	-1837	-1615	-1597
(b)	-122	-780	-978	-1184	-4205	-3397	-2751	-3247	-2928	-2905	-2653	-3071	-2820	-2806	-2584	-2565
(c)	-122	-840	-1081	-1375	-2679	-1619	-910	-1422	-1104	-1081	-828	-1249	-998	-983	-761	-754

R-Creep Strain

	1	2	3	4	5	6	7	8	9	10	11	12	13	14	15	16
(a)	0	0	0	0	-2739	-2739	-2739	-2739	-2739	-2739	-2739	-2739	-2739	-2739	-2739	-2739
(b)	0	0	0	0	-3632	-3632	-3632	-3632	-3632	-3632	-3632	-3632	-3632	-3632	-3632	-3632
(c)	0	0	0	0	-1233	-1233	-1233	-1233	-1233	-1233	-1233	-1233	-1233	-1233	-1233	-1233

Z-Total Strain

	1	2	3	4	5	6	7	8	9	10	11	12	13	14	15	16
(a)	-835	-1643	-1885	-2144	-5341	-4370	-3599	-1947	-2494	-2580	-3059	-1847	-2271	-2338	-2732	-2717
(b)	-835	-1643	-1885	-2144	-5732	-4756	-3978	-2323	-2871	-2957	-3436	-2223	-2648	-2714	-3109	-3095
(c)	-835	-1762	-2076	-2467	-4018	-2720	-1858	-202	-749	-835	-135	-73	-496	-563	-957	-952

Z-Creep Strain

	1	2	3	4	5	6	7	8	9	10	11	12	13	14	15	16
(a)	0	0	0	0	-4706	-4706	-4706	-4706	-4706	-4706	-4706	-4706	-4706	-4706	-4706	-4706
(b)	0	0	0	0	-5159	-5159	-5159	-5159	-5159	-5159	-5159	-5159	-5159	-5159	-5159	-5159
(c)	0	0	0	0	-1643	-1643	-1643	-1643	-1643	-1643	-1643	-1643	-1643	-1643	-1643	-1643

Table XVII. Total Strain.

	Time, hour			
	0.05	0.1	0.5	1.0
● Effective-Strain				
EPC	6568	6956	8484	9327
EC	4446	5134	7303	8334
● R-Strain				
EPC	-2736	-2852	-3340	-3636
EC	-1963	-2164	-2849	-3215
● Z-Strain				
EPC	-4388	-4600	-5431	-5885
EC	-3301	-3644	-4788	-5341
● T-Strain				
EPC	6181	6591	8203	9084
EC	3931	4684	7001	8079
● R-Z Strain				
EPC	-385	-412	-515	-596
EC	-270	-313	-424	-521
All strains X10^{-6}				

Table XVIII. Creep Strain.

	Time, hour			
	0.05	0.1	0.5	1.0
● Effective-Strain				
EPC	779	1306	3327	4388
EC	2193	3239	6233	7535
● R-Strain				
EPC	-301	-502	-1268	-1683
EC	-735	-1105	-2226	-2739
● Z-Strain				
EPC	-472	-793	-2028	-2666
EC	-1420	-2082	-3926	-4706
● T-Strain				
EPC	772	1294	3296	4349
EC	2155	3187	6152	7445
● R-Z Strain				
EPC	-36	-64	-178	-259
EC	-137	-201	-355	-448

Table XIX. Eight-Element Patch Total Strain.

	Time, hour			
	0.05	0.1	0.5	1.0
• Effective-Strain				
EPC	6966	7419	9160	10024
EC	4863	5794	8543	9650
• R-Strain				
EPC	-3086	-3272	-4028	-4429
EC	-2221	-2564	-3698	-4205
• Z-Strain				
EPC	-4491	-4706	-5489	-5857
EC	-3547	-3994	-5255	-5732
• T-Strain				
EPC	6588	7069	8923	9842
EC	4319	5323	8267	9445
• R-Z Strain				
EPC	-223	-187	-26	68
EC	-163	-129	55	160

Table XX. Eight-Element Patch Creep Strain.

	Time, hour			
	0.05	0.1	0.5	1.0
• Effective-Strain				
EPC	821	1408	3684	4801
EC	2427	3725	7502	8835
• R-Strain				
EPC	-347	-601	-1649	-2203
EC	839	-1336	-2932	-3632
• Z-Strain				
EPC	-471	-802	-2027	-2591
EC	-1552	-2344	-4420	-5159
• T-Strain				
EPC	817	1404	3677	4794
EC	2391	3679	-7352	-8791
• R-Z Strain				
EPC	-5.9	4.1	127	227
EC	-104	-121	-13	92

2. These operating conditions define the individual misison points for each component and are intended to encompass the expected range of engine operation.

C. Component Analysis

1. Total structural response of the generic component will be obtained through detailed finite element anlaysis procedures.

2. A detailed analysis will be performed for each set of operating conditions (mission points) and critical locations can be identified for the component under study. This procedure can be user-defined or automated.

3. Critical Locations - Once the critical locations are identified, procedures will be implemented to store information on (a) nodal displacements, and (b) elemental stresses and strains for the nodes and elements defining the region. This information will form the data base on which the synthesis techniques will be based.

D. Structural Response and Load Application

1. The structural response at the critical location can fall into these categories:

    ● Uniaxial
    ● Biaxial
    ● Triaxial

2. The generic mode of load application can be identified and a hierarchy defining the overall influence and effect on overall structural response can be formed.

E. Material Response

1. Material response can be modeled in a number of ways. The following limitations can be imposed on the material behavior:

    ● Elastic only
    ● Elastic/plastic
    ● Elastic/creep
    ● Elastic/plastic/creep
    ● Flow rule and yield criteria
    ● Creep formulation

F. Decomposition Procedures and Models

1. Serving as baseline data sets are models previously validated under other NASA programs.

- Turbine blade tip durability
- Inelastic

2. These models will be used to create a preliminary data base from which we will evaluate our stress/strain decomposiiton techniques.

3. These models represent actual engine conditions and are intended to economically and efficiently evaluate the stress/strain decomposition and synthesis techniques.

II. SYNTHESIS TECHNIQUES

A. Component-Specific Synthesis Techniques

1. The synthesis techniques will be based on a defined set of mission-segment/component station characteristics.

- The comnponent station characteristics are defined in the thermomechanical load (TML) matrix.

- The structural data base will supply the necessary mission segment response upon which the synthesis alrogithms will operate.

B. Synthesis Algorithms

1. Algorithms used to compute fixed point mission-time profiles of "local" (critical point location) stresses, strains, and displacements. These algorithms will be limited to local level response. These algorithms may be based on empirical relations between loads and deformation states.

III. COMPONENT DATA BASE STRUCTURE

A. Component Dependent

1. Three distinct data bases will arise from the component specific modeling effort:

- Turbine blade data base (TBDB)
- Turbine vane data base (TVDB)
- Combustor data base (CBDB)

2. The component data bases will be identical in structure but dissimilar in content.

3. A simple set of access routines will be used to construct and access the three data bases.

```
                    ┌──────────────────────┐
                    │  Component Specific   │
                    │   Modeling Effort     │
                    └──────────┬───────────┘
         ┌─────────────────────┼─────────────────────┐
         ▼                     ▼                     ▼
┌──────────────────┬──────────────────┬──────────────────┐
│  Turbine Blade   │   Turbine Vane   │    Combustor     │
│   Data Base      │   Data Base      │    Data Base     │
└──────────────────┴──────────────────┴──────────────────┘
```
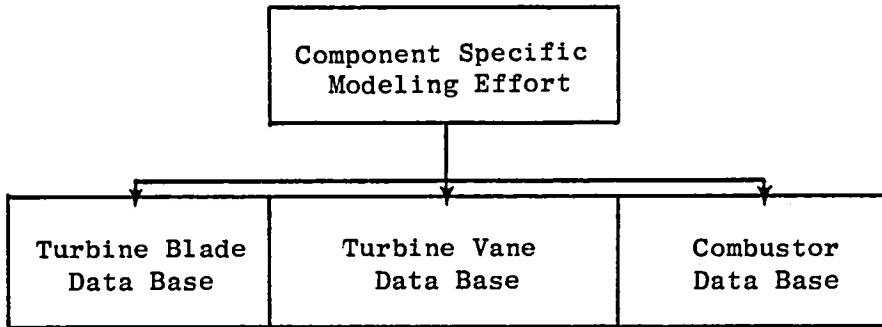
B.   Component Data Base Attributes

1.   Random access

2.   Self-contained sizing

3.   Simple structure

4.   Three consitutent parts

   ● Control includes

      - Overall problem sizing
      - Critical region and mission point specifications
      - Assorted pointers and counters
      - Descriptions and titles

   ● Critical Region Specification Includes

      - Location and number of critical points are defined

      - Assorted pointers and counters for the mission points
        are defined.

   ● Mission Point Specification Includes

      - Local control information
      - Node and element information and data

50

The following sketch shows how three constituent parts interact.


```
┌─────────────────────┐  ┌─────────────────────┐
│                     │  │  CR1 ──────► MP(1)  │
│      Overall        │  │             MP(2)   │
│      Control        │  │             MP(3)   │
│         │           │  │              .      │
│         │           │  │              .      │
│         ▼           │  │             MP(n)   │
├─────────────────────┤  ├─────────────────────┤
│ Critical Region (CR)│  │  CR2 ──────► MP(1)  │
│   Specification     │  │             MP(2)   │
│         │           │  │              .      │
│         ▼           │  │              .      │
├─────────────────────┤  │             MP(n)   │
│ Mission Point (MP)  │  ├─────────────────────┤
│   Specification     │  │  CR3 ──────► MP(1)  │
│         │           │  │             MP(2)   │
│         │           │  │              .      │
│         ▼           │  │              .      │
│                     │  │             MP(n)   │
│                     │  ├─────────────────────┤
└─────────────────────┘  │         ▼           │
                         └─────────────────────┘
```

General Data Base   Detail: Mission Point
Structure.   Specification
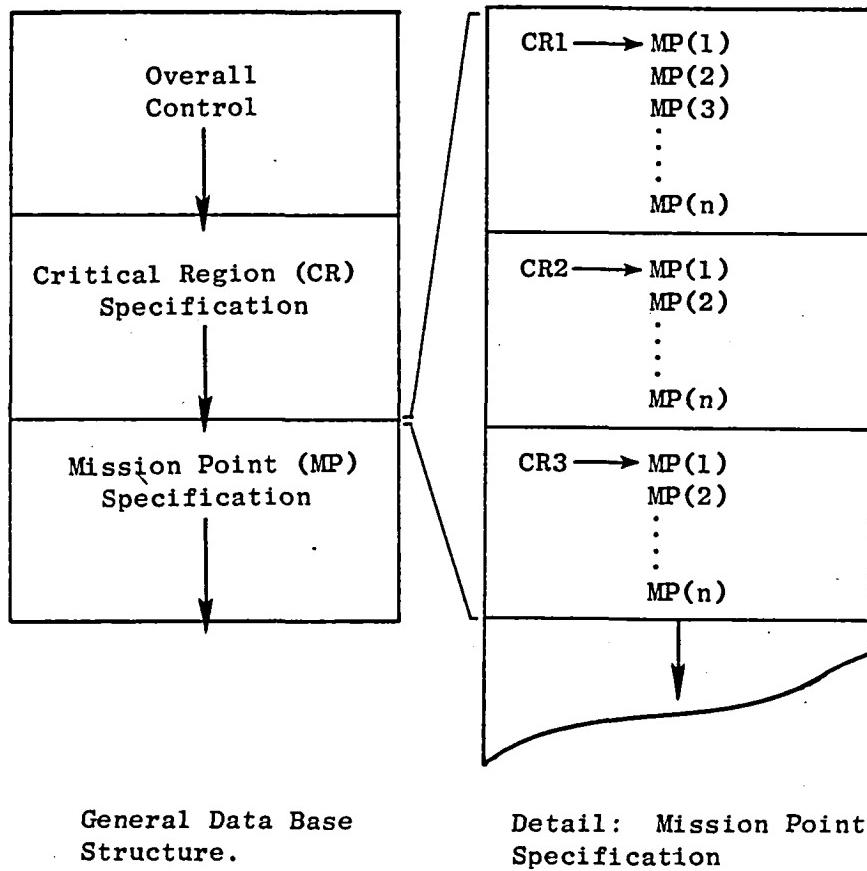
2.6 TASK II - STRUCTURAL ANALYSIS METHODS EVALUATION

This task was completed during 1983. The selections outlined in 2.1 are the result of this effort.

2.7 TASK VII - THERMODYNAMIC LOADS MODEL

The general form of the input, output, and calculations for blades, vanes, and combustor thermodynamic loads was defined during 1983, and work was initiated on the software coding. The final software specification is shown in the following paragraphs.

Thermodynamic Loads Features for TDE Model:

I. BLADES AND VANES

A. Input will be:

1. A series of midspan station temperatures at a specified SS reference case condition, and for each station a percent cord envelope dimension

2. A set of _output_ percent cord envelope dimensions

3. A table of percent radial span versus cooling effectiveness factors. RF, where:

$$RF = \frac{\eta_{cs}}{\eta_{cms}}$$

η_{cs} = cooling effectiveness at specified span dim.

η_{csm} = cooling effectiveness at midspan

The point density in this table will be such that spanwise linear interpolation will suffice.

B. Calculations

1. For each temperature a nominal cooling effectiveness will be calculated from:

$$\eta_c = \frac{T41-Tm}{T41-T3}$$

2. At each new condition, all station η_c values will be modified by a factor, CF, as follows:

$$CF = \frac{(1 - \eta_c)}{(1 - \eta_c)REF} = ((T3 * T41_{REF})/(T3_{REF} * T41))\alpha, \text{ where } \alpha \text{ is input}$$

3. Output η_c values will be linearly interpolated based on percent cord envelope at adjacent input stations

4. For each output radial distance (specified in the input) all station temperatures will be calculated as follows:

$$Tij = T3 + (1 - \eta_{c_R}) * CF(T41-T3) * RF$$

Where i = station index

j = radial station index

II. COMBUSTOR

A. Inputs will be:

1. Metal bulk made temperatures at axial stations on inner and outer liners, and for each station, x and y dimensions of node centers at a specified reference case condition. Both hot streak and average metal temperature values will be input.

2. It is assumed that output node dimensions will match the input nodes. If cross-meshing is to be required, it will be done before the input is defined.

3. A set of linear equation constants will be input for a sparse set of axial locations, identified by "ΔT station" numbers. Output ΔT locations will be same as input locations.

4. A set of ΔP scaling constants will be inpout at a sparse set of locations, identified by ΔP station numbers. Output ΔP stations will be same as input.

B. Calculations

1. A nominal cooling effectiveness will be calculated for each input combustor average and hot streak temperature.

2. At each flight condition, each metal temperature will be recalculated from:

$$Tm_{ij} = T3_j + (1 - \eta_{c_i})(T41_j - T3_j)$$

where i = station index and j = flight phase index

3. At each flight condition, each ΔT will be recalculated from:

$$\Delta T_{ij} = [T3_j + (1 - \eta_{c_i})(T41 - T3)][b_i + m_i * P3_j]$$

4. At each flight condition, each ΔP will be recalculated from:

$$\Delta P_{ij} = P3_j * K_i * \left(\frac{W41}{P3}\right)_j^2 * T3_j$$

The accuracy of the thermodynamic engine model has been evaluated, relative to the engine steady-state performance computer model (cycle deck). In a model based on interpolation methods, the maximum error must occur in regions where the "distance" from known data points is greatest. Figure 13 shows the altitude versus Mach No. map of stored data points used in the thermodynamic engine model (TEM). The X symbols on this map indicate the worst-case points selected for the error evaluation.

The interpolation logic varies from quadrant to quadrant within a rectangle bounded by stored data points. The nearest point is always used as the base from which the interpolation process is started, for example. Figure 14 shows a typical set of four stored data points. The shaded area is a quadrant. The evaluation test point is at the center. The hypothetical error magnitude curves drawn from two corners to the center illustrate two facts:

- In any quadrant, the error surface is approximately parabolic in shape and maximum at the center of the stored data.

- The four quadrants have different error surfaces, and a discontinuity occurs where they meet.

Since there can be four different maximum error values at each test point, the error analysis was performed four times at each point. The results were summarized by a computer program. The right-hand four columns of Table XXI
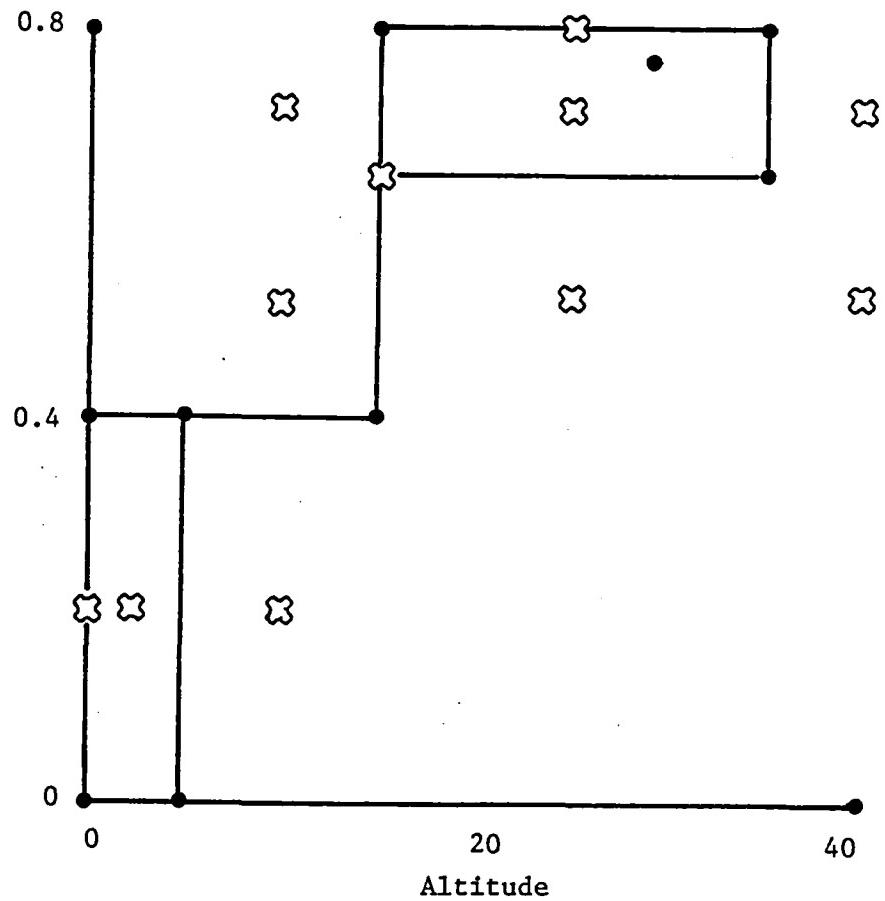
Figure 13. Data Points Used for Interpolation Routines in the TEM.
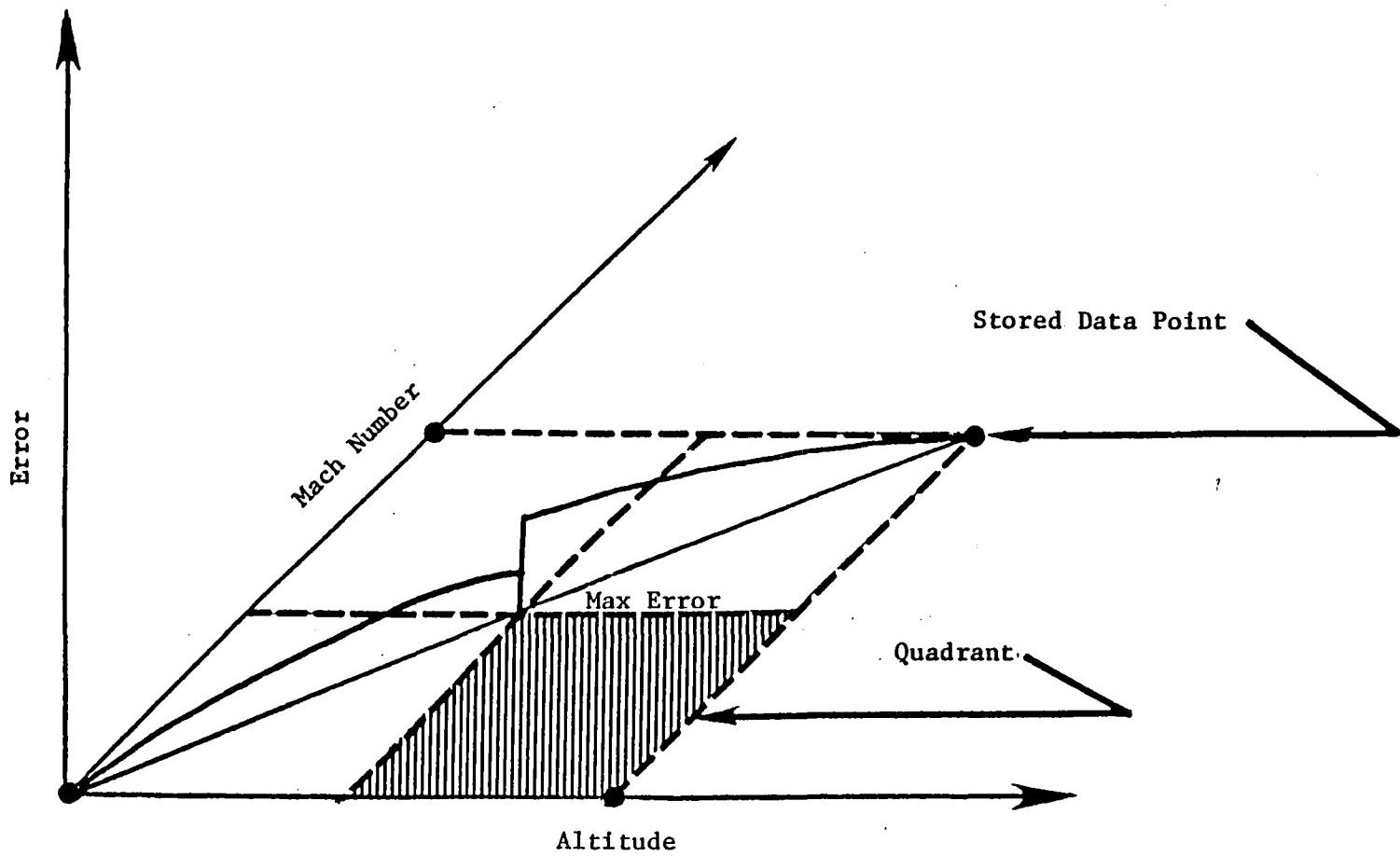
Figure 14. Quadrant Error Distribution.

Table XXI. Error Summary.

C	MACH	ALT	T2	PCHLR	BLEED	DT48	PERCENT =	0.50			X M 2 5			04/04/84
1	0.20	2500.	513.8620	106	3.2579	-1.0	-0.5519	0.	-0.6205	0.	0.	0.	0.	0.
2	0.20	2500.	513.8620	96	3.1946	-1.0	-0.5045	-0.6257	-0.5277	0.	0.	0.	0.	0.
3	0.20	2500.	513.8620	84	3.1303	-1.0	0.	0.	0.	0.	0.	0.	0.	0.
4	0.20	2500.	513.8620	65	3.0411	-1.0	-1.1828	-1.1591	-0.9959	-0.8267	-0.5578	-0.5565	-0.7176	-0.7255
5	0.20	2500.	513.8620	46	1.9375	-1.0	0.	0.5660	0.	0.	0.	0.	0.	0.
8	0.52	2500.	537.3528	84	3.1620	-1.0	-0.7501	-0.7983	-0.7340	-0.6966	0.	0.	0.	0.
13	0.20	10000.	486.8993	114	2.9939	-1.0	0.	0.	-0.5631	0.	0.	0.	0.	0.
14	0.20	10000.	486.8993	103	2.9393	-1.0	0.	0.	0.	0.	0.	0.	0.	0.
15	0.20	10000.	486.8993	87	2.8665	-1.0	-0.5497	0.	0.	0.	0.	0.	0.	0.
16	0.20	10000.	486.8993	68	1.7500	-1.0	-1.1465	-1.0691	-1.0257	-0.9836	-0.5193	-0.5197	-0.8407	-0.8453
17	0.20	10000.	486.8993	51	1.7500	-1.0	0.	0.	0.	0.	0.	0.	0.	0.
20	0.52	10000.	509.1575	87	2.8930	-1.0	-0.6744	-0.7065	0.	0.	0.	0.	0.	0.
23	0.72	10000.	533.1161	87	2.9232	-1.0	-1.2963	-1.2814	-0.5555	-0.5555	0.	0.	0.	0.
25	0.52	25000.	452.7669	105	2.6150	-1.0	0.	0.	-0.8555	-0.8591	0.	0.	0.	0.
26	0.52	25000.	452.7669	90	1.5000	-1.0	-0.5666	0.	0.	0.	-0.5408	-0.5441	-0.5406	0.
27	0.52	25000.	452.7669	81	1.5000	-1.0	-0.7112	-0.6162	0.	0.	0.	0.	0.	0.
28	0.52	25000.	452.7669	54	1.5000	-1.0	0.	0.6721	0.6806	0.5485	0.	0.	0.	0.
30	0.72	25000.	474.0719	105	2.6439	-1.0	0.	0.	-0.9923	-0.9042	0.	0.	0.	0.
31	0.72	25000.	474.0719	81	1.5000	-1.0	-0.5029	-0.6023	0.	0.	0.	0.	0.	0.
33	0.52	40000.	411.0791	113	2.2351	-1.0	-0.9334	-0.9349	-0.9335	-0.9349	0.	0.	0.	0.
34	0.52	40000.	411.0791	81	1.5000	-1.0	0.	0.	0.	0.	0.	0.	0.	0.
36	0.72	40000.	430.4226	113	2.2523	-1.0	-1.0978	-1.0829	-1.0979	-1.0829	0.	0.	0.	0.
37	0.72	40000.	430.4226	81	1.5000	-1.0	0.	0.	0.	0.	0.	0.	0.	0.
44	0.20	2500.	564.2620	108	3.2390	-1.0	-0.7879	-0.7140	-0.9580	-0.7769	0.	0.	0.	0.
45	0.20	2500.	564.2620	84	3.1178	-1.0	-0.6657	0.	-0.5454	0.	0.	0.	0.	0.
48	0.52	10000.	540.7799	87	2.8857	-1.0	-0.5813	-0.7143	-0.5642	-0.5642	0.	0.	0.	0.
50	0.72	25000.	507.1823	105	2.6368	-1.0	0.	0.	-1.4901	-1.3956	0.	0.	0.	0.
51	0.72	25000.	507.1823	81	1.5000	-1.0	0.	-0.5206	0.	0.	0.	0.	0.	0.
53	0.20	2500.	463.4620	106	3.2789	-1.0	-0.6021	-0.5373	-0.5777	0.	0.	0.	0.	0.
54	0.20	2500.	463.4620	84	3.1446	-1.0	-0.5541	0.	-0.6280	0.	0.	0.	0.	0.
57	0.52	10000.	488.0759	87	2.8983	-1.0	-0.7158	-0.7473	0.	0.	0.	0.	0.	0.
59	0.72	25000.	451.9983	105	2.6489	-1.0	0.	0.	-0.7757	-0.6905	0.	0.	0.	0.
60	0.72	25000.	451.9983	81	1.5000	-1.0	-0.6487	-0.7383	0.	0.	0.	0.	0.	0.
62	0.20	2500.	513.8620	106	3.0626	25.0	-0.6785	-0.6130	-0.8573	-0.6909	0.	0.	0.	0.
63	0.20	2500.	513.8620	84	2.9988	25.0	0.	0.	0.	0.	0.	0.	0.	0.
66	0.52	10000.	509.1575	87	2.7726	25.0	-0.6360	-0.6682	0.	0.	0.	0.	0.	0.
68	0.72	25000.	474.0719	105	2.5327	25.0	0.	0.	-1.3583	-1.2696	0.	0.	0.	0.
69	0.72	25000.	474.0719	81	1.5000	25.0	0.	-0.5975	0.	0.	0.	0.	0.	0.
71	0.20	2500.	513.8620	106	0.3914	-1.0	0.	0.	0.	0.	0.	0.	0.	0.
72	0.20	2500.	513.8620	84	0.2626	-1.0	0.	0.	0.	0.	0.	0.	0.	0.
75	0.52	10000.	509.1575	87	0.2405	-1.0	0.	0.	0.	0.	0.	0.	0.	0.
77	0.72	25000.	474.0719	105	0.2225	-1.0	0.	0.	0.	0.	0.	0.	0.	0.
78	0.72	25000.	474.0719	81	0.1383	-1.0	0.	0.	0.	0.	0.	0.	0.	0.
81	0.20	0.	522.8496	90	0.3171	-1.0	0.	0.	0.	0.	0.	0.	0.	0.
82	0.20	0.	622.8496	55	0.1548	-1.0	0.	0.	0.	0.	0.	0.	0.	0.
84	0.80	25000.	484.5183	104	0.2333	-1.0	0.	0.	0.	0.	0.	0.	0.	0.
85	0.80	25000.	484.5183	65	0.0961	-1.0	0.	0.	0.	0.	0.	0.	0.	0.
87	0.40	5000.	496.2553	84	0.3169	-1.0	0.	0.	0.	0.	0.	0.	0.	0.
88	0.40	5000.	496.2553	57	0.1455	-1.0	0.	0.	0.	0.	0.	0.	0.	0.
89	0.65	15000.	482.8221	106	0.3220	-1.0	0.	0.	0.	0.	0.	0.	0.	0.
90	0.65	15000.	482.8221	94	0.2551	-1.0	0.	0.	0.	0.	0.	0.	0.	0.
91	0.65	15000.	482.8221	59	0.1184	-1.0	0.	0.	0.	0.	0.	0.	0.	0.
92	0.40	5000.	616.8962	114	0.2197	25.0	0.	0.	0.	0.	0.	0.	0.	0.
93	0.40	5000.	616.8962	94	0.1566	25.0	0.	0.	0.	0.	0.	0.	0.	0.
94	0.40	5000.	616.8962	57	0.0718	25.0	0.	0.	0.	0.	0.	0.	0.	0.
					AVG		0.2622	0.2650	0.2875	0.2626	0.1125	0.1064	0.1119	0.1196
					MAX		-1.2963	-1.2814	-1.4901	-1.3956	-0.5578	-0.5565	-0.8407	-0.8453
					NVAL		22	21	21	15	3	3	3	2

show the error values that exceed the target value which is listed in the center of the heading. The left-hand five columns identify the test points. The middle four columns show the accuracy level available before the improvements developed in this program were incorporated. The average of the absolute errors, the max error, and the number of "Exceedances" are given at the bottom of each column. Note that speed, pressure, and horsepower errors are expressed as percent of the rated standard day, sea level value. It seemed more meaningful to express temperature errors in degrees.

Table XXII shows a brief summary of the accuracy level achieved. Column 2 shows the average of all test point errors. Columns 3, 4, and 5 show the value that is exceeded 2, 4, and 11 times (1%, 2%, and 5% of the 220 error values). Note that all data in this figure refers to the worst-case test points. Since the error surfaces are approximately parabolic in shape, the average error in each quadrant is approximately half of the maximum error, and the overall error is approximately half of the average error listed.

Table XXII. CF6-50C2 Validation Case
Error Analysis.

		Error Exceeded N Times		
	Average	N = 2	N = 4	N = 11
P_2	0.03%	<1%	<1%	<1%
P_3	0.23%	1.3%	1.2%	1.0%
FNIN1	0.49%	1.8%	1.8%	1.8%
XN25	0.17%	0.7%	0.6%	0.5%
T_2	0.08%	<5°	<5°	<5°
T_3	2.1°	<10°	<10°	<10°
T_{41}	11°	47°	47°	35°

The maximum error of 47° F listed for T41 may seem large. This was one of the most difficult parameters to fit. However, note that 47° is only 2% of

the rated T41 value (expressed in ° F) and the true average error is only approximately 0.23%.

Work is continuing toward the completion of the thermodynamic loads features to be incorporated in the thermodynamic engine model.

2.8 TASK VIII - COMPONENT SPECIFIC MODEL DEVELOPMENT

2.8.1 Geometric Modeling

A recipe for a segment of a combustor liner has been completed. Figure 15 shows the typical nugget of a combustor liner. The recipe describes the geometry of a nugget as a function of a prescribed set of physical parameters. These parameters include the thicknesses of the liner skin, the radii of the internal and external surfaces of the nugget, the height and length of the nugget, and the overall length of the panel. Generic master regions are then constructed using these key points. The coordinates of these key points and the connectivity of the master regions are then used as input into a 20-noded mesh generator to obtain the final mesh. In addition, the key information is written into an ESMOSS recipe format. This recipe is then used in conjunction with the ESMOSS mesh-generating logic to obtain a discretized mesh. Figure 16 shows a typical nugget, some of the physical input parameters, and the master region definition based on these parameters. Figure 17 shows representative 2D and 3D models generated from the master region.

We came to the decision that we could not use exactly the same procedure for the turbine blade model. This is because of the significant differences in the two geometries. A typical turbine blade geometry is shown in Figure 18. The outside of this airfoil is a complex curve defined by aero requirements. There are no reasonable number of physical parameters which could be used to describe this geometry. We evaluated many options and believe that the best course is to use a data file of coordinates which define this closed curve. The capability to work with a file of points is present in ESMOSS. The interior of the cross section (wall thicknesses, location and number of spars, etc.) will be specified as physical parameters. The interior cross section can be defined using a data file or by specifying a constant wall thickness as a physical parameter. Figure 19 shows a plot of the exterior and interior points for a typical airfoil.

Once the basic cross section is defined, the location and size of the interior spars can be controlled by the user through selection of paired points on the interior surface. The generator will then automatically insert the spars at the desired locations. The user can vary the number of spars

60
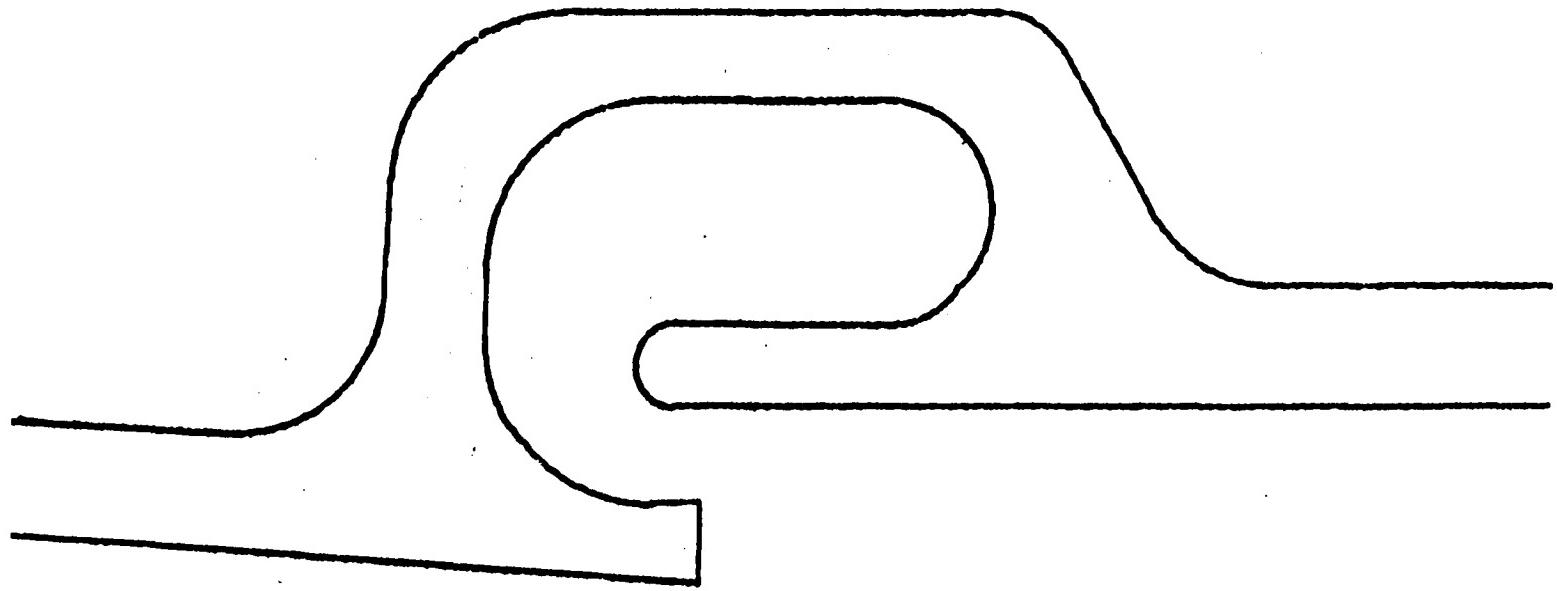
Figure 15.   Typical Nugget.
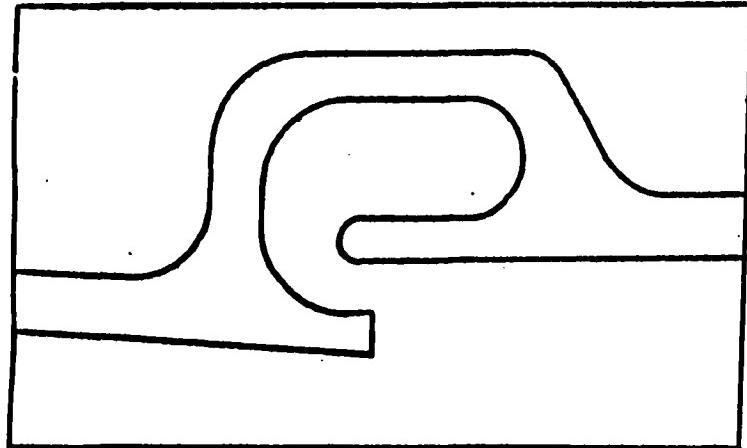
Typical Nugget
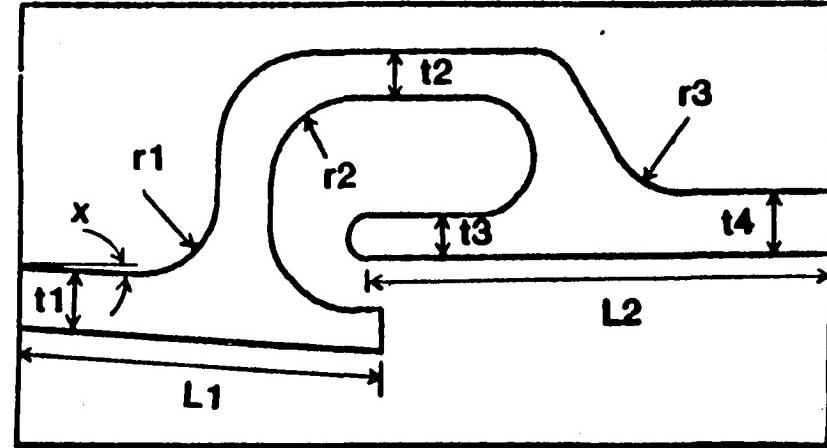
Physical Input Parameters
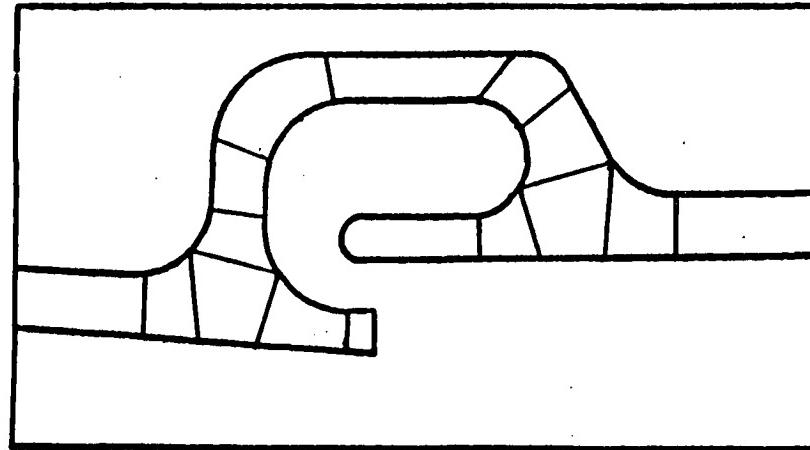
Master Region Definition

Figure 16. Combustor Recipe Process.
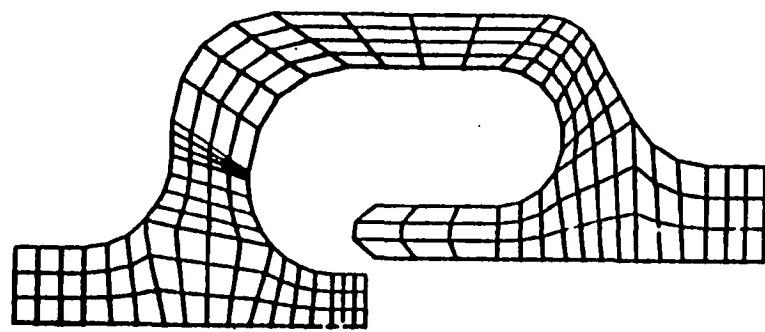
2D Model
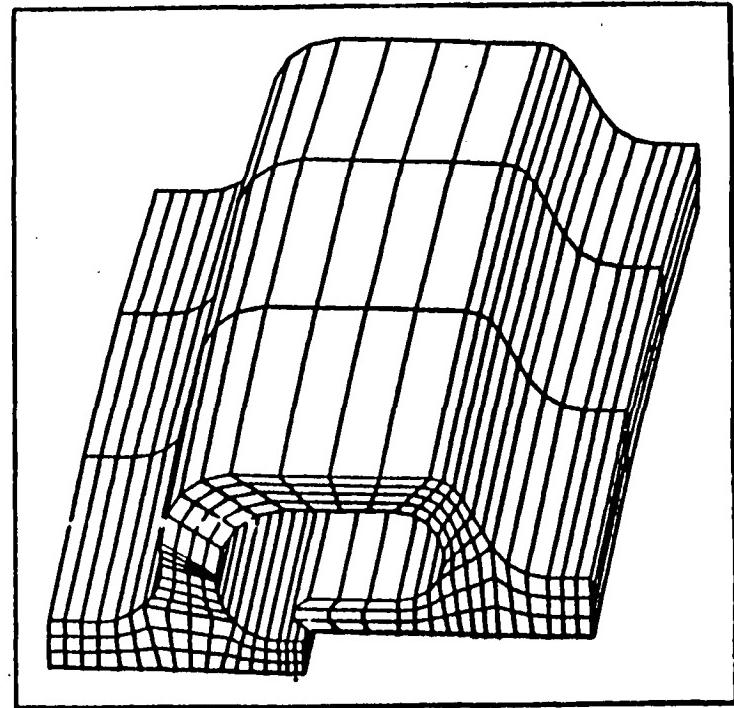
3D Model

Figure 17.   Combustor Nugget Finite Element Models.
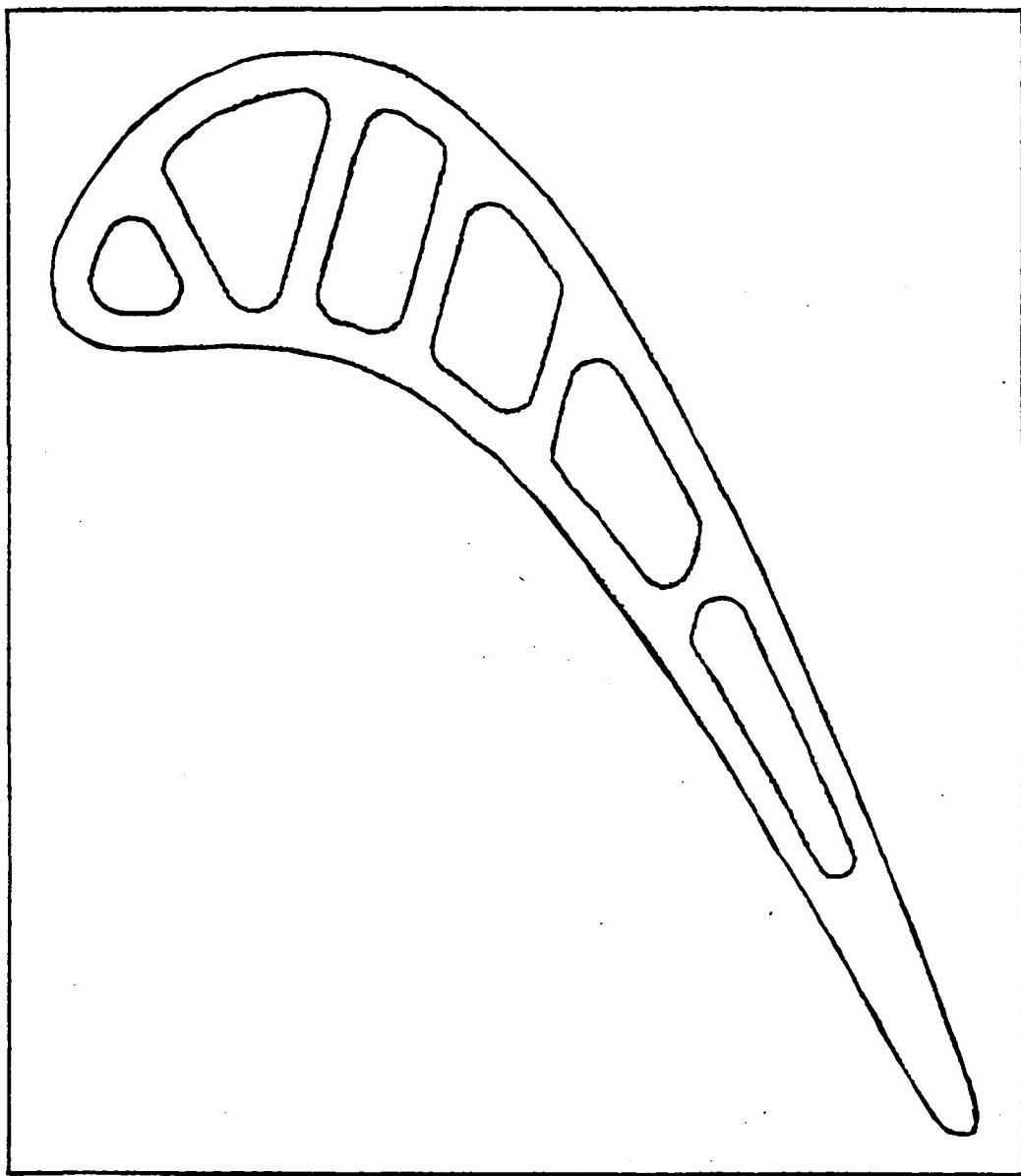
Figure 18. Cooled Turbine Blade Cross Section.
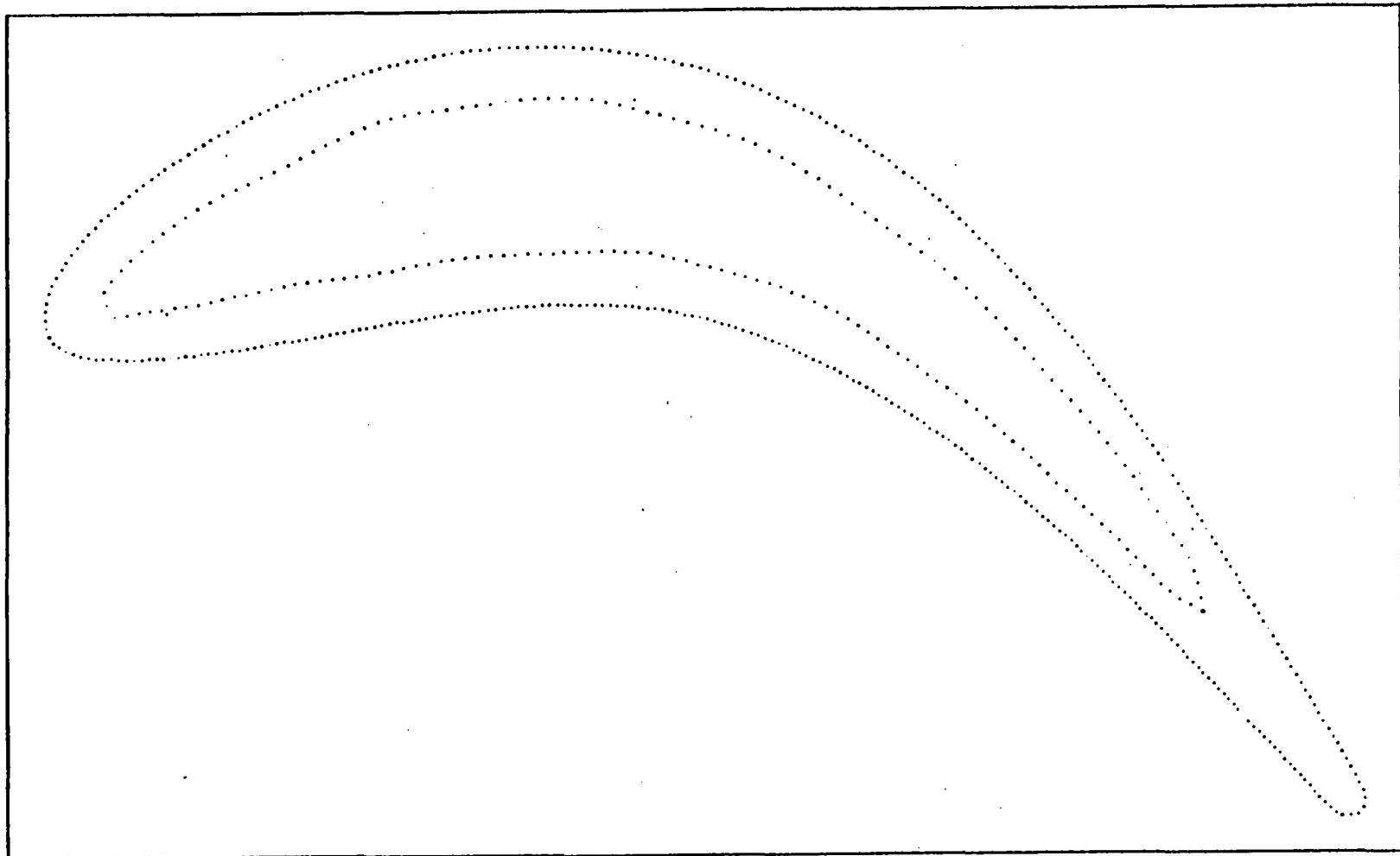
Figure 19. Plot of Exterior and Interior Points for a Typical Airfoil.

and the geometry of each spar. Figure 20 shows the pointer selected for a spar configuration. Figures 21 and 22 show coarse meshes for a blade with and without cavities. This software is complete and integrated with ESMOSS.

2.8.2 Remeshing and Mesh Refinement

This area and the next, Self-Adaptive Solution Strategies, touch on each other synergistically. What is sought in this program is the best combination of both. This involves two major areas of investigation: (1) the method to be used to refine, upgrade, and rearrange the mesh, and (2) the criteria to be used to activate this process.

There are a number of ways to refine a mesh to get a better answer: (1) one way is to progressively subdivide a coarse mesh, always retaining all previous meshes within the finer mesh; (2) a second family of techniques totally realigns the mesh based on some criteria such as strain energy density; (3) a third method is to leave the mesh unchanged but upgrade the order of the elements.

The first method, progressive subdivision, has certain theoretical and computational advantages. If the finite element interpolating functions used meet the requirements for completeness and continuity, convergence is mathematically guaranteed when we refine the mesh by progressive subdivision. The computational process of remeshing by progressive subdivision is straightforward; however, it guarantees a larger problem to solve.

For a solution of the finite element system of equations:

$$[K] \{\delta\} = \{F\}$$

suppose there is a numerical solution for the displacement, $\{\delta^*\}$. Then the equilibrium or residual force vector is generated:

$$\{R\} = \{F\} - [K] \{w^*\}$$

A perfect solution would result in this vector containing all zeros. Given the finite numerical accuracy of the computer, this is impossible. Therefore, a measure of the numerical "goodness" of the solution is to be found in how much this vector deviates from zero. Decisions on whether to

66
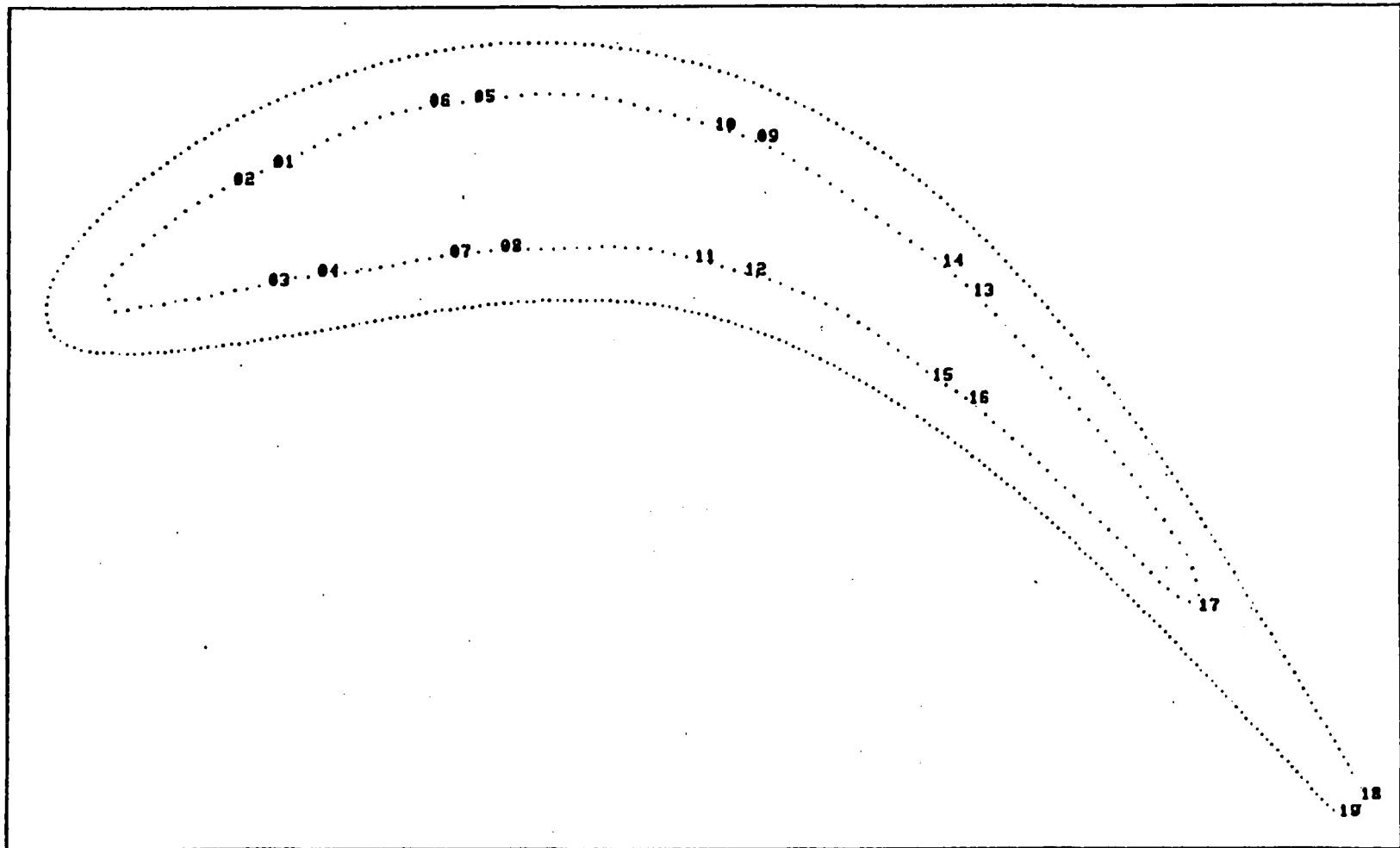
Figure 20. Points Chosen for a Spar Configuration.
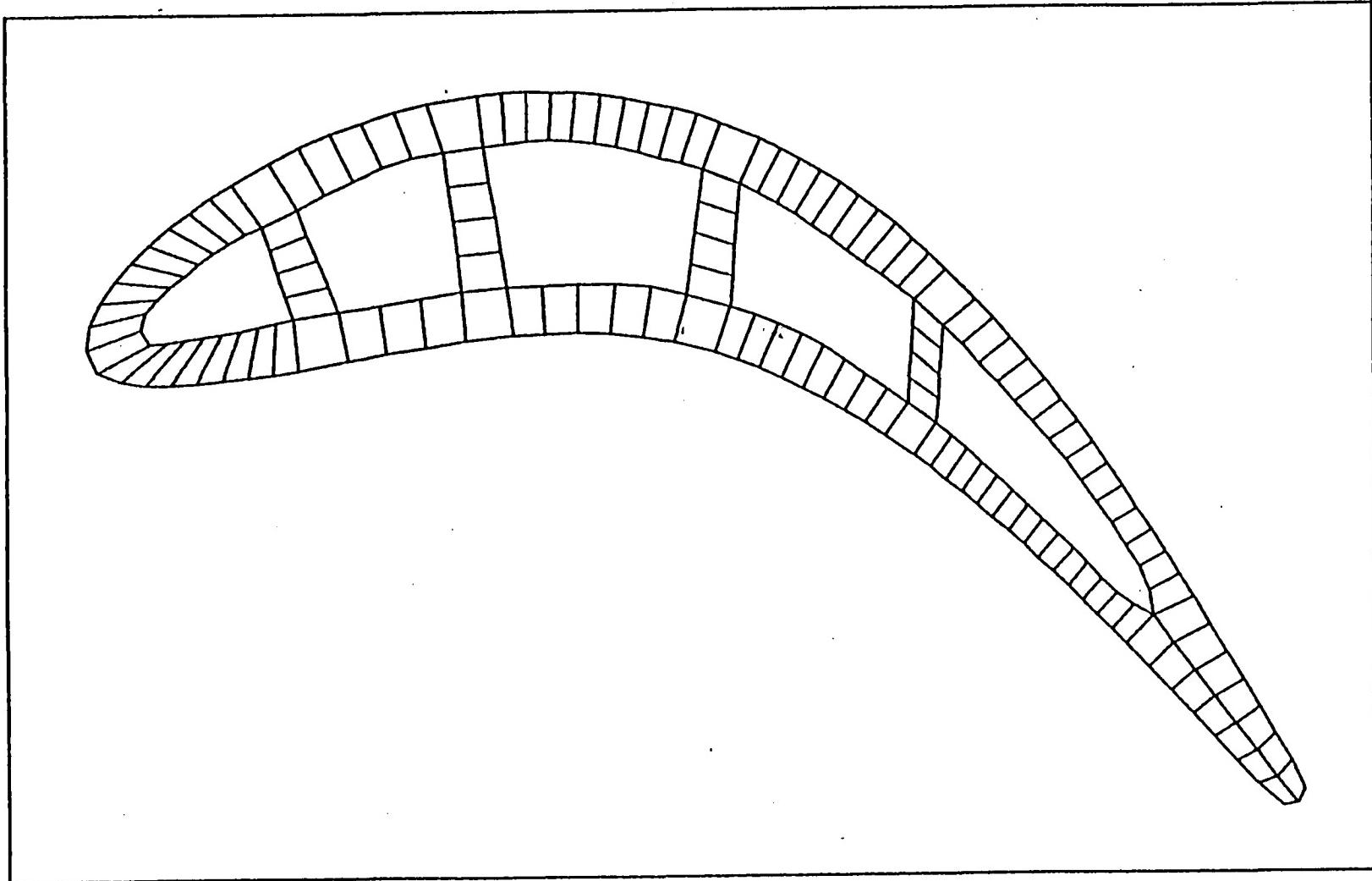
Figure 21. Coarse Mesh Selection for a Blade With Cavities.
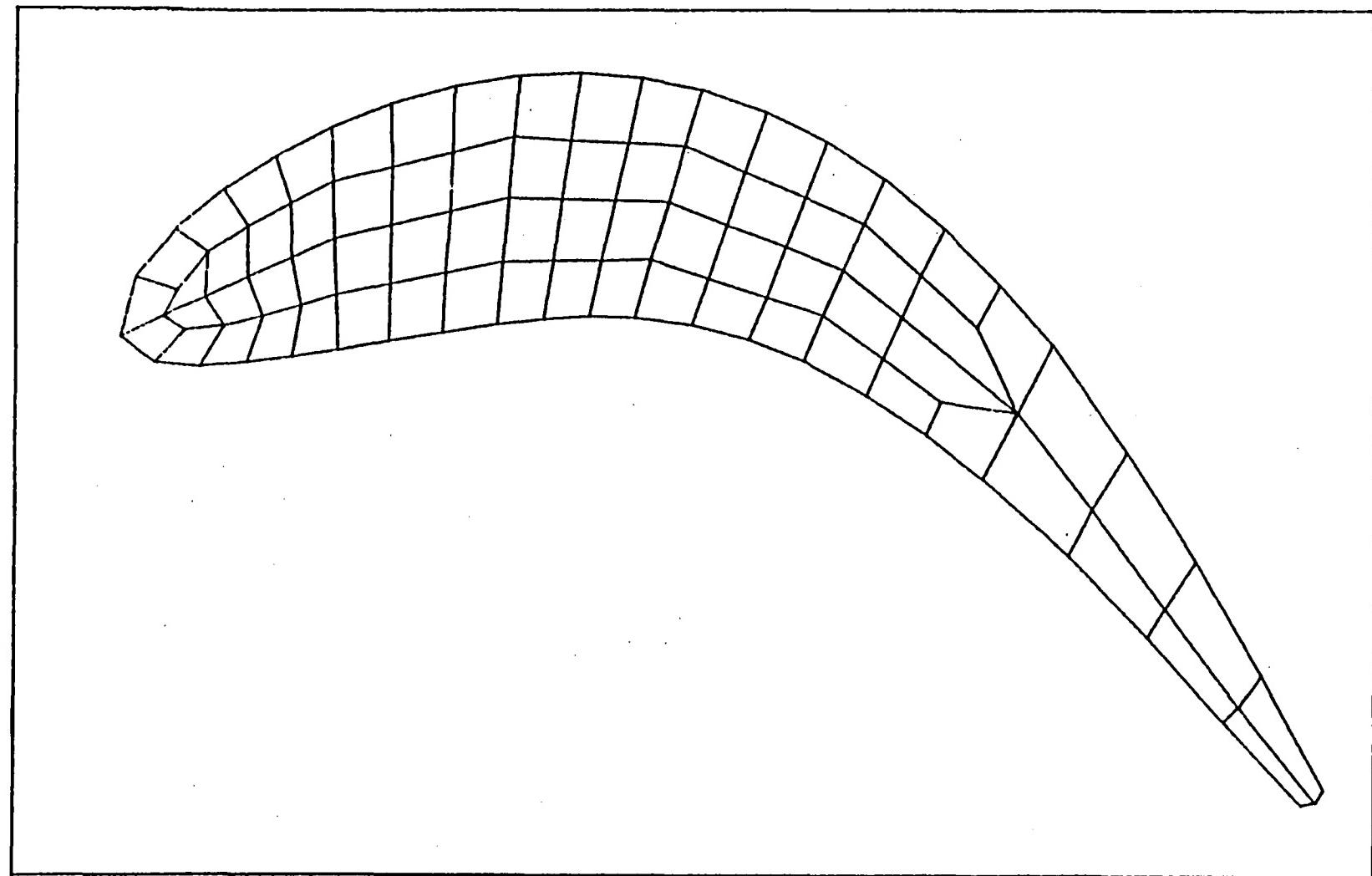
Figure 22.   Coarse Mesh Selection for a Blade Without Cavities.

re-solve or redefine the problem can be based on the total and local deviations from zero. If a few local degrees of freedom are out of equilibrium, this might suggest a local remeshing. If the total equilibrium is deficient, this will require remeshing and/or re-solving with greater numerical accuracy.

The decision tree for this is as follows

1. $\left\{ \begin{array}{l} \text{If } \Sigma R_i < C_R \\ \text{and all } R_i < C_{RiL} \end{array} \right\}$ the solution is good

2. If $\Sigma R_i > C_R$
   and [Number of nodes with $CR_{iL} < R_i < C_{R_{iu}}$] $> C_s$
   then re-solve

3. If $\Sigma R_i > C_R$
   and [Number of nodes with $R_i > C_{R_{iu}}$] $< C_s$
   then remesh and re-solve

4. If $R_i < C_R$
   but some $R_i > C_{R_{iu}}$
   then remesh and re-solve

where:

R_i = i^{th} residual-free vector

C_R = Maximum allowable sum of R_i

$C_{R_{iL}}$ = Lower bound for R_i for possible remeshing

$C_{R_{iu}}$ = Maximum allowable upper bound for R_i

Once an acceptable displacement solution has been reached, proceed to the element level. If, at the elastic level, stresses and strains are linearly connected, only one of these two needs to be evaluated. Strain will be checked. The total strain at each calculation point in an element is made up of an elastic strain and a thermal strain:

$$\varepsilon_i = \varepsilon_i^e + \varepsilon_i^\tau$$

One aspect of this program is the establishment of acceptable strain gradients for different element types. Between adjacent strain calculation points in one element, and probably over the entire element, a strain gradient would not be chosen that could encompass an elastic-plastic-elastic or a plastic-elastic-plastic variation. Therefore,

if

$$\varepsilon_i^e - \varepsilon_j^e \geq \mid 2\varepsilon_{yield} \mid,$$

remesh this element.

Additionally, there will be a change in sign. Therefore,

if

$$\frac{\varepsilon_i^t}{\varepsilon_j^t} < 0$$

remesh this element.

Once the nonlinear solution has been entered, the element level checks become more complex and more important. The total strain is now made up of the elastic strain, thermal strain, plastic strain, and creep strain:

$$\varepsilon_i = \varepsilon_i^e + \varepsilon_i^t + \varepsilon_i^\rho + \varepsilon_i^c$$

Now stress and strain are no longer linearly connected; stress is a function of elastic strain only. Once again, between any two adjacent calculation points within one element, an elastic strain gradient greater than the allowable material elastic gradient is not desirable. Thus,

if

$$\varepsilon_i^e - \varepsilon_j^e \geq \mid 2\varepsilon_{yield} \mid,$$

remesh this element. The limit on the thermal strain would still be retained.

If

$$\frac{\varepsilon_i^\tau}{\varepsilon_j^\tau} < 0, \text{ remesh this element.}$$

The next check is on the computed plastic and creep strain. No sign changes in either of these are allowed. In addition, a maximum gradient is set.

If

$$\frac{\varepsilon_i^\rho}{\varepsilon_j^\rho} < 0$$

or

$$\frac{\varepsilon_i^c}{\varepsilon_j^c} < 0$$

or

$$| \varepsilon_i^\rho - \varepsilon_j^\rho | > C_P$$

or

$$| \varepsilon_i^c - \varepsilon_j^c | > C_C,$$

remesh this element.

Next, proceed to the interelement level check. These are of the same nature as the above, but now involve adjacent calculation points in adjacent elements.

Our strategy for proceeding in this area consists of the following:
- Select an analytical model with known solutions.
- Use the "recipe procedure" to generate several meshes of different density.
- Use the 20-noded finite element to evaluate remeshing criteria.

For our first model, we selected a semi-infinite plate with a circular hole near the edge. The stress concentration solutions for this problem for various loadings is known. Figure 23 shows the recipe parameters and master region definition for this problem. Figure 24 is a master region generated for a particular case. Figures 25 and 26 show a coarse discretized model based on this master region breakdown. Figures 27 and 28 show a refined discretized model. With these models we will evaluate such correlative parameters as:

- Strain energy density
- Elemental stress/strain gradients
- Interelement stress/strain comparison
- Nodal stress comparison.

In order to evaluate these criteria, three models were created for the problem of a hole with an edge effect in a semi-infinite plate. These three models represent three different mesh densities. The first load case run was a constant membrane stress condition applied to the right-hand edge of the model with symmetric conditions on the left-hand edge. This case has been run for all three mesh densities using 2D plane stress elements. Figures 29, 30, and 31 are plots of the three models.

The objective of this evaluation is to determine if the interelement stress distribution can be used to "monitor" the adequacy of the mesh density. An additional objective is to compare various methods of approximating the surface stresses based on the stress output at the centroid of the elements. These two efforts are synergistic since a good measure of the mesh adequacy is the correct surface stress and the surface stress is certainly a function of the element stress distribution. There are two approaches to approximating the surface stress from 2D elements. The first extrapolates the elemental stresses to the surface. The second method uses the nodal displacement at the surface to compute the surface strain. This surface stress is then computed based on this strain and the appropriate material properties. Figure 32 shows the extrapolated stresses for each mesh density and the calculated stress based on strain. The vertical axis is stress and the horizontal axis is "wall thickness" which is the distance from the surface.

Master Region Model
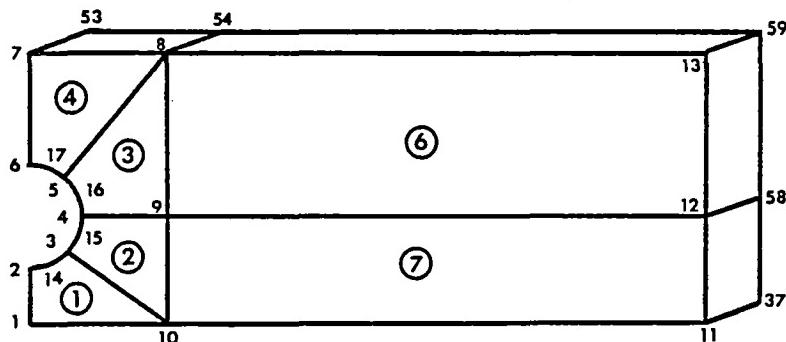
Parameters
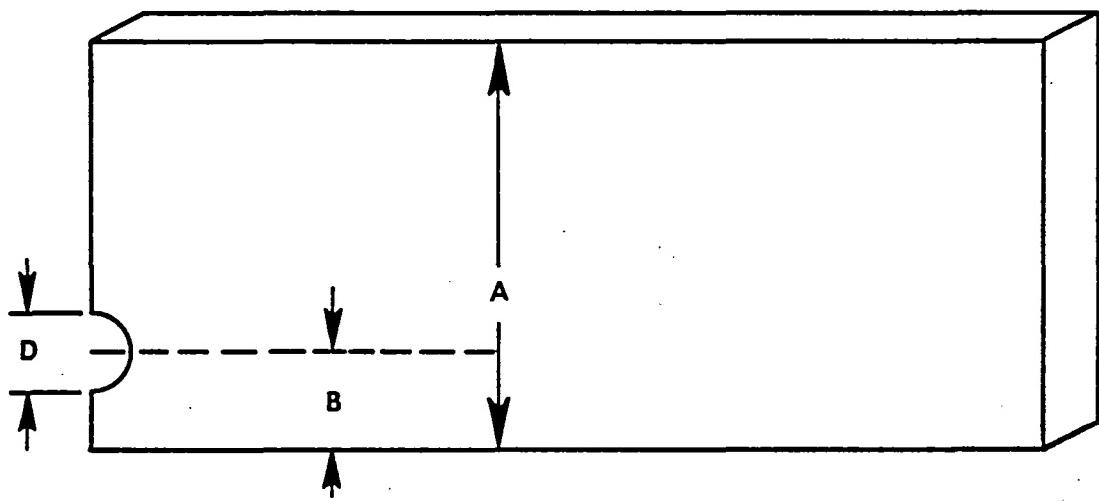
A = Height
B = Relative Placement of Center
    of Hole Relative to A
D = Diameter of Hole

Input: D as a Percentage of the Height
        B as a Percentage of the Height

Note: The Hole Cannot be Placed Beyond the
        Limits of the Beam

(Ex) Input = 20%, 23.334%
     Set a 0.2A Hole
          0.2334 A Center

Figure 23.   Recipe Parameters and Master Region Model for Plate
             With Hole.

74
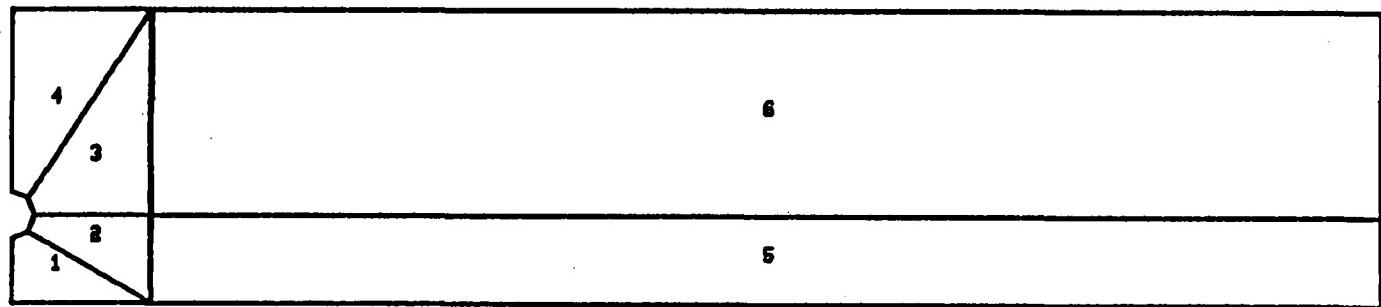
Figure 24. Generated Master Region.

AFMAP PLOT
UIEU X1,Y1,Z1,PHI   1.000   1.000   1.000   0
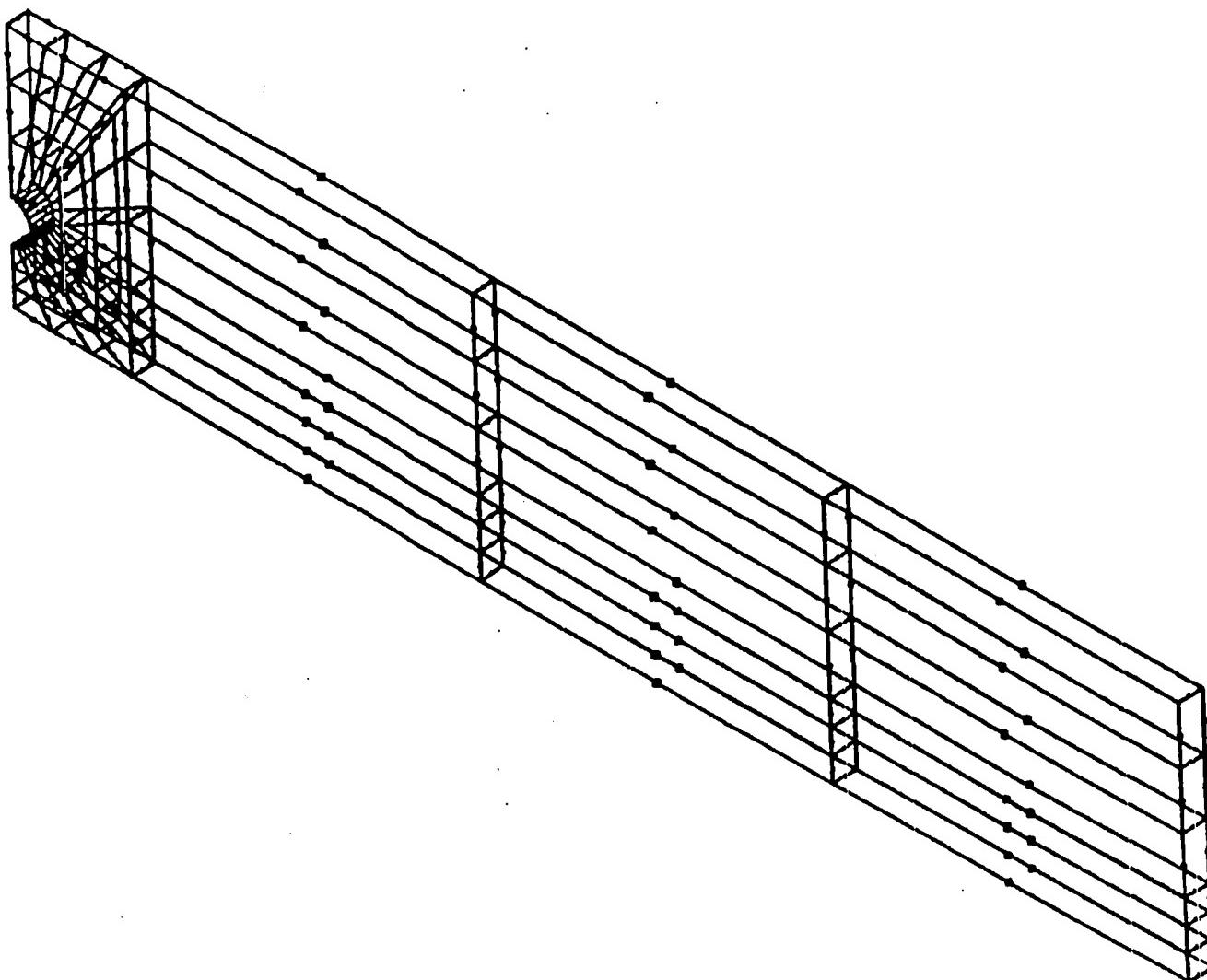
Figure 25.   Coarse Discretized Model.
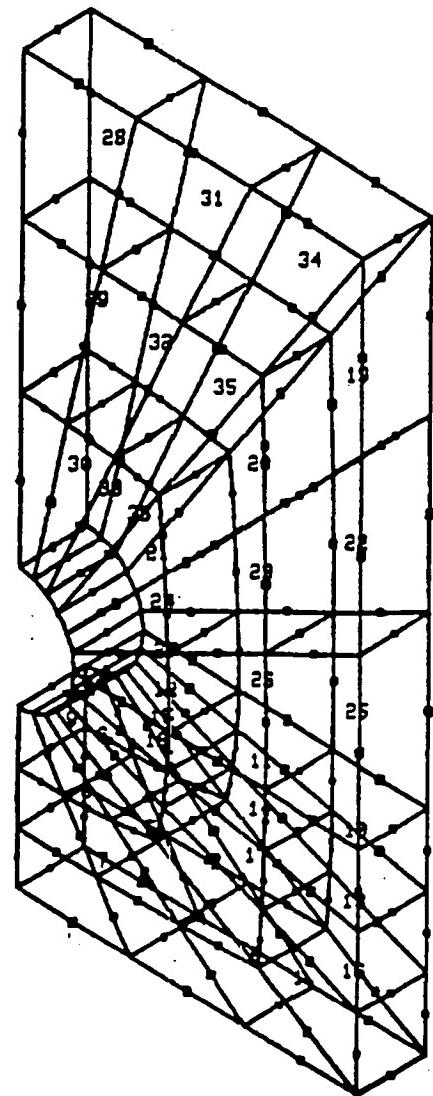
Figure 26. Magnification of Hole Region for Coarse Model.

AFMAP PLOT
UIEW X1,Y1,Z1,PHI   0.   0.   1.000   0
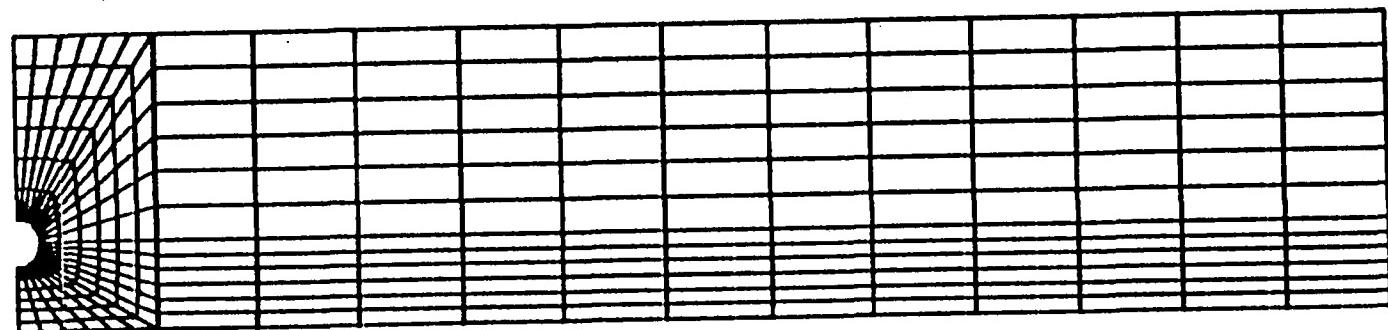
Figure 27.   Refined Discretized Model.
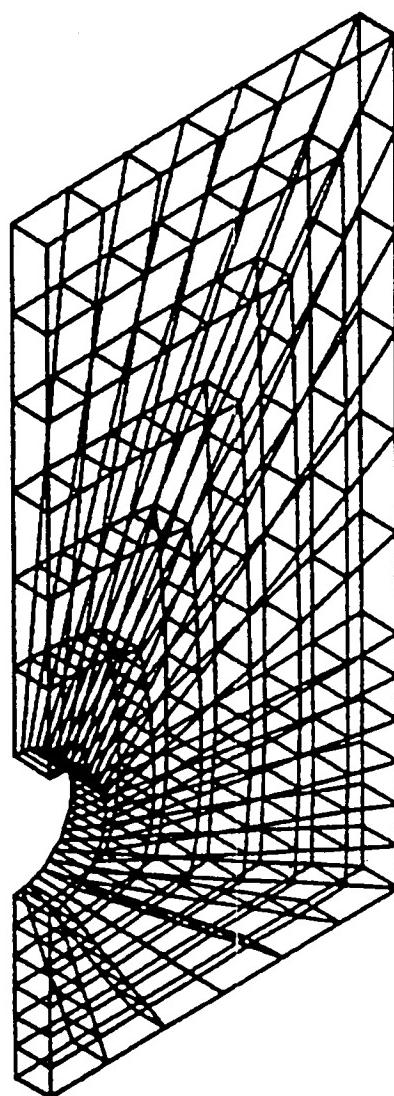
Figure 28.   Magnification of Hole Region of Refined Model.
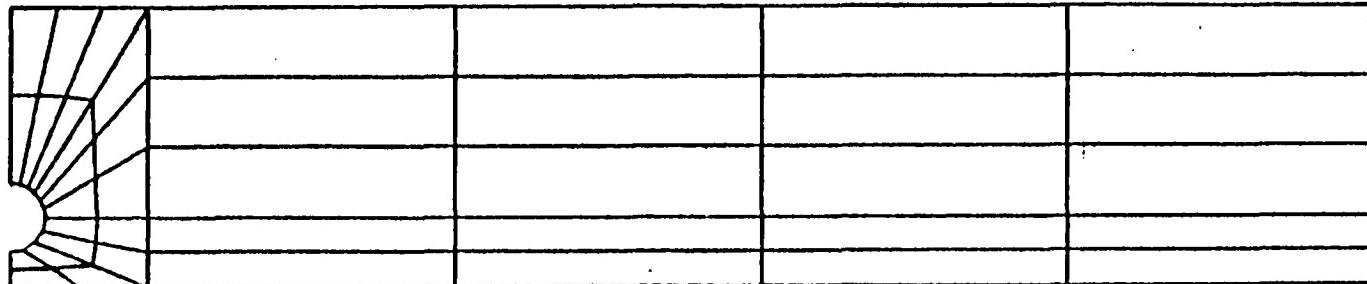
Figure 29. Coarse Mesh.
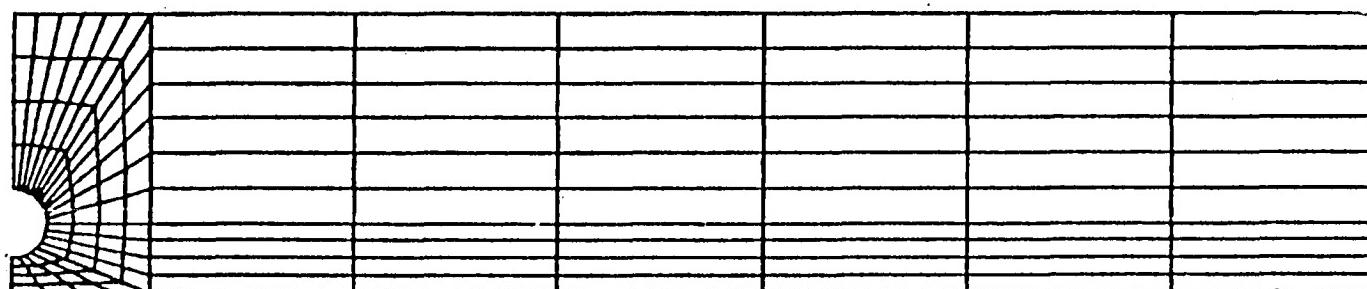
Figure 30. Medium Mesh.
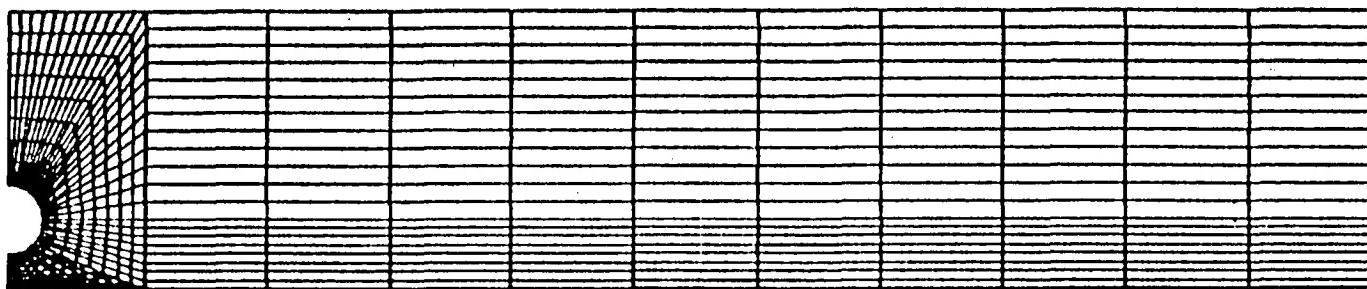
Figure 31. Fine Mesh.
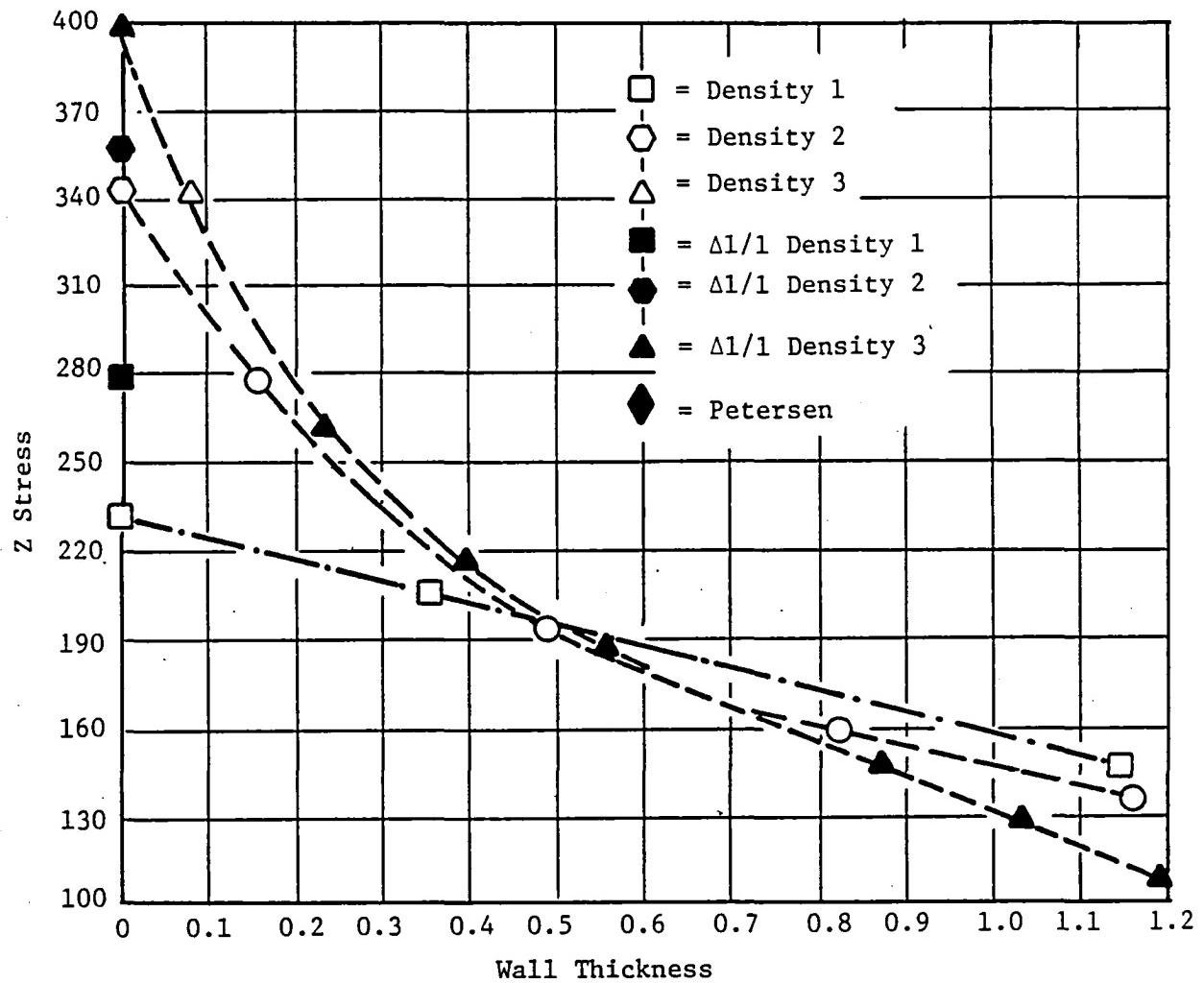
Figure 32.   Effect of Mesh Density on Stress Prediction.

The correct value obtained from Petersen is $K_t = 3.9$. Note that the two coarse meshes underestimate the surface stress using both the extrapolation method and the surface strain method. The fine mesh model underestimates very slightly, but gets almost the same answer by both techniques.

A fourth model was created and run for the tensile loading conditions. The basic geometrical model with the applied boundary conditions is shown in Figure 33. Also shown in Figure 33 are blow-ups of the mesh around the bottom of the hole for all fan mesh densities.

The interelement stress distribution has been evaluated for these four models by approximating the stresses at the nodal points. These nodal point stresses were computed by weighted averaging of the elemental centroid stresses. The weighting coefficient is inversely proportional to the distance between the centroid and the node point. The maximum difference of the stress at any node was computed as the maximum difference of any of the centroid stresses of elements adjacent to the node. The percent difference is a measure of the mismatch of nodal stress normalized by the local average stress. Figure 34 is a tabulation that represents the maximum difference and percent difference of nodal stress for seven points that are common in all four models. Notice that for all the points, the maximum stress difference and the percent difference decreases as the mesh density gets finer. This indicates that the percent difference could be used as a mesh refinement criteria. Further work is needed to determine if this criteria holds for other loadings and different models and to select the acceptable levels of the percent difference at which no further refinement is required.

Different loading conditions are being generated for these models. In addition, an 8-noded and 20-noded 3D model are also being created.

2.8.3 Self-Adaptive Solution Strategies

We have successfully developed and incorporated a dynamic time increment-ing scheme into a version of the two-dimensional nonlinear structural analysis program. The dynamic time incrementing technique is intended to provide for
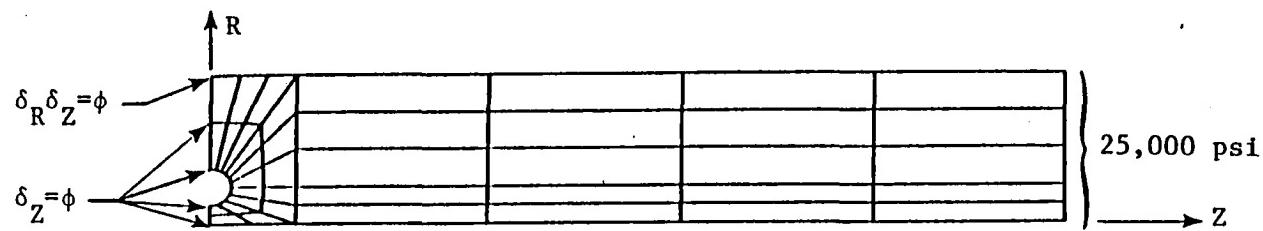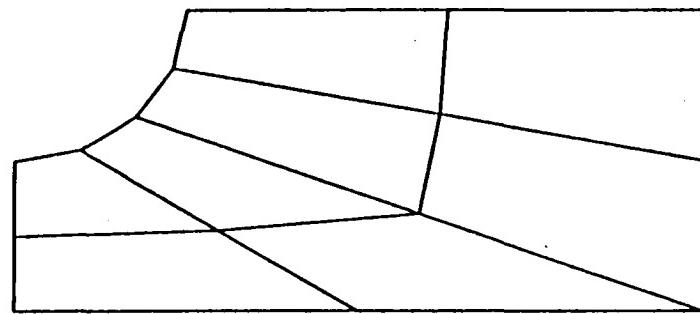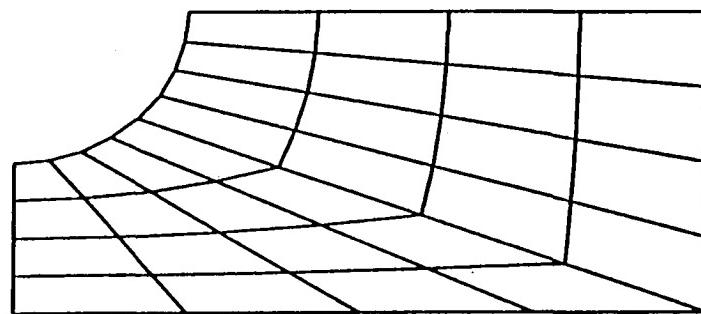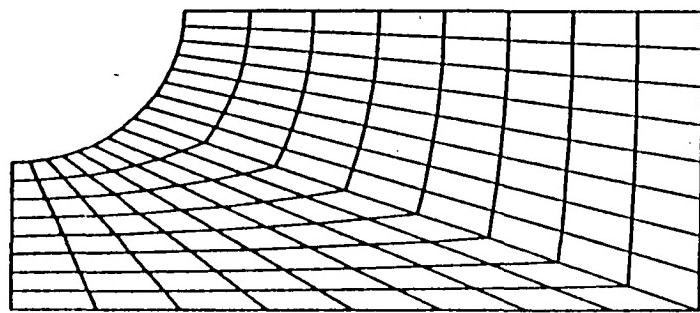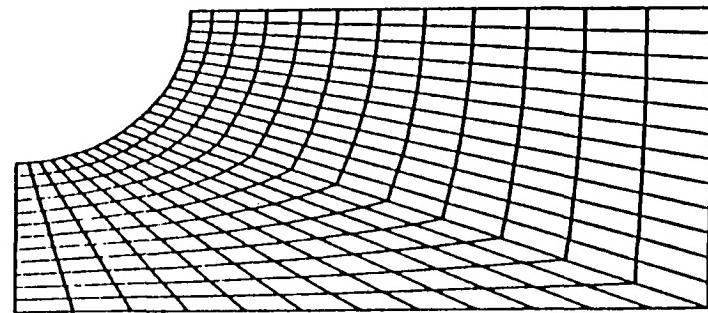
Figure 33. Problem Boundary Conditions and FEM Meshes.

Grid	1		2		3		4	
	σ_{Max} Diff ksi	$\frac{\sigma_{Max} \text{Diff}}{\sigma_{Avg}}$x100	σ_{Max} Diff ksi	$\frac{\sigma_{Max} \text{Diff}}{\sigma_{Avg}}$x100	σ_{Max} Diff ksi	$\frac{\sigma_{Max} \text{Diff}}{\sigma_{Avg}}$x100	σ_{Max} Diff ksi	$\frac{\sigma_{Max} \text{Diff}}{\sigma_{Avg}}$x100
A	71	42	58	30	42	20	34	15
B	46	42	38	37	26	30	20	35
C	29	38	19	26	11	15	8	11
D	46	53	28	33	16	19	11	13
E	46	41	18	16	11	9	8	7
F	83	55	29	20	12	8	7	4
G	58	33	34	20	22	12	16	9

Figure 34.   Results of the Effect of Mesh Density.

convergence and promote stability in the nonlinear iteration schemes currently being used.

In the analysis code, the constitutive model prepared by Bodner is being utilized to model time dependent inelastic flow. Bodner's model requires that constitutive equations be numerically integrated over finite time intervals. This procedure is iterative as is the method of solution we use to solve the finite element equations. The dynamic time incrementing scheme developed is specific to these methods.

In the implementation of the dynamic time incrementation scheme, the determination of an appropriate time increment can be computed three separate ways when the following simplified assumptions are made.

1. <u>Inelastic strain varies linearly with time</u> - This allows the time increment to be computed by limiting the maximum change in the inelastic strain that can occur during the time interval.

$$\Delta t_{i+1} = \Delta t_i \frac{(\Delta \varepsilon_e^I)_{allowable}}{(\Delta \varepsilon_e^I)_{max}}$$

where,

Δt_{i+1} = next time subincrement

Δt_i = current time subincrement

$(\Delta \varepsilon_e^I)_{max}$ = maximum inelastic strain increment occurring in the current time step

$(\Delta \varepsilon_e^I)_{allowable}$ = maximum allowable inelastic strain increment. User input or set to default value.

2. <u>Stress varies linearly with time</u> - This allows the time increment to be computed by limiting the maximum change in stress that can occur during the time interval.

$$\Delta t_{i+1} = \Delta t_i \frac{(\Delta \delta_e)_{allowable}}{(\Delta \delta_e)_{max}}$$

where

$(\Delta\delta_e)_{max}$ = maximum change in stress occurring in the current time step

$(\Delta\delta_e)_{allowable}$ = maximum allowable stress change. User input or set to default value.

3. <u>Control integration error</u> - This allows for the control of the local integration error when computing the inelastic strain during the time increment. The local integration error is not allowed to exceed a predefined tolerance.

$$\Delta t_{i+1} = \left[\frac{12*TOL + (\Delta\varepsilon^I)_{allowable}}{\overset{...I}{\varepsilon}_i}\right]^{1/3}$$

where,

TOL = user input

$\overset{...I}{\varepsilon}$ = second derivative of the inelastic strain rate.

The results in Table XXIII help illustrate the utility and stability of the dynamic time incrementing technique. In the generation of Table XXIII we illustrate the effect on creep response of Inco 100 when we control the maximum allowable inelastic strain $(\Delta\varepsilon^I)$ and the maximum allowable stress $(\Delta\sigma)$ that can occur during any time increment.

We have included in our nonlinear analysis code an alternate method for determining convergence of the numerical solution. A global Euclidian norm was defined as follows:

$$\frac{\left|\sum_{j=1}^{N}(\theta_j^i)^2\right| - \left|\sum_{j=1}^{N}(\theta_j^{i-1})^2\right|}{\left|\sum_{j=1}^{N}(\theta_j^i)^2\right|} \leq Tolerance$$

N = No. of structural DOF

i = Iteration No.

Table XXIII. Stability of Dynamic Time Incrementing.

Material Constants

$E = 21.3E6$ psi
$D = 10^4$ Sec^{-1}
$N = .7$
$Z_0 = 915$ ksi
$Z_1 = 1015$ ksi
$Z_2 = 600$ ksi
$A = 0.0019$ Sec^{-1}
$r = 2.66$

(a). Strain Control.

σ	130	130	130
#t	126	628	5751
# Iteration	252	1256	11502
$\Delta\sigma$	4000	4000	2000
ΔE^I	.001	.0001	.00001
CPU/SNUB	14.37/4U38	58.44/4U040	504.6/4U260

t	E_T	E^I	E_T	E^I	E_T	E^I
10 sec.	6136	33	6136	33	6136	33
5 min.	12059	5956	12060	5956	12060	5957
10	16034	9931	16039	9936	16039	9936
15	19958	13855	19964	13861	19964	13861
20	23880	17777	23886	17782	23886	17783
25	27802	21699	27808	21704	27808	21705
30	31724	25621	31730	25626	31730	25627
35	35646	29543	35651	29548	35652	29548
40	39568	33465	39573	33470	39574	33470
45	43490	37386	43495	37392	43496	37392
50	47412	41308	47417	41314	47417	41314
55	51333	45230	51339	45235	51339	45236
60	55255	49152	55261	49157	55261	49158
65	59177	53074	59182	53079	59183	53080
70	63099	56966	63104	57001	63105	57001

(b). Stress Control.

σ	130	130	130
#t	117	126	152
# Iteration	234	252	304
$\Delta\sigma$	6000	4000	2000
ΔE^I	.001	.001	.001
CPU/SNUB	13.76/4U464	14.37/4U938	16.96/4U406

t	E_T	E^I	E_T	E^I	E_T	E^I
10 sec.	6138	35	6136	33	6135	32
5 min.	12059	5956	12059	5956	12059	5956
10	16034	9931	16034	9931	16034	9931
15	19959	13855	19958	13855	19958	13855
20	23881	17777	23880	17777	23880	17777
25	27803	21699	27802	21699	27802	21699
30	31724	25621	31724	25621	31724	25621
35	35646	29543	35646	29543	35646	29543
40	39568	33465	39568	33465	39568	33464
45	43490	37387	43490	37386	43490	37386
50	47412	41309	47412	41308	47411	41308
55	51334	45230	51333	45230	51333	45230
60	55256	49152	55255	49152	55255	49152
65	59177	53074	49177	53074	59177	53074
70	63099	56966	63099	56966	63099	56996

Convergence is assumed when the difference in the norm of the unknowns (displacements in this instance) is less than or equal to some predefined tolerance. This concept represents a global test of convergence rather than a local or point-by-point method as we currently use.

The model presented for illustration of such a technique is presented in Figure 35. Linear springs are used to connect nodes along the crack face and theoretically should carry no load when the crack has opened. The displacements of several nodes on this face are followed and presented in the following tables. The true elastic solution for such a model is located in the first column of each table and represents the solution attained when an infinitesimal tolerance is prescribed for convergence. For this model all stresses remain in the elastic region and no time-dependent material behavior is assumed.

For the model shown, a study was conducted to determine the quality of solution obtained when either a global or a local convergence criteria was used. Tables XXIV and XXVI are the results of utilizing local criteria and Table XXV when the global criteria is used. Attention should be directed to the number of iterations for solution as well as the quality of the solution.

We are continuing the effort to incorporate such concepts into our finite element code and evaluate their applicability to self-adaptive solution strategies currently under development. Our current work has focused upon vector norms due to their direct applicability and the ease with which they can be computed. The definition of the vector norm is essential to the development of techniques in error analysis for the vector norm provides the means by which quantitative and comparative statements of size and distance can be made between associated vectors. The theory and development of vector and matrix norms can be found in most texts on numerical methods and only the necessary concepts are presented here.

The norm of an "N" dimensional vector is written as $\|\overline{X}\|$, and represents a single number. The norm is a function of all the elements in $\overline{X}$ and should not be confused with the definition of the vector (Euclidian) length $|\overline{X}|$. The norm of $\overline{X}$ satisfies the following conditions:
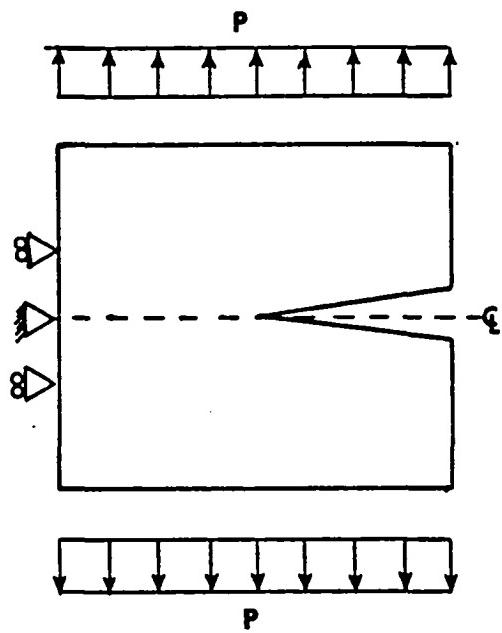
Figure 35. Cycle Crack Growth Model.

Table XXIV. Displacement Tolerance Criteria.

Node No.	Elastic	10^{-4}	10^{-5}	10^{-6}
50	0.9224	0.8905	0.919	0.922
61	1.575	1.518	1.569	1.575
71	2.1557	2.075	2.147	2.155
80	2.7001	2.595	2.689	2.70
90	3.219	3.091	3.205	3.217
100	3.719	3.566	3.703	3.718
No of Iterations to Convercence		(13)	(22)	(31)
All Displacements ($X10^{-3}$)				

Table XXV. Global Euclidian Criteria.

Node #	Elastic	10%	5%	1%
50	0.9224	0.8362	0.8815	0.9152
61	1.5750	1.4211	1.5021	1.5624
71	2.1557	1.9366	2.0571	2.1374
80	2.7001	2.4172	2.5658	2.6766
90	3.2190	2.8723	3.0544	3.1901
100	3.7190	3.3061	3.5233	3.6851
No. of Iterations to Convergence		(9)	(12)	(19)
All Displacements (X10^{-3})				

Table XXVI. Percentage Change Criteria.

Node #	Elastic	10%	5%	1%
50	0.9224	0.9193	0.9193	0.9174
61	1.575	1.5685	1.5685	1.5661
71	2.1557	2.1429	2.1429	2.142
80	2.7001	2.6778	2.6778	2.6814
90	3.219	3.1868	3.1868	3.1951
100	3.719	3.6768	3.6768	3.6901
No. of Iterations to Convergence		(8)	(8)	(9)
All displacements (X10^{-3})				

1. $\|\overline{X}\| \geq 0$ and $\|\overline{X}\| = 0$ if and only if $\overline{X} = \overline{N}$

   where $\overline{N}$ is the null vector

2. $\|\alpha\overline{X}\| = |\alpha| \, \|\overline{X}\|$ for all scales α and
   vectors $\overline{X}$

   $\|\overline{X+Y}\| \geq \|\overline{X}\| + \|\overline{Y}\|$ for all vectors $\overline{X}$ and $\overline{Y}$

There can be defined infinitely many norms but the three most common norms are the ℓ_p norms $\| \cdot \|_P$ for $P = 1, 2,$ and ∞.

$$\| \cdot \|_1 = |\overline{X}_1| + |\overline{X}_2| + |\overline{X}_3| + \ldots \ldots |\overline{X}_N|$$

$$\| \cdot \|_2 = \left[|\overline{X}_1|^2 + |\overline{X}_2|^2 + |\overline{X}_3|^2 + \ldots \ldots |\overline{X}_N|^2 \right]^{1/2}$$

$$\| \cdot \|_\infty = \max \left\{ |\overline{X}_1|, |\overline{X}_2|, |\overline{X}_3|, \ldots \ldots |\overline{X}_N| \right\}$$

The above norms are special cases of the vector norm:

$$\left(\sum_{i=1}^{N} (\overline{X}_i)^P \right)^{1/P}$$

To utilize the norms defined above the concept of relative and absolute error can be defined (1) for any two vectors, the absolute error can be written as:

$$E^A = \|\overline{X}_i\| - \|\overline{X}_{i-1}\|$$

And the relative error written as:

$$E^R = \frac{\|\overline{X}_i\| - \|\overline{X}_{i-1}\|}{\|\overline{X}_{i-1}\|}$$

The expression for relative error tends to be far more applicable to our needs and its structure lends itself conveniently to the formulation of convergence

criteria in iterative methods. When compared to a predefined tolerance, the relative error reflects the percentage change that has occurred.

To simplify the task of evaluating new convergence criteria, we have chosen to limit the present study to a class of problems that exhibit only geometric nonlinearity. We will use the nodal displacement as the control vector for which we compute the assorted vector norms, assemble the error expressions, and hopefully determine convergence. Noting that our solution scheme is an iterative technique, we are looking for the convergence of a series of vectors. For our application it is necessary to determine when a solution has been obtained as well as to determine the quality of the computed solution.

Convergence of the numerical solution can be determined on either the local or global level. Currently within our code we use a local or point-by-point method and the present work represents an effort to see if a global scheme has applicability. Six separate convergence criteria were generated from the error expressions mentioned above and represent those most commonly used in the literature.

$$1. \quad \frac{\|\overline{x}_i\|_1 - \|\overline{x}_{i-1}\|_1}{\|\overline{x}_{i-1}\|_1} \qquad\qquad 2. \quad \frac{\|\overline{x}_i\|_1 - \|\overline{x}_{i-1}\|_1}{\|\overline{x}_1\|_1}$$

$$3. \quad \frac{\|\overline{x}_i\|_2 - \|\overline{x}_{i-1}\|_2}{\|\overline{x}_{i-1}\|_2} \qquad\qquad 4. \quad \frac{\|\overline{x}_i\|_2 - \|\overline{x}_{i-1}\|_2}{\|\overline{x}_1\|_2}$$

$$5. \quad \frac{\|\overline{x}_i\|_\infty - \|\overline{x}_{i-1}\|_\infty}{\|\overline{x}_{i-1}\|_\infty} \qquad\qquad 6. \quad \frac{\|\overline{x}_i\|_\infty - \|\overline{x}_{i-1}\|_\infty}{\|\overline{x}_1\|_\infty}$$

In the above expressions, the subscripts are indicative of the iteration used.

The model presented for the illustration of global convergence criteria is presented in Figure 35. This model is that presented in the March and April narratives. Linear springs are used to connect the nodes along the crack face and theoretically should carry no load when the crack has opened. We have limited ourselves to small strain/small displacements to reduce our test matrix.

The results of our work are presented in Tables XXVII, XXVIII, and XXIX. During each iteration the assorted vector norms are computed and the necessary error terms are formed. In all instances the solution has terminated when a local convergence criteria had been satisfied. The local criteria states that convergence can be assumed when during any iteration less than 0.5% change has occurred in the local displacement. As can be noted in the tables, the measure of relative error is in excellent agreement with the measure of local convergence and thus the expression of relative error has potential application in our work as a measure of convergence when small displacement/small strain problems are encountered.

Table XXVII. Utilization of $L_{(1)}$ Vector Norms.

Iterations	Absolute Error $\|\bar{V}_i\| - \|\bar{V}_{i-1}\|$	Relative Error $\dfrac{\|\bar{V}_i\| - \|\bar{V}_{i-1}\|}{\|\bar{V}_{i-1}\|}$	Relative Error $\dfrac{\|\bar{V}_i\| - \|\bar{V}_{i-1}\|}{\|\bar{V}_i\|}$
3	0.403030E-02	0.268721E 00	0.403030E 00
4	0.318589E-02	0.166441E 00	0.341290E 00
5	0.249554E-02	0.111846E 00	0.267334E 00
6	0.195128E-02	0.784618E-01	0.209031E 00
7	0.152432E-02	0.569722E-01	0.163294E 00
8	0.119919E-02	0.422954E-01	0.127500E 00
9	0.929067E-03	0.316458E-01	0.995202E-01
10	0.725017E-03	0.239712E-01	0.776677E-01
11	0.565730E-03	0.192889E-01	0.606040E-01
12	0.441403E-03	0.148639E-01	0.472855E-01
13	0.344368E-03	0.187724E-01	0.368906E-01
14	0.268678E-03	0.933461E-02	0.287822E-01
15	0.209589E-03	0.741137E-02	0.224523E-01
16	0.163509E-03	0.475493E-02	0.175159E-01

Table XXVIII. Utilization of $L_{(2)}$ Vector Norms.

Iterations	Absolute Error $\|\bar{V}_i\| - \|\bar{V}_{i-1}\|$	Relative Error $\dfrac{\|\bar{V}_i\| - \|\bar{V}_{i-1}\|}{\|\bar{V}_{i-1}\|}$	Relative Error $\dfrac{\|\bar{V}_i\| - \|\bar{V}_{i-1}\|}{\|\bar{V}_i\|}$
3	0.371980E-01	0.285964E 00	0.382371E 00
4	0.315477E-01	0.172524E 00	0.307744E 00
5	0.247281E-01	0.115255E 00	0.241220E 00
6	0.192872E-01	0.869854E-01	0.188144E 00
7	0.151037E-01	0.584852E-01	0.147334E 00
8	0.118487E-01	0.435963E-01	0.115583E 00
9	0.924242E-02	0.322419E-01	0.901586E-01
10	0.722271E-02	0.243764E-01	0.704566E-01
11	0.564067E-02	0.185682E-01	0.550182E-01
12	0.439950E-02	0.142235E-01	0.429165E-01
13	0.343170E-02	0.109411E-01	0.334758E-01
14	0.267746E-02	0.844391E-02	0.261144E-01
15	0.208808E-02	0.653173E-02	0.203690E-01
16	0.162887E-02	0.506257E-02	0.158894E-01

Table XXIX. Utilization of $L_{(3)}$ Vector Norms.

Iterations	Absolute Error $\|\bar{V}_i\| - \|\bar{V}_{i-1}\|$	Relative Error $\dfrac{\|\bar{V}_i\| - \|\bar{V}_{i=1}\|}{\|\bar{V}_{i-1}\|}$	Relative Error $\dfrac{\|\bar{V}_i\| - \|\bar{V}_{i=1}\|}{\|\bar{V}_i\|}$
3	0.710577E-03	0.277796E 00	0.430516E 00
4	0.554693E-03	0.169667E 00	0.336071E 00
5	0.432763E-03	0.113170E 00	0.262198E 00
6	0.337589E-03	0.793064E-01	0.204534E 00
7	0.263337E-03	0.573175E-01	0.159548E 00
8	0.205415E-03	0.422866E-01	0.124455E 00
9	0.160228E-03	0.316462E-01	0.970771E-01
10	0.124988E-03	0.239288E-01	0.757264E-01
11	0.974963E-04	0.182293E-01	0.596699E-01
12	0.760492E-04	0.139647E-01	0.466758E-01
13	0.593200E-04	0.107427E-01	0.359401E-01
14	0.462757E-04	0.829138E-02	0.280376E-01
15	0.360952E-04	0.641412E-02	0.218689E-01
16	0.281566E-04	0.497154E-02	0.170592E-01

APPENDIX A

TASK II - DESIGN OF STRUCTURAL ANALYSIS
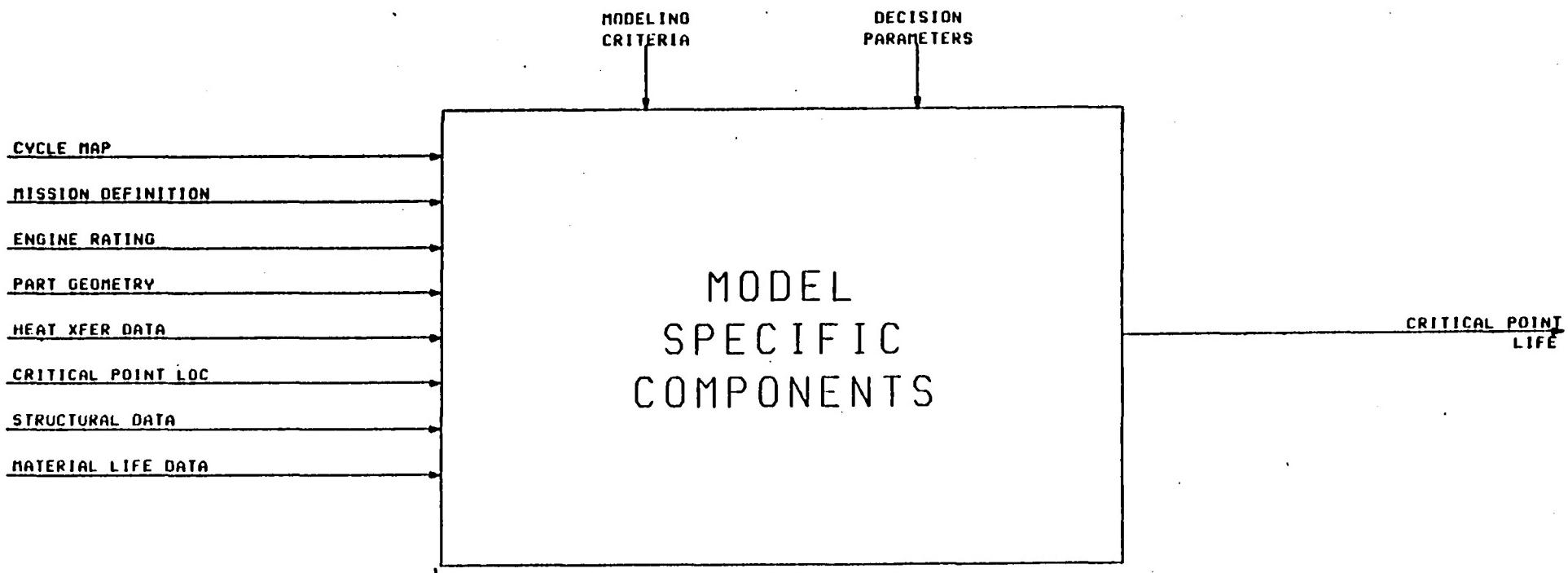
SOFTWARE ARCHITECTURE

MODELING
CRITERIA

DECISION
PARAMETERS

CYCLE MAP

MISSION DEFINITION

ENGINE RATING

PART GEOMETRY

HEAT XFER DATA

CRITICAL POINT LOC

STRUCTURAL DATA

MATERIAL LIFE DATA

MODEL SPECIFIC COMPONENTS

CRITICAL POINT
LIFE

97

COSMOS - CONTEXT

A-0

Model Specific Component

A4

REVISION- 1

7-22-83

66

100
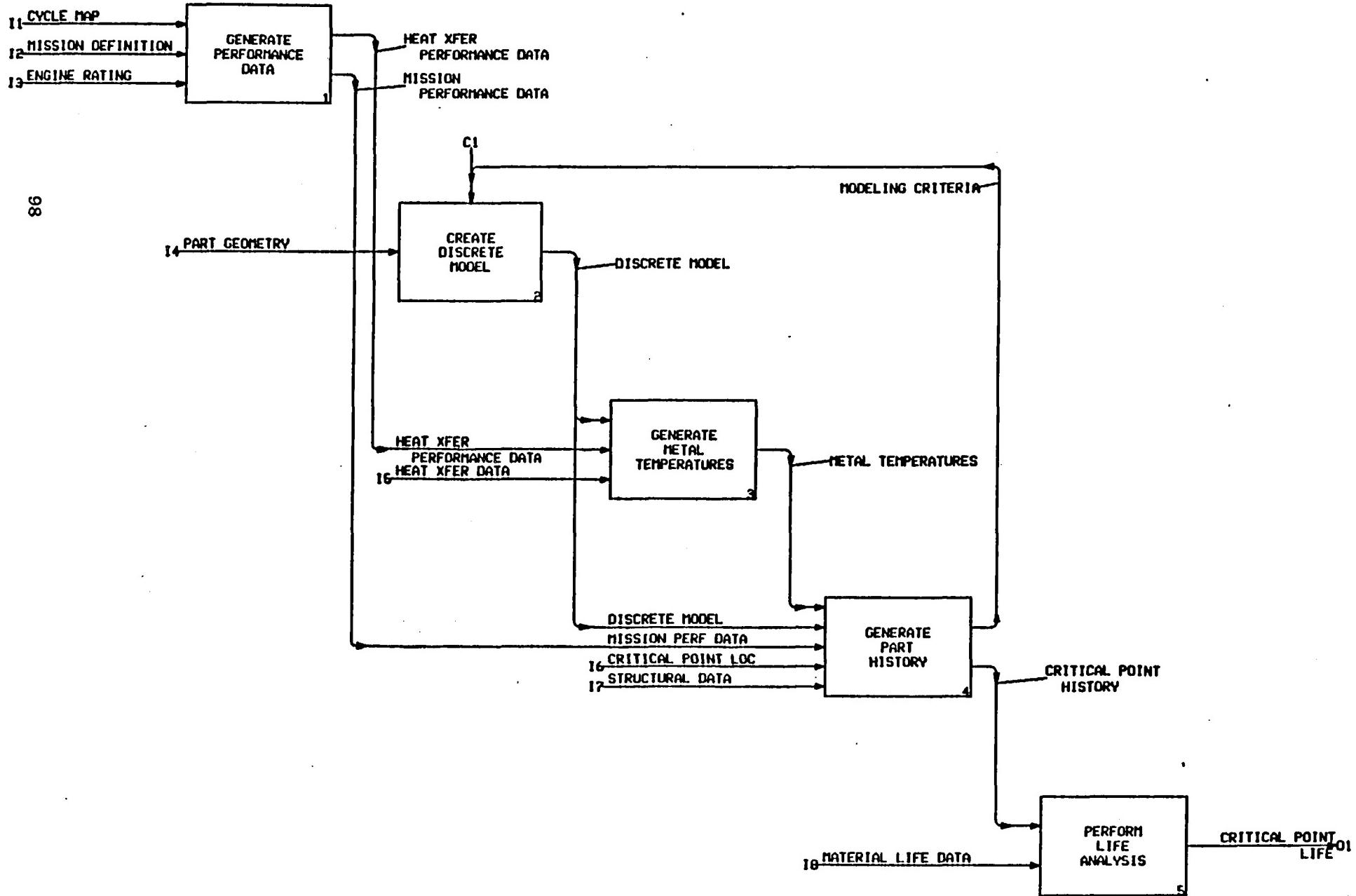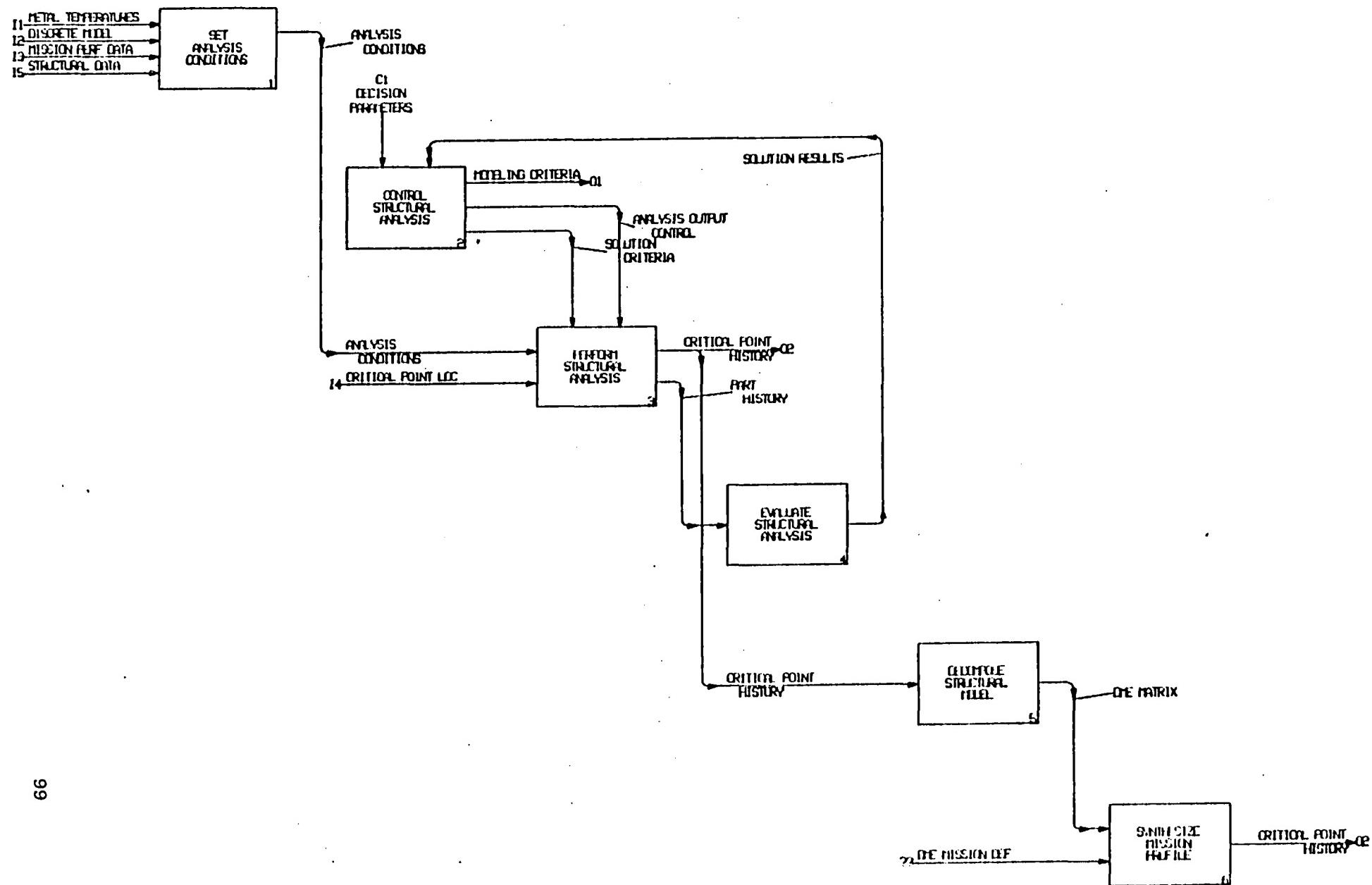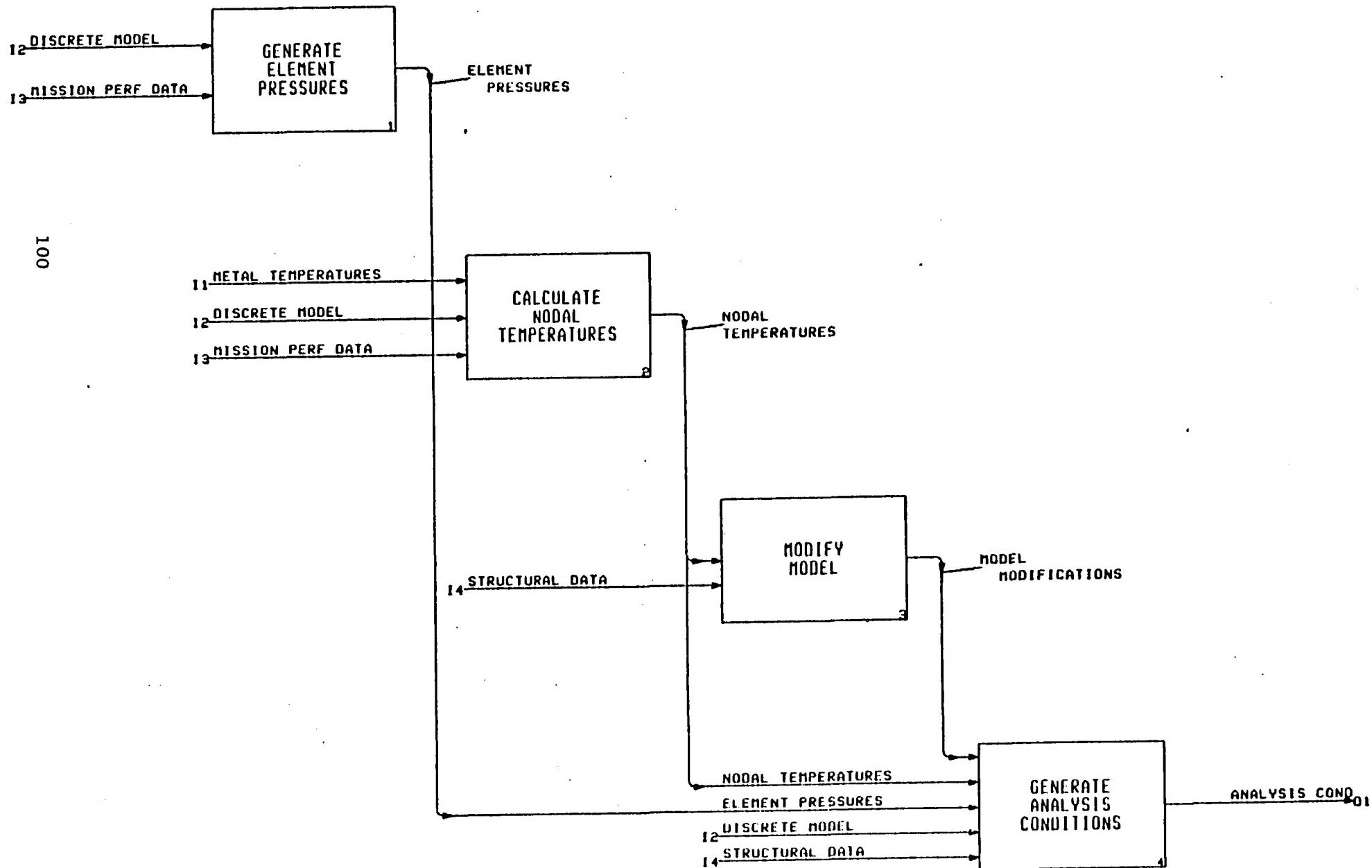
SET ANALYSIS CONDITIONS

A4.1
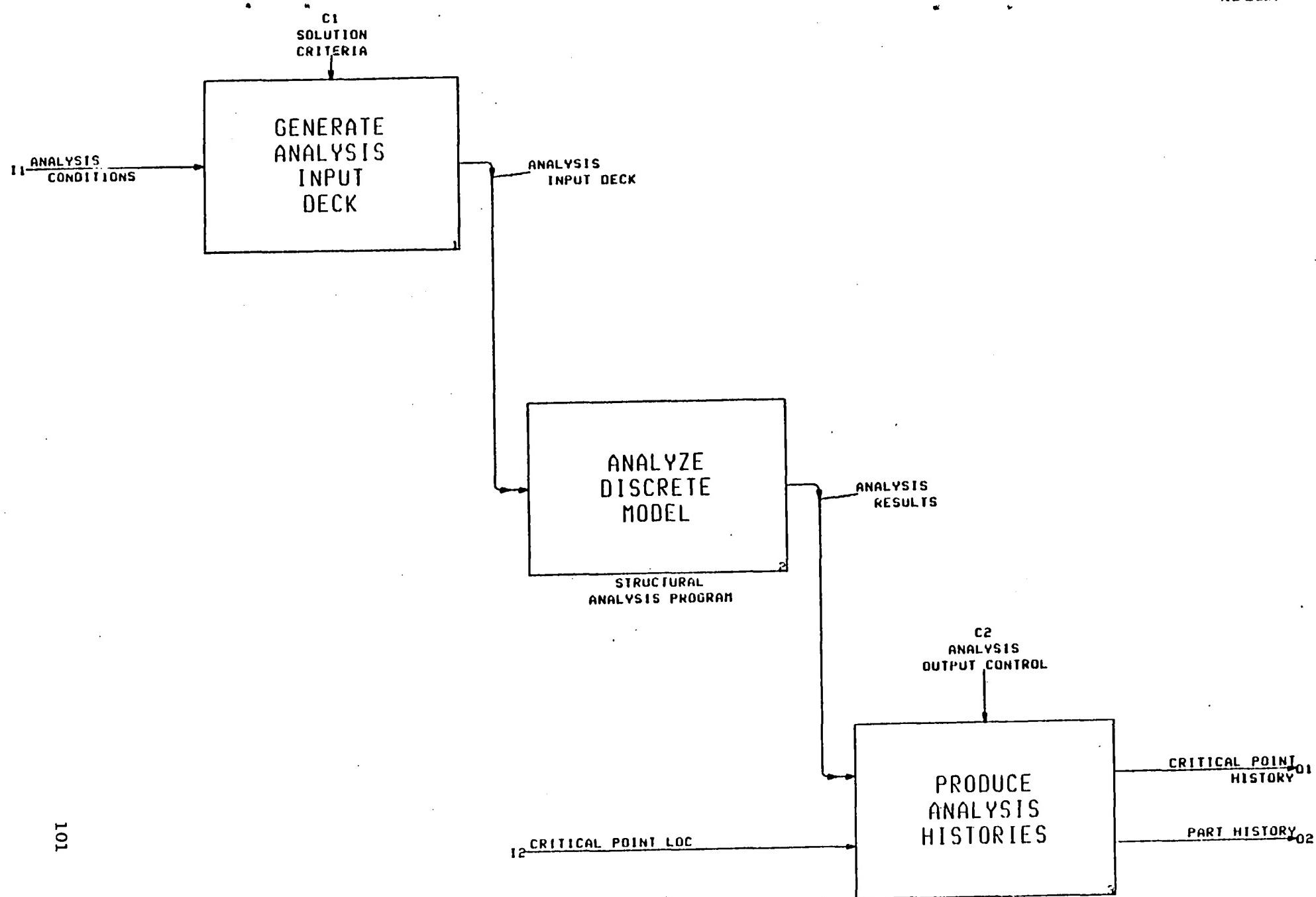
PERFORM STRUCTURAL ANALYSIS

A4.3

REVISION- 1

0-10-83
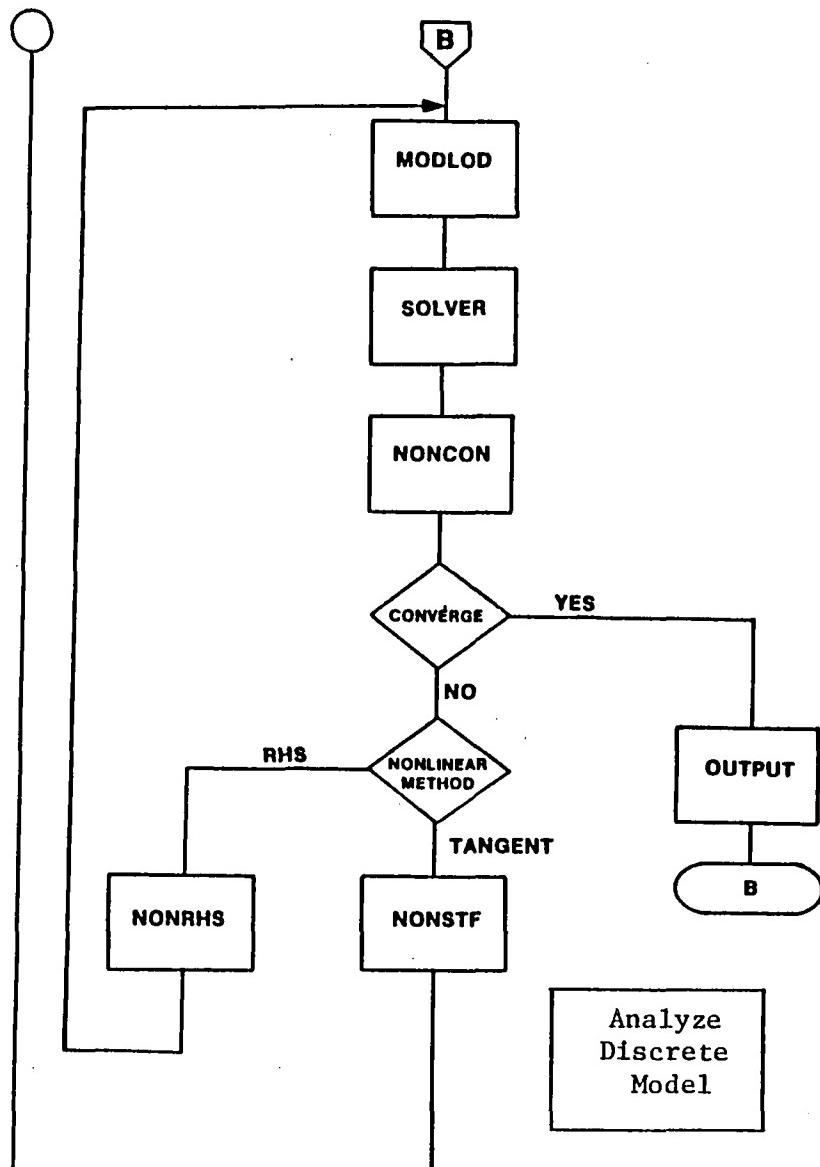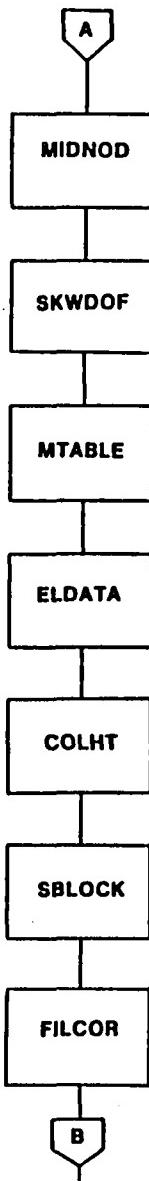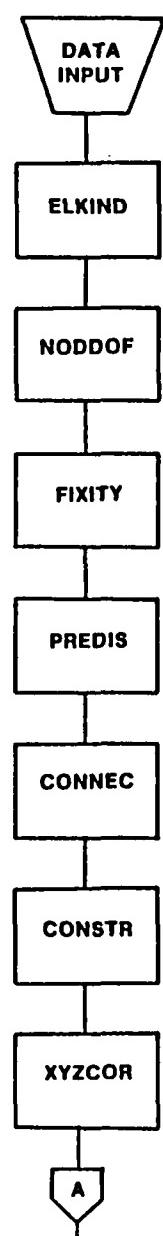
Structural
Analysis Program

PREPROCESSOR ATTRIBUTES:

    A.   SOFTWARE
- Modular in Structure
- Machine Independent
- Low Core Requirement
- Extensive Documentation

    B.   FEATURES/OPERATION
- User Friendly
- Extensive Diagnostics
- Complete Data Summary
- Interactive Graphics
  - Model Geometry
  - Material Physical Properties
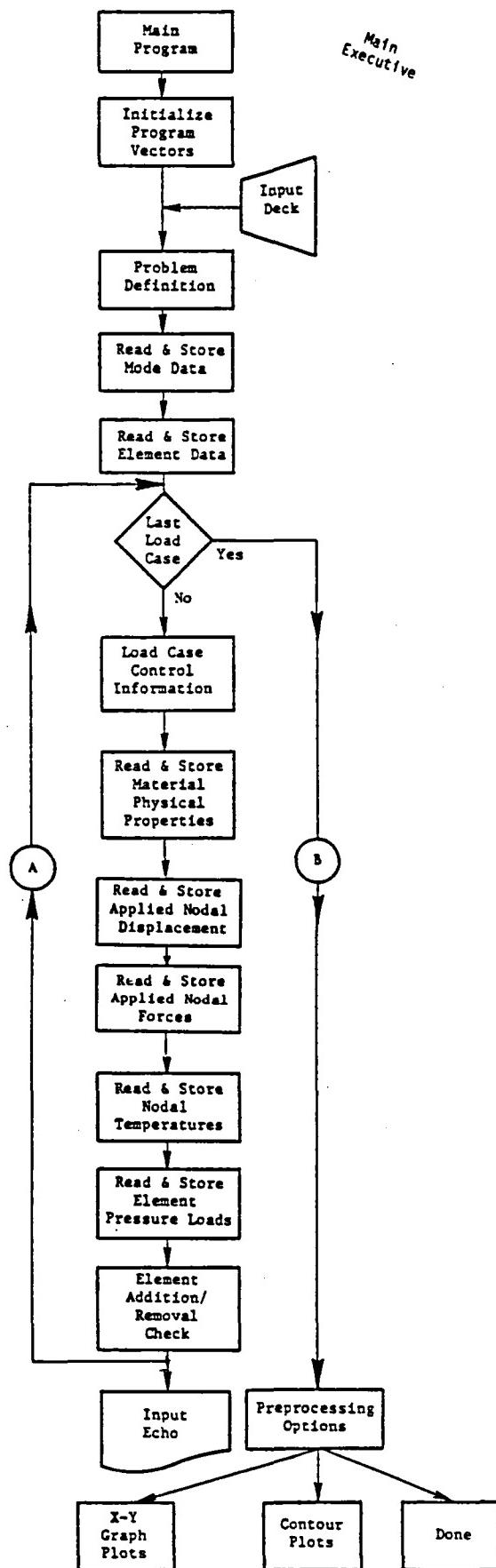
POSTPROCESSOR ATTRIBUTES:

A.   SOFTWARE
   ●   Modular in Structure
   ●   Machine Independent
   ●   Low Core Requirement
   ●   Extensive Documentation

B.   FEATURES/OPERATION
   ●   User Friendly
   ●   Will Function in Batch or Time-Share Environment
   ●   Will Have Extensive Graphics Capabilities
       -   X-Y Graph Plots
       -   Contour and Deflected Shape Plots at Defined Planes
   ●   Will Have Built-in Data Manipulation Routines (User Controlled)
       -   User Friendly Data Base

```
                    ┌──────────────┐
                    │    Main      │
                    │  Executive   │
                    └──────┬───────┘
                           │
                           ▼
                    ┌──────────────┐
                    │  Initialize  │
                    │   Program    │        ╱────────────╲
                    │   Vectors    │        │   Input    │
                    └──────┬───────┘        │  File(s)   │
                           │                ╲────────────╱
                           ▼                      │
                        ╱─────╲                   │
                       ╱ Create ╲                 │
                      ╱  Data    ╲◄───────────────┘
                      ╲  Files   ╱────────────────────────────────┐
                       ╲        ╱   No                            │
                        ╲──┬──╱                                   │
                           │ Yes                                  │
                           ▼                                      │
                    ┌──────────────┐                              │
                    │   Problem    │                              │
                    │   Sizing     │                              │
                    │ Information  │                              │
                    └──────┬───────┘                              │
                           ▼                                      │
                    ┌──────────────┐                              │
                    │ Read & Store │                              │
                    │  Node Data   │                              │
                    └──────┬───────┘                              │
                           ▼                                      │
                    ┌──────────────┐                              │
           ┌───────►│ Read & Store │                              │
           │        │ Element Data │                              │
           │        └──────┬───────┘                              │
           │               ▼                                      │
           │            ╱─────╲                                   │
           │           ╱ Last  ╲                                  │
           │          ╱  Load   ╲   Yes                           │
           │          ╲  Case    ╱──────────┐                     │
           │           ╲        ╱            │                    │
           │            ╲──┬──╱              │                    │
           │               │ No             │                    │
           │               ▼                │                    │
           │        ┌──────────────┐        │                    │
          ╱─╲       │ Read & Store │       ╱─╲                  ╱─╲
         │ A │      │Material Data │      │ B │                │ C │
          ╲─╱       └──────┬───────┘       ╲─╱                  ╲─╱
           ▲               ▼                │                    │
           │        ┌──────────────┐        │                    │
           │        │ Read & Store │        │                    │
           │        │    Nodal     │        │                    │
           │        │Displacements │        │                    │
           │        └──────┬───────┘        │                    │
           │               ▼                │                    │
           │        ┌──────────────┐        │                    │
           │        │ Read & Store │        │                    │
           │        │   Element    │        │                    │
           └────────│   Results    │        │                    │
                    └──────────────┘        ▼                    ▼
                                     ┌──────────────┐
                                     │Postprocessing│
                                     │  Operations  │
                                     └──────┬───────┘
              ┌─────────────────────────────┼──────────────────────┐
              ▼                              ▼                      ▼
      ┌──────────────┐              ┌──────────────┐        ┌──────────────┐
      │  Graphical   │              │ Calculation  │        │    Done      │
      │   Display    │              │   Options    │        │              │
      └──────┬───────┘              └──────┬───────┘        └──────────────┘
     ┌───────┼────────┐              ┌─────┴───────┐
     ▼       ▼        ▼              ▼             ▼
┌─────────┐┌────────┐┌─────────┐┌──────────┐┌─────────────┐
│X-Y Graph││Deflected││ Contour │││  Life    ││    Data     │
│  Plots  ││ Shape  ││  Plots  │││Prediction││ Manipulation│
└─────────┘└────────┘└─────────┘└──────────┘└─────────────┘
```
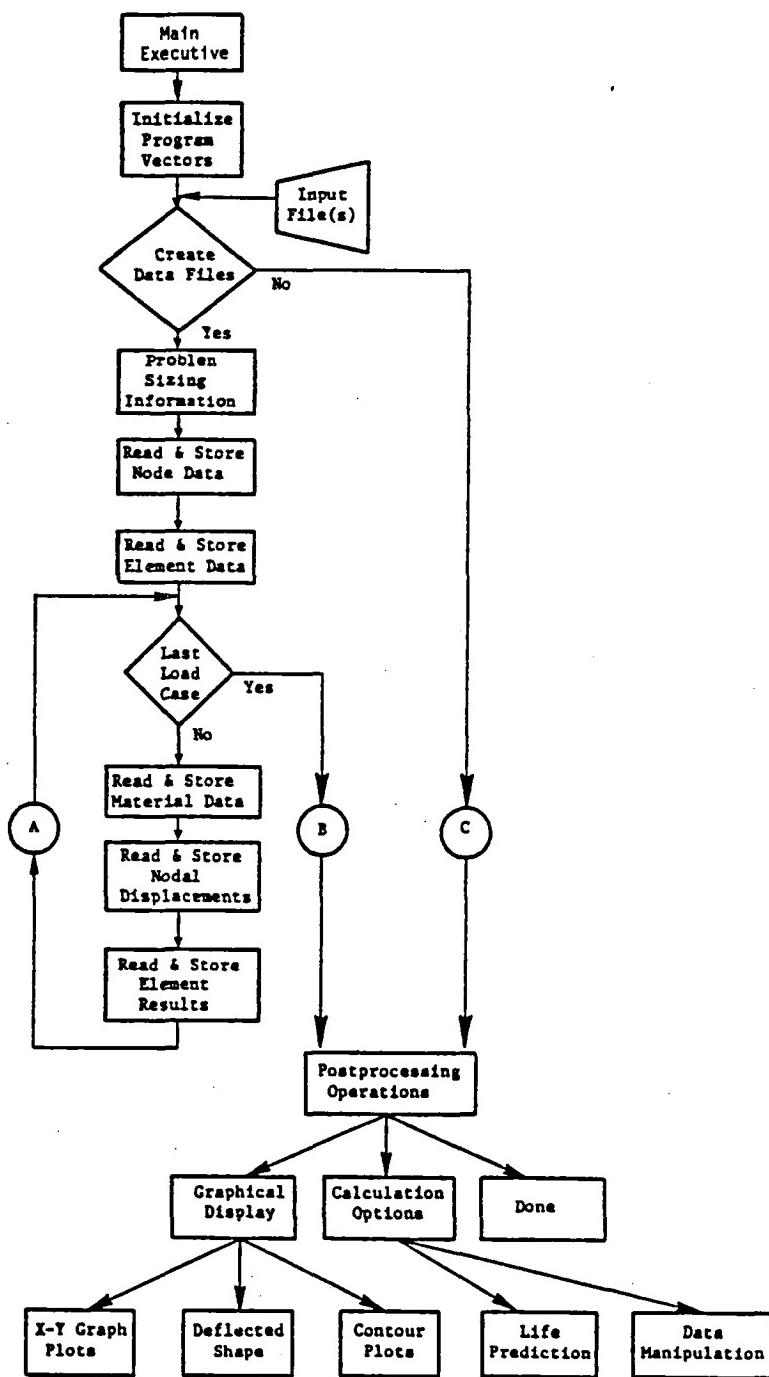
COMPONENT TEMPERATURE AND PRESSURE DECOMPOSITION

AND SYNTHESIS PLAN

I.   Blades and Vanes

     A.   Input will be:

          1.   A series of mid-span station temperatures at a specified SS
               reference case condition, and for each station a percent cord
               envelope dimension.

          2.   A set of output percent cord envelope dimensions.

          3.   A table of percent radial span (or radii) versus temperature
               factors, RF, where:

               $$RF = \frac{Ts-T3}{Tms-T2}$$

               Ts = temperature at specified span dim.

               Tms = temperature at midspan.

     The point density in this table will be such that spanwise linear interpo-
lation will suffice.

     B.   Calculations

          1.   For each temperature a nominal cooling effectiveness will be
               calculated from:

               $$\eta_c = \frac{T41-Tm}{T41-T3}$$

          2.   At each new condition, all station η_c values will be modified
               by a factor, CF, as follows:

               $$CF = \frac{(1-\eta_c)}{(1-\eta_c)REF} = (T3 \ast T41)^{\alpha}/(T3 \ast T41)^{\alpha}_{REF} \quad \text{where } \alpha \text{ is input}$$

          3.   Output Nc values will be linearly interpolated based on percent
               cord envelope at adjacent input stations.

          4.   For each output radial distance (specified in the input) all
               station temperatures will be calculated as follows:

$$Tij = T3 + (1-\eta_{c_R})*CF(T41-T3)*RF$$

Where i = station index

j = radial station index

II. Combustor

A. Inputs will be:

1. Metal bulk made temperatures at axial stations on inner and outer liners, and for each station, x and y dimensions of node centers at a specified reference case condition. Both hot streak and average metal temperature values will be input.

2. It is assumed that output node dimensions will match the input nodes. If cross-meshing is to be required, it will be done before the input is defined.

3. A set of linear equation constants will be input for a sparse set of axial locations, identified by ΔT station: numbers. Output ΔT locations will be same as input locations.

4. A set of ΔP scaling constants will be input at a sparse set of locations, identified by ΔP station numbers. Output ΔP stations will be same as input.

B. Calculations

1. A nominal cooling effectiveness will be calculated for each input combustor average and hot streak temperature.

2. At each flight condition, each metal temperature will be recalculated from:

$$Tm_{ij} = T3_j + \left(1-\eta_{c_i}\right)\left(T41_j - T3_j\right)$$

Where i = station index

j = flight phase index

3. At each flight condition, each ΔT will be recalculated from:

$$\Delta T_{ij} = \left[\left(1-\eta_{c_i}\right)*T41_j + \left(\eta_{c_i}-1\right)*T3_j\right]\left[b_i+m_i*P3_j\right]$$

4. At each flight condition, each ΔP will be recalculated from:

$$\Delta P_{ij} = P3_j*K_i*\frac{W41}{P3}_j^2 * T3_j$$